University of Alberta

The Development and Application of an Electrospray Ionisation Ion Trap/Linear Time-of-Flight Mass Spectrometer

by

Randall William Purves ©

A thesis submitted to the Faculty of Graduate Studies and Research in partial fulfilment of the requirements for the degree of Doctor of Philosophy

Department of Chemistry

Edmonton, Alberta

Fall 1997

National Library
of Canada

Acquisitions and
Bibliographic Services

395 Wellington Street
Ottawa ON K1A 0N4
Canada

Bibliothèque nationale
du Canada

Acquisitions et
services bibliographiques

395, rue Wellington
Ottawa ON K1A 0N4
Canada

Your file Votre référence

Our file Notre référence

The author has granted a non-exclusive licence allowing the National Library of Canada to reproduce, loan, distribute or sell copies of this thesis in microform, paper or electronic formats.

The author retains ownership of the copyright in this thesis. Neither the thesis nor substantial extracts from it may be printed or otherwise reproduced without the author's permission.

L'auteur a accordé une licence non exclusive permettant à la Bibliothèque nationale du Canada de reproduire, prêter, distribuer ou vendre des copies de cette thèse sous la forme de microfiche/film, de reproduction sur papier ou sur format électronique.

L'auteur conserve la propriété du droit d'auteur qui protège cette thèse. Ni la thèse ni des extraits substantiels de celle-ci ne doivent être imprimés ou autrement reproduits sans son autorisation.

0-612-23059-7

Canada

University of Alberta

Library Release Form

Name of Author: Randall William Purves

Title of Thesis: The Development and Application of an Electrospray Ionisation Ion Trap/Linear Time-of-Flight Mass Spectrometer

Degree: Doctor of Philosophy

Year This Degree Granted: 1997

Permission is hereby granted to the University of Alberta Library to reproduce single copies of this thesis and to lend or sell such copies for private, scholarly, or scientific research purposes only.

The author reserves all other publication and other rights in association with the copyright in the thesis, and except as hereinbefore provided, neither the thesis nor any substantial portion thereof may be printed or otherwise reproduced in any material form whatever without the author's prior written permission.

Randy Purves

32 Sinclair Crescent S.W.
Calgary, AB.
T2W 0L7

September 23, 1997.

University of Alberta

Faculty of Graduate Studies and Research

The undersigned certify that they have read, and recommend to the Faculty of Graduate Studies and Research for acceptance, a thesis entitled The Development and Application of an Electrospray Ionisation Ion Trap/Linear Time-of-Flight Mass Spectrometer submitted by Randall William Purves in partial fulfillment of the requirements for the degree of Doctor of Philosophy.

Liang Li

Dr. L. Li, Associate Professor of Chemistry

Fred Cantwell

Dr. F. F. Cantwell, Professor of Chemistry

Monica Palcic

Dr. M. Palcic, Professor of Chemistry

Mark T. McDermott

Dr. M. McDermott, Assistant Professor of Chemistry

Peter Sporns.

Dr. P. Sporns, Professor of Agricultural Food and Nutritional Science

Murray Johnston

Dr. M. V. Johnston, Professor of Chemistry and Biochemistry

Sept. 22, 1997

to my wife, Andrea

Abstract

Electrospray is arguably the most successful technique for producing intact gas-phase ions from highly polar and nonvolatile compounds. Coupling electrospray ionisation with a time-of-flight mass spectrometer (TOFMS) allows for a very rapid and sensitive analysis of these compounds. One method of combining electrospray ionisation with a TOFMS involves the use of a quadrupole ion trap for temporary ion storage. The quadrupole ion trap not only accumulates the ions, but it also functions as part of the extraction region of the TOFMS. The development and application of an electrospray ionisation ion trap/linear TOFMS are described.

Adduct formation occurring both in solution and in the ion trap are discussed. In particular, the type of diffusion pump fluid was a critical parameter as silicon-based fluids caused the formation of unwanted adducts in the ion trap.

At present, the instrument is most applicable to the analysis of small analytes (i.e., molecular weights less than ~1000). For these analytes, mass resolution values in excess of 1000 fwhm are routinely obtainable. For larger analytes, the use of high flow rates of buffer gas, necessary for efficient trapping, is shown to decrease the mass spectral quality. Space-charge effects and mass-to-charge ratio discrimination are also observed for large analytes. The use of a quadrupole focussing lens and electronic cooling methods are suggested as ways to help alleviate these problems. The same limitations are not observed for small analytes. Furthermore, mass accuracy errors of less than 100 ppm are routinely obtainable and errors as low as ~10 ppm can be obtained with this instrument using an internal standard when the isotopes of the analyte are resolved.

The use of this instrument for quantitative purposes is investigated using sulphonamides. The linear range of a calibration curve and the reproducibility of the instrument are examined. Twenty phenylthiohydantoin (PTH)-amino acids are also investigated, and all were detected at the 100 fmol level. In all applications, the chemical background noise is a limiting factor for trace analysis. The use of tandem mass spectrometry techniques to improve the detection limits is discussed.

Acknowledgment

I would like to thank my supervisor, Dr. Liang Li for his advice, support and enthusiasm during the past five years. I also thank all members of Dr. Li's research group with whom I have worked with. I especially thank Mr. Wojciech Gabryelski whose contributions are especially noticeable in Chapters 4, 6 and 7. I also thank Dr. Randy Whittal for his discussions in regards to the initial design of the instrumentation.

I thank the personnel in both the electronics shop and the machine shop of the chemistry department. In particular, I thank Erich Schartner for his invaluable assistance in the design and manufacturing of the instrumentation. I also thank Mr. Larry Coulson and Mr. Ed Feschuk for their assistance in the development of the electronic circuitry described in Appendix A.

Finally, I thank the University of Alberta and the Department of Chemistry for funding.

Table of Contents

Chapter 1 1

Introduction: Electrospray Ionisation Ion Trap/Time-of-Flight Mass Spectrometry . . . 1

1.1 Electrospray Ionisation 1
1.2 Time-of-Flight (TOF) Mass Spectrometry 6
1.3 Electrospray Ionisation/TOF Mass Spectrometry 10
    1.3.1 Beam Deflection 11
    1.3.2 Ion Storage TOFMS 11
    1.3.3 Orthogonal TOFMS 12
    1.3.4 Ion Trap/TOFMS 13
        1.3.4.1 Quadrupole Ion Trap 14
    1.3.5 Other Methods 17
1.4 Comparison of Ion Trap/TOFMS with Other Methods 18
1.5 Literature Cited 19

Chapter 2 29

Development of Instrumentation for Atmospheric Pressure Ionisation/Time-of-Flight Mass Spectrometry 29

2.1 Introduction 29
    2.1.1 Ion Transport and Cluster Formation 30
2.2 Experimental 31
    2.2.1 Interface 31
    2.2.2 Vacuum System and Orthogonal TOFMS 34
    2.2.3 Data Collection 36
    2.2.4 Ionisation Sources 37
    2.2.5 Sample Preparation 37
    2.2.6 Operating Conditions 38

2.3 Results ... 39
  2.3.1 Corona Discharge ... 39
  2.3.2 Electrospray ionisation ... 41
  2.3.3 Limitations ... 42
2.4 Literature Cited ... 44

Chapter 3 ... 53

Development of an Electrospray Ionisation Ion Trap/Linear Time- of-Flight Mass Spectrometer for Micro-Column Liquid Chromatography Detection ... 53
... 53
3.1 Introduction ... 53
3.2 Experimental ... 54
  3.2.1 Ion Trap/Linear TOFMS ... 54
  3.2.2 Ion Trap Operation and Ion Extraction. ... 56
  3.2.3 Data Collection and Analysis. ... 56
  3.2.4 Sample Injections. ... 57
  3.2.5 Chemicals and Solutions. ... 58
3.3 Results and Discussion ... 58
  3.3.1 Evaluation of Linear TOFMS ... 58
  3.3.2 Detection Limits ... 59
  3.3.3 On-line Separations ... 61
  3.3.4 Summary ... 61
3.4 Literature Cited ... 62

Chapter 4 ... 70

Adduct Formation in an Electrospray Ionisation Ion Trap/Time-of-Flight Mass Spectrometer 70
4.1 Introduction ... 70

4.2 Experimental 71
4.3 Results and Discussion 72
  4.3.1 Adducts From Silicon-Based Diffusion Pump Fluid 72
  4.3.2 Solution Adduct Formation 76
4.4 Literature Cited 78

Chapter 5 88

Characterization of an Electrospray Ionisation Ion Trap/Linear Time-of-Flight Mass Spectrometer 88
5.1 Introduction 88
5.2 Experimental Section 89
  5.2.1 Calibration of Helium Flow Rate Into the Ion Trap 89
  5.2.2 Bipolar Extraction 90
5.3 Results and Discussion 91
  5.3.1 Mass Resolution 91
  5.3.2 Mass Range. 94
  5.3.3 Effect of the Buffer Gas and Trapping Time. 96
  5.3.4 Space Charge Effects. 99
  5.3.5 Mass-to-Charge Ratio Discrimination. 100
  5.3.6 Mass Accuracy 101
    5.3.6.1 Considerations for Ion Trap/TOFMS 101
    5.3.6.2 Mass Accuracy Values for Electrospray Ion Trap/TOFMS 103
  5.3.7 Bipolar Extraction 109
  5.3.8 Summary 111
5.4 Literature Cited 112

Chapter 6 126

Quantitative Analysis Using an Electrospray Ionisation Ion Trap/Linear Time-of-Flight Mass Spectrometer . . . 126
6.1 Introduction . . . 126
6.2 Experimental . . . 127
6.3 Results and Discussion . . . 129
    6.3.1 Solution Properties . . . 129
    6.3.2 Detection limits and Linear Range . . . 130
    6.3.3 Reproducibility . . . 133
    6.3.4 Multicomponent Analysis . . . 134
    6.3.5 Summary . . . 135
6.4 Literature Cited . . . 136

Chapter 7 . . . 146

Detection of Phenylthiohydantoin Amino Acids Using Electrospray Ionisation Ion Trap/Linear Time-of-Flight Mass Spectrometry . . . 146
7.1 Introduction . . . 146
7.2 Experimental . . . 147
7.3 Results and Discussion . . . 148
    7.3.1 Mass Spectra of PTH-Amino Acids . . . 148
    7.3.2 Detectability of PTH-Amino Acids . . . 148
    7.3.3 Mixture Analysis . . . 150
    7.3.4 Summary . . . 151
7.4 Literature Cited . . . 151

Chapter 8 . . . 155

Conclusions and Future Work . . . 155

Appendix A . . . 158

Electronic Circuitry 158

List of Tables

Table 5.1 Effect of concentration on the observed peak width for various analytes. 99

Table 5.2 Comparison of peak area, peak width, and mass accuracy at different delay times of ion extraction after the rf voltage is turned off. 102

Table 5.3 Mass accuracy obtained using an internal standard with isotopic resolution. 105

Table 5.4 Mass accuracy obtained using an external standard (isotopic resolution). 106

Table 5.5 Mass accuracy obtained using an internal standard (non isotopic resolution). 107

Table 5.6 Mass accuracy values obtained using an external standard (non isotopic resolution). 108

Table 5.7 Comparison of negative extraction (only) versus bipolar extraction for PEG. 110

Table 6.1 S/N ratios for 5 sulphonamides examined in this study. 130

Table 6.2 Determination of the Upper Limit of Quantitation. 132

Table 7.1 Signal-to-noise ratios of 20 PTH-amino acids using the ion trap/linear TOFMS. 149

Table A.1 List of parts for electronic circuitry. 161

List of Figures

Figure 1.1 (A) Schematic of the electrospray ionisation process. (B) Close up of the Taylor cone, liquid filament and droplet formation. 24

Figure 1.2 Schematic of a time-of-flight mass analyser. (A) At time zero, (B) during mass analysis. See text for details. 25

Figure 1.3 Two of the earlier methods used to combine electrospray ionisation and TOFMS. (A) Beam deflection using the gate model and (B) "ion storage" TOF. See text for details. 26

Figure 1.4 A schematic of two commonly used methods for coupling electrospray ionisation and TOF. (A) Orthogonal extraction and (B) ion trap/TOF. A description is given in the text. 27

Figure 1.5 The quadrupole ion trap. (A) A schematic of the various components of the ion trap. (B) A part of the a versus q stability diagram. The dashed line indicates the mass-selective storage mode of operation. (C) A representation of the depth of the trapping well in the z-direction; point 'a' represents an ion entering the ion trap from an external source. See text for details. 28

Figure 2.1 Schematic of the two-stage interface constructed at the University of Alberta. Drawing is not to scale, dimensions are given in the text. 46

Figure 2.2 Schematic of the electrospray ionisation/linear TOFMS in the orthogonal configuration. Drawing is not to scale, a description of the instrument is given in the text. 47

Figure 2.3 The effect of floating the detector on the quality of the mass spectra for background water clusters. (A) Normal MCP operation, detector voltage = -2170 V, liner = -2100 V. (B) Detector voltage = -4800 V, liner= -4000 V. 48

Figure 2.4 Mass spectrum of tributylamine obtained using a corona discharge source. Operating conditions are given in the text. 49

Figure 2.5 Corona discharge mass spectrum obtained from water vapour. The result was the extensive formation of $(H_2O)_nH^+$ clusters with n = 1 to 62 observed.

Shown in the inset is the expanded view of the n = 38 water cluster with a mass resolution of ~ 710 fwhm. 50

Figure 2.6 Electrospray ionisation mass spectra of (A) kyotorphin (YR) with isotopic resolution of the $[M + H]^+$ peak (inset) and (B) bradykinin with mass resolution of ~ 600 fwhm for the $[M + 2H]^{2+}$ peak (inset). 51

Figure 2.7 Electrospray ionisation mass spectra of (A) a synthetic peptide (Ac-DIKHLEAEYRFLDTEVKSLEDEIRALDADVKACES-Amide) and (B) equine cytochrome c. Operating conditions are given in the text. 52

Figure 3.1 Schematic of the electrospray ionisation ion trap/linear time-of-flight mass spectrometer. Drawing is not to scale, dimensions are given in the text. 64

Figure 3.2 Timing diagram for one ion extraction event using an ion trap/linear time-of-flight mass spectrometer. 65

Figure 3.3 Electrospray ionisation mass spectra of (A) equine cytochrome c and (B) equine apomyoglobin obtained using an electrospray ionisation ion trap/linear TOFMS. An expanded view of the most intense peak in each mass spectrum is shown in the inset. 66

Figure 3.4 Flow injection profiles for four different amounts of bradykinin injected. (A) 3 pmol, (B) 300 fmol, (C) 150 fmol, and (D) 75 fmol. A Savitzky-Golay 2nd order algorithm (15 points) was used to smooth the data. 67

Figure 3.5 Mass spectra of bradykinin for four different amounts injected using the electrospray ionisation ion trap/linear TOFMS. (A) 3 pmol, (B) 300 fmol, (C) 150 fmol, and (D) 75 fmol. 68

Figure 3.6 Extracted ion chromatogram of (A) equine cytochrome c and (B) equine apomyoglobin obtained using micro-LC electrospray ionisation ion trap/linear TOFMS and (C) a UV chromatogram of the same mixture. The chromatographic conditions are given in the text. A Savitzky-Golay 2nd order algorithm (15 points) was used to smooth the data in (A) and (B). 69

Figure 4.1 (A) Mass spectrum of equine cytochrome c obtained using DC 7040 diffusion pump fluid and a trapping time of 330 ms. (B) Expanded view of the adducts of the $[M + 16H]^{16+}$ ion. 80

Figure 4.2 Mass spectrum of a solution of 2 mM ammonium acetate in 80% acetonitrile and 20% water with no bath gas in the desolvation region. The diffusion pump fluid was DC 7040. 81

Figure 4.3 (A) Plot of the intensity of the $[M + 21H]^{21+}$ and the $[M + 21H + 484]^{21+}$ peaks for equine apomyoglobin as a function of trapping time; DC 7040 diffusion pump fluid was present in the instrument. (B) Plot of the peak width (ns) of the $[M + 21H]^{21+}$ peak for the same experiment. 82

Figure 4.4 (A) Mass spectrum of equine cytochrome c obtained using a detergent in the cleaning procedure and changing the diffusion pump fluid to DC 7050. The trapping time used was 500 ms. (B) Expanded view of the 17^+ charge state and its adducts. (C) Expanded view of the 15^+ charge state and its adducts. 83

Figure 4.5 Mass spectrum of equine cytochrome c obtained using Santovac 5 diffusion pump fluid and a trapping time of 1 s. 84

Figure 4.6 (A) Mass spectrum of a solution of equine cytochrome c containing Cu(I). (B) Expanded view of the 14^+ charge state and its corresponding adducts. 85

Figure 4.7 Reduction of adduct peaks in a mass spectrum of equine apomyoglobin by changing the voltage drop between the nozzle and sampling plate in the interfacial region. (A) ΔV = 13 V, (B) ΔV = 18 V, and (C) ΔV = 23 V. 86

Figure 4.8 Reduction of adduct peaks in a mass spectrum of bovine trypsinogen by changing the voltage drop between the nozzle and sampling plate in the interfacial region. (A) ΔV = 40 V, (B) ΔV = 50 V, and (C) ΔV = 60 V. 87

Figure 5.1 A plot of the flow rate of helium into the ion trap as a function of the change in pressure observed in the flight tube. 115

Figure 5.2 Resolution capabilities of the ion trap/linear time-of-flight mass spectrometer. (A) Mass spectrum of a small peptide, FIPK, showing isotopic resolution (inset). The rf voltage was 730 V_{p-p} and the flow rate of helium into the trap was 0.20 mL/min. (B) Mass spectrum of bradykinin with mass resolution of 560 fwhm (inset). The rf voltage was 750 V_{p-p} and flow rate of helium into the trap was 0.08 mL/min. The extraction conditions for both spectra are listed in the text. 116

Figure 5.3 Mass resolution capabilities of the ion trap/linear time-of-flight mass spectrometer for larger analytes. (A) Mass spectrum of equine cytochrome c with a mass resolution of 1020 (inset). The rf voltage was 1650 V_{p-p} and the flow rate of helium into the ion trap 0.03 mL/min. (B) Mass spectrum of bovine serum albumin. The rf voltage was 2200 V_{p-p} and the rf frequency was 740 kHz. The trapping time was 100 ms and flow rate of helium into the trap was 0.17 mL/min. 117

Figure 5.4 Mass spectra of (A) chicken lysozyme with a mass resolution of 980 (inset) and (B) bovine carbonic anhydrase II with a mass resolution of 400 (inset). (A) The rf voltage was 2150 V_{p-p} and flow rate of helium into the trap was 0.03 mL/min. (B) The rf voltage was 1240 V_{p-p} and flow rate of helium into the trap was 0.05 mL/min. 118

Figure 5.5 The effect of trapping time, for different flow rates of the helium buffer gas, on the peak area of FIPK. (A) 0 mL/min, (B) 0.03 mL/min, (C) 0.12 mL/min, (D) 0.40 mL/min, (E) 0.54 mL/min, (F) 0.72 mL/min. The rf voltage was 730 V_{p-p}. 119

Figure 5.6 The effect of trapping time, for different flow rates of the helium buffer gas, on the peak width of FIPK. Conditions were the same as those given in Figure 5.5. The value of the minimum peak width is displayed for each helium flow rate. 120

Figure 5.7 The effect of trapping time, for different flow rates of helium buffer gas, on the peak area of equine cytochrome c. (A) 0 mL/min, (B) 0.03 mL/min, (C) 0.07 mL/min, (D) 0.20 mL/min, (E) 0.40 mL/min. The rf voltage was 1650 V_{p-p}. 121

Figure 5.8 The effect of trapping time, for different flow rates of the helium buffer gas, on the peak width of equine cytochrome c. Conditions are the same as those given in Figure 5.7. The value of the minimum peak width is displayed for each helium flow rate. 122

Figure 5.9 Mass-to-charge ratio discrimination observed for equine apomyoglobin. (A) rf voltage of 2250 V_{p-p}, (B) rf voltage of 2000 V_{p-p}, (C) rf voltage of 1750 V_{p-p} and (D) rf voltage of 1500 V_{p-p}. 123

Figure 5.10 Effect of buffer gas on mass-to-charge ratio discrimination observed for equine cytochrome c. The helium flow rates are (A) 0.03 mL/min and (B) 0.32 mL/min. 124

Figure 5.11 A mass spectrum of PEG with the three principle distributions (inset) and its corresponding structure. 125

Figure 6.1 Effect of changing the concentration of ammonium acetate on the mass spectra of SDM. (A) No ammonium acetate added, (B) 0.5 mM ammonium acetate, (C) 2 mM ammonium acetate, and (D) 10 mM ammonium acetate. 139

Figure 6.2 Mass Spectrum obtained from an injection of a mixture of SDM, SCP, SMZ, SMR, and STZ. The mixture contained 100 fmol of each sulphonamide. See description in text. 140

Figure 6.3 Calibration curve for a series of loop injections of SDM with an expanded view of the low end of the curve shown in the inset. 141

Figure 6.4 Mass spectrum of an injection of 5 fmol of SDM showing the limitations due to the chemical background noise using an electrospray ionisation ion trap/linear TOFMS. Note that only 25 ion extraction events were summed for this mass spectrum. 142

Figure 6.5 Reproducibility of the electrospray ionisation ion trap/TOFMS illustrated using repeat injections of SDM at 10 fmol, 100 fmol and 1 pmol. 143

Figure 6.6 Repeat injections of SDM over an eight hour period. (A) Area calculated using a calibration curve, (B) a ratio of peak areas calculated using SMZ as an internal standard. 144

Figure 6.7 Calibration curves for (A) SDM, (B) STZ, (C) SMZ, (D) SCP, (E) SMR obtained simultaneously from a mixture. 145

Figure 7.1 Mass spectra of (A) PTH-alanine, (B) PTH-(PTC-cysteine). See text for details. 153

Figure 7.2 Mass spectra of a mixture of six PTH-amino acids, (A) 1 pmol and (B) 250 fmol of each compound injected. See text for details. 154

Figure A.1 Circuit developed to protect the electronic components. 162

Figure A.2 Circuit developed to ground induced rf noise on the exit endcap electrode. 163

List of Abbreviations

API	atmospheric pressure ionisation
CID	collision induced dissociation
DC 7040	tetraphenyl tetramethyl trisiloxane (Dow Corning)
DC 7050	pentaphenyl trimethyl trisiloxane (Dow Corning)
fwhm	full width at half maximum
HPLC	high performance liquid chromatography
ID	inner diameter
LC	liquid chromatography
M	molecular ion
MALDI	matrix-assisted laser desorption/ionisation
MCP	multichannel plate detector
MOSFET	metal oxide semiconductor field effect transistor
MS	mass spectrometry
MS^n	tandem mass spectrometry to the n
MS/MS	tandem mass spectrometry
m/z	mass-to-charge ratio
OD	outer diameter
PEG	poly(ethylene glycol) monomethyl ether
PITC	phenylisothiocyanate
ppm	parts per million
PTC	phenylthiocarbamyl
PTH	phenylthiohydantoin
rf	radio frequency
RSD	relative standard deviation
SCP	sulphachlorpyridazine
SDM	sulphadimethoxine
SIDT	single ion in droplet theory
SMR	sulphamerazine

SMZ	sulphamethazine
STZ	sulphathiazole
S/N	signal-to-noise
TFA	trifluoroacetic acid
TOF	time-of-flight
TOFMS	time-of-flight mass spectrometry
u	unified atomic mass unit
UV	ultraviolet
v/v	volume-to-volume ratio

Chapter 1

Introduction: Electrospray Ionisation Ion Trap/Time-of-Flight Mass Spectrometry

The application of mass spectrometry to the analysis of very large, complex, and fragile compounds had been restricted due to the difficulties in transforming these compounds into intact gas-phase ions. Recently, the development of soft ionisation techniques, such as electrospray, has made this transformation possible. Consequently, the mass spectrometric analysis of several biological molecules can now be carried out when only a couple of decades ago this was not possible. Time-of-flight (TOF) offers several potential advantages for mass analysis of ions produced from biological molecules compared with traditional mass analysers (e.g., quadrupole). However, only with recent improvements in technology have these advantages been realized. The development of a mass spectrometer capable of fast, sensitive analyses is of interest to the biological community. The primary objective of this work is to develop and characterize a mass spectrometer of this type.

1.1 Electrospray Ionisation

The need to produce intact molecular ions for increasingly larger and less volatile compounds has resulted in the recent development of several soft ionisation techniques. Usually, these techniques are classified as either energy sudden methods, or field desorption methods [1]. Energy sudden methods, such as fast atom bombardment and laser desorption, involve a nearly instantaneous implementation of a high energy density in a sample of analyte. Although this leads to the formation of highly energetic ions, these are considered "soft ionisation methods" because they produce intact molecular ions for large analytes. Matrix-assisted laser desorption/ionisation (MALDI) [2] is the most successful of these techniques in terms of the highest molecular weight detected.

Field desorption methods use very strong electric fields to extract ions into the gas phase. When electrical energy is used, there is no localized heating and very little internal energy is given to the ions. Field desorption is subdivided into techniques that either desorb ions into vacuum, or those that desorb ions into a bath gas [1]. Desorption of ions from a nonvolatile liquid into vacuum (i.e., electrohydrodynamic ionisation) produces ions with varying degrees of solvation and a wide range of energies. A major improvement in field desorption methods occurred when ions were desorbed into a bath gas instead of into vacuum. The bath gas was vital in overcoming problems associated with field desorption into vacuum for two main reasons [1]. First, evaporation of solvent is much more efficient at atmospheric pressure because of a more effective heat transfer. Also, the bath gas helps to moderate the internal and translational energy of the ions to the level corresponding to the bath gas temperature. Electrospray ionisation is one of three techniques that desorbs ions from a liquid into a bath gas.

The study of electrospray phenomena extends back to Zeleny who observed nebulization occurring from the surface of ethanol solutions when they were exposed to high electric fields in 1917 [3]. In the late 1960's, the use of electrospray as an ionisation technique was investigated by Dole et al. [4,5]. During these experiments, a Faraday cage was used to measure ion currents produced from solutions of polystyrene. This was the first evidence that gas-phase macroions were obtained from the electrospray process [4]. However, it was not until 1984 that electrospray ionisation mass spectrometry was introduced independently by Yamashita and Fenn [6], and Alexsandrov et al. [7]. Fenn and coworkers later applied electrospray ionisation to the analysis of protein samples [8]. Since these results were reported, the popularity of electrospray ionisation in the mass spectrometry community has dramatically increased. This increase in popularity is illustrated by the fact that 387 of the 1527 abstracts submitted to the 45th American Society for Mass Spectrometry Conference in Palm Springs in 1997 contained "electrospray ionization" as a key word in their abstract.

Kebarle has described four major processes that occur in electrospray ionisation mass spectrometry; the production of charged droplets, shrinkage of charged droplets, repeated droplet disintegrations, and formation of gas phase ions [9]. This overall process is briefly summarized below for positive ion generation using Figure 1.1 as an illustration [9]. Figure 1.1 (A) shows a liquid sample continually flowing through a stainless steel capillary. A high voltage is applied to the metal capillary, which is in close proximity ($x \approx 1$ cm) to a large counter electrode, thereby producing an electric field. The strength of the electric field is dependent upon several variables, including the internal radius of the capillary, the voltage applied to the capillary, and the distance from the needle tip to the counter electrode, x [9]. The electric field causes positive charges to accumulate on the surface of the liquid. Consequently, the surface becomes destabilized resulting in the formation of a Taylor cone, Figure 1.1 (B) [10]. At sufficiently high electric field strengths, a liquid filament is emitted from the tip of the Taylor cone. This filament becomes unstable and produces droplets enriched with positive charges. The size and charge of these droplets are dependent upon the electrospray conditions used. The rest of this discussion is concerned with droplets produced using optimal conditions for high gas-phase ion yields. This corresponds to a flow rate of 5 μL/min and a total electrolyte concentration of 10^{-3} M to 10^{-5} M [9].

These initial droplets, rich in positive charges, shrink in size as solvent molecules evaporate. To assist in this process, a cross-countercurrent flow of a drying gas (typically dry nitrogen) is used [6]. These droplets continue to shrink until the coulombic repulsion forces overcome the surface tension forces thereby causing a coulombic explosion to occur. The condition where this occurs is given by the Rayleigh equation [11]; a simplified version of this equation is given by:

$$Q_R^2 = k\gamma R_R^3 \tag{1.1}$$

Where Q_R is the charge on the droplet, R_R is the radius of the droplet, k is a numerical constant and γ is the surface tension of the solvent. A coulombic explosion results in the emission of several small droplets that contain about 15% of the charge and only 2% of the mass of the original droplet [9]. The solvent molecules in the smaller droplets continue to evaporate until another coulombic explosion occurs. Different theories have been put forth to explain the process that ultimately leads to the formation of gas phase ions from these small droplets. The single ion in droplet theory (SIDT) [4,12] and the ion evaporation theory [13,14] are the two most common theories. The mechanism of the SIDT involves the formation of extremely small droplets from repeated solvent evaporation and coulombic explosions. These small droplets convert to gas phase ions upon evaporation of the last solvent molecule. Conversely, the ion evaporation theory assumes that small ions evaporate from small, highly charged droplets. That is, the droplet does not undergo subsequent fission, but instead emits gas-phase ions. A detailed discussion of theories dealing with the formation of gas-phase ions from electrospray ionisation is presented in a recent paper by Kebarle that discusses the mechanism of electrospray ionisation mass spectrometry [9].

With possibly the exception of MALDI, no other technique has been as successful as electrospray ionisation for producing intact gas phase ions from large or very fragile compounds [15]. In addition, there are several other advantages of using electrospray ionisation. First, unlike the energy sudden ionisation methods, electrospray ionisation mass spectrometry is used to characterize noncovalent interactions in solution. A recent review article by Przybylski and Glocker discusses several successful applications that demonstrate the widespread use of electrospray ionisation for direct analysis of specific noncovalent interactions [16]. However, if structural information is desired, fragmentation is carried out by adjusting instrumental parameters (described in Chapter 2) [17]. Furthermore, the solvents used for electrospray ionisation are generally compatible with separation methods and therefore electrospray ionisation mass spectrometry can be readily used for on-line detection. A recent review article by Gelpí discusses several applications of liquid chromatography electrospray ionisation mass spectrometry [18].

Since the electrospray process results in the formation of highly charged liquid droplets, multiple charges are inherent with this technique. Multiple charging allows for a wider mass range to be observed on scanning type mass analysers through the reduction of m/z (mass-to-charge) ratio values. Furthermore, because of multiple charging, collision induced dissociation (CID) is now carried out on larger analytes (i.e., albumin with molecular weight 66 000) [19].

The two other techniques that desorb ions from solution into a bath gas are ionspray and thermospray. Ionspray is different from electrospray ionisation in that mechanical energy from a high velocity gas flow is used to assist in nebulization [20]. This energy input allows ionspray to be used at higher flow rates than electrospray ionisation, therefore, it is more compatible with liquid chromatography/mass spectrometry techniques. Thermospray is different from electrospray ionisation and ionspray in that a voltage is not applied to the metal capillary. Instead, thermospray involves heating the capillary tube to vaporize the majority of the solvent [21,22]. This results in the formation of droplets in solvent vapour that emerge from the capillary tip. Statistical fluctuations of ions in solution cause the formation of an equal number of positively and negatively charged droplets. The conversion of these droplets to gas-phase ions involves the same mechanism as described for electrospray.

1.2 Time-of-Flight (TOF) Mass Spectrometry

The concept of TOF mass analysis was first described by Stephens in 1946 [23]. In 1955, Wiley and McLaren developed a TOF mass spectrometer (MS) [24], the design of which provides the basis for modern day TOF instruments. The principles of TOF mass analysis are briefly explained using the simplified diagram shown in Figure 1.2 [25]. The TOF mass analyser consists of an extraction region, a drift region (i.e., the flight tube), and a detection region. Ions generated from an external source (i.e., electrospray) are allowed to fill the extraction region, Figure 1.2 (A). Note that methods of introducing electrosprayed ions into the extraction region are discussed in section 1.3. A voltage pulse, V, is applied to the back electrode at time zero, thereby accelerating the ions in this region toward the grounded electrode according to:

$$\frac{m \cdot v^2}{2} = z \cdot E \cdot s \tag{1.2}$$

Where E is the electric field, V/d; m/z is the mass-to-charge ratio of the ion; v is the velocity; and s is the initial distance of the ion from the grounded electrode. When the ions cross the grounded electrode and enter the drift region, their velocities are given by:

$$v = \left(\frac{2z \cdot E \cdot s}{m}\right)^{1/2} \tag{1.3}$$

Consequently, ions in the drift region separate based on their differences in velocity (which is inversely proportional to m/z) as is illustrated in Figure 1.2 (B). The time that the ions spend in the drift region, t_D, is therefore:

$$t_D = \left(\frac{m}{2z \cdot E \cdot s}\right)^{1/2} D \tag{1.4}$$

The total flight time of an ion, t_T, is a sum of the time the ion spends in all three regions, more specifically that being:

$$t_T = t_E + t_D + t_d \tag{1.5}$$

Where t_E represents the time the ion spends in the extraction region and t_d represents the time the ion spends in the detection region. In the extraction region, if the ions are assumed to have an initial velocity of zero in the direction normal to the flight tube, then the time spent in this region is:

$$t_E = \left(\frac{2m \cdot s}{z \cdot E} \right)^{1/2} \tag{1.6}$$

If the detector is operated at the same voltage as the ground grid, then equation 1.4 is modified by replacing D with (D + D'). If the ions are post accelerated (i.e., the detector is operated at a negative voltage in Figure 1.2), then the treatment is analogous to equation 1.6. Consequently, the total flight time, t_T, can be determined.

The above equations illustrate that the time spent in any region of a TOF is proportional to the square root of the mass-to-charge ratio. Consequently, a calibration involving two points with known m/z values is carried out to solve for k and b in the following equation:

$$t = k(m/z)^{1/2} + b \tag{1.7}$$

Where k represents several instrumental parameters and b corresponds to an offset used to account for various delays in timing. The delay between applying the voltage pulse and the start of the data acquisition system is an example of a timing delay.

The resolving power of a mass spectrometer is given by m/Δm and for a TOFMS it is also defined as:

$$\frac{m}{\Delta m} = \frac{t}{2\Delta t} \qquad \textbf{(1.8)}$$

The value of Δm is determined using the full width at half the maximum peak height (fwhm). In mass spectrometry literature, the resolving power of a mass spectrometer is commonly reported using the term mass resolution. Note, however, that a reported mass resolution value of 1000 fwhm does not enable two peaks centred at m/z values of 1000 and 1001 to be distinguished.

Mass resolution values can be limited by both spatial distributions and kinetic energy distributions. Electrosprayed ions have a large kinetic energy spread [26] and therefore this is usually the limiting factor for mass resolution when these ions are analysed using a TOFMS. To compensate for these differences in initial kinetic energy, reflectrons are commonly used [26]. Spatial distributions occur when ions are located at different positions in the extraction region when the voltage pulse is applied. This causes ions with the same mass-to-charge ratios to be accelerated through different distances in the extraction region ('s' changes in equation 1.2). Consequently, the ion velocities entering the drift region will not be the same for ions with the same m/z values (equation 1.3). When the spatial distribution is the same for all ions, then methods to compensate for it can be used [25].

The TOF is unique in its ability to analyse ions of all m/z ratios simultaneously. This ability, in combination with the high ion transmission (i.e., no slits) capabilities of the TOF allow for highly sensitive mass analysis. Another advantage of using a TOF is that it is the only mass analyser that has a theoretically unlimited m/z range. In practice, the m/z range is limited by the detection system. Furthermore, the TOF generates a complete mass spectrum in a very short time (less than 1 ms), thereby allowing very fast data acquisition rates to be used. These potential advantages were unrealized until recent years in which there has been a significant improvement in electronics technology. For example, fast (>1 × 10^9 samples/s) digital oscilloscopes with long recording memories are now available.

1.3 Electrospray Ionisation/TOF Mass Spectrometry

Initially, electrospray ionisation mass spectrometry was almost exclusively carried out using quadrupole mass analysers [19]. Compared with the quadrupole and other mass analysers, a TOF mass analyser offers several advantages when used as a detector for electrospray ionisation. First, the extremely high data acquisition rates are well suited for coupling electrospray ionisation with fast separation techniques such as capillary electrophoresis and fast liquid chromatography. Second, the TOF allows for very sensitive analyses, as was discussed in the previous section. Finally, for some applications, electrospray ionisation generates ions with m/z values that are outside of the m/z range of a quadrupole mass analyser [27]. For these applications, the TOF is the preferential mass analyser.

The idea of combining electrospray ionisation and TOF was first proposed over a quarter of a century ago by Dole in his pioneering experiments with electrospray [28]. A major challenge in combining electrospray ionisation with TOF mass spectrometry arises because electrospray is a continuous ionisation source while TOF requires a starting point. Recently, several methods have been presented for coupling various continuous ionisation sources with TOF mass analysers. This section discusses only the configurations used to couple electrospray ionisation and TOF mass spectrometry. Note that the methods are presented in the chronological order in which they appeared in the literature. Figure 1.3 shows a schematic of the set-up for two early attempts at combining electrospray with a TOFMS, beam deflection and "ion storage TOF."

1.3.1 Beam Deflection

Beam deflection techniques produce ion packets for mass analysis from continuous electrospray ion beams. Different types of beam deflection methods are described by Yefchak et al. [29]; a schematic of the "gate model" is shown in Figure 1.3 (A). This method uses a voltage pulse to generate a discrete packet of ions for TOF mass analysis. The sensitivity of this type of analysis is drastically reduced, however, because the pulse duration must be restricted to only a few nanoseconds to maintain acceptable mass resolution values. For this discussion, duty cycle is defined as the fraction of ions, of those which entered the ion extraction region, that reach the detector. A study by Ma et al. estimated a duty cycle of only ~0.01% for a beam deflection technique [30].

1.3.2 Ion Storage TOFMS

Due to the inherently low duty cycle of beam deflection techniques, subsequent attempts at coupling electrospray ionisation and TOF involved some form of temporary ion storage. A schematic of the design of an early attempt at temporary ion storage, proposed by Boyle and Whitehouse [31], is shown in Figure 1.3 (B). With this configuration, ions enter the extraction region in a direction that is coaxial with the flight tube of the TOF mass analyser. These ions are slowed by applying a stopping voltage to the electrode V_{ex} in the extraction region. During ion storage, the voltage applied to V_{ex} is slightly repulsive compared with the voltage applied to V_{bac}, consequently, the ions in this region are driven back toward the electrospray ionisation source. The ions stored in this region were extracted into the flight tube by applying a negative voltage pulse to V_{ex}.

The mass spectra presented in this initial study [31] suffered from low sensitivity and poor mass resolution. Since this initial paper, further studies using this technique have not been reported.

1.3.3 Orthogonal TOFMS

Figure 1.4 shows a schematic of two commonly used techniques for coupling electrospray ionisation and TOF mass spectrometry. In the first method, shown in Figure 1.4 (A), ions enter the extraction region of the TOF in an orthogonal direction compared with the flight tube. After the ions fill this region, a voltage pulse is applied to extract the ions into the flight tube. This method was introduced for electrospray generated ions by Dodonov et al. at the 12th International Mass Spectrometry Conference in 1991 [32], and later reported by others as well [27,33,34]. The sensitivity and mass resolution obtained with this configuration are vastly improved in comparison with the ion storage TOFMS discussed in section 1.3.2. The maximum duty cycle for orthogonal TOF instruments is restricted by the ratio of the time required to fill the ion extraction region to the total flight time of the largest ion. One of the earlier estimates of the duty cycle of an orthogonal TOFMS was ~ 20% [27].

Recent developments in instrumentation for the orthogonal TOFMS have focussed on improving the transportation of ions into the ion extraction region. The presence of a radio frequency (rf)-only quadrupole lens, operated at high pressures, drastically reduces the velocity of the ions entering the ion extraction region [35]. The presence of a rf field also constrains the ions close to the axis of the quadrupole thereby reducing the ion spread. Krutchinsky et al. used a rf-only quadrupole to improve the sensitivity of their orthogonal TOFMS [36]. An electrostatic beam guide, consisting of a wire and a concentric cylinder, has also been used to improve the performance of an orthogonal TOFMS [37]. Other recent designs that were based on this original orthogonal TOF configuration, discussed in section 1.5, are capable of tandem mass spectrometry (i.e., isolation of a specific m/z ion followed by the production and analysis its fragment ions).

1.3.4 Ion Trap/TOFMS

Another common method of temporarily storing ions prior to TOF mass analysis involves the use of a quadrupole ion trap. This design, shown schematically in Figure 1.4 (B), was first used to analyse electrosprayed ions by Lubman and coworkers [38]. Ions entering the ion trap are temporarily stored before a voltage pulse is applied to the ion trap to extract the ions into the flight tube. A simplified discussion of the theory of an ion trap, with emphasis on its function in combining electrospray ionisation and TOF, is given in section 1.3.4.1. A detailed discussion of the theory and operation of the ion trap is given elsewhere [39]. When used to couple electrospray ionisation and TOF, the ion trap not only serves to accumulate and focus the ions into a tight packet, but it also serves as part of the extraction region of the TOF during the mass analysis step. Note that the sensitivity and mass resolution obtained using this configuration are similar in comparison with orthogonal extraction techniques discussed in section 1.3.3.

1.3.4.1 Quadrupole Ion Trap

The components of a quadrupole ion trap consist of two endcap electrodes (separated by a distance of z_o) and one ring electrode (internal radius r_o) all having hyperboloidal geometry. A schematic of a cross-sectional view of the quadrupole ion trap is shown in Figure 1.5 (A). During the operation of the quadrupole ion trap, a rf voltage (with a maximum potential, V) and a DC potential (U) is applied between the ring and endcap electrodes. The motion of an ion (with mass, m, and charge, z) in a quadrupole ion trap is described mathematically by the solutions to a second-order linear differential equation, the Mathieu equation [40]. These solutions are defined as:

$$a_z = \frac{-8eU}{mr_o^2\Omega^2} \tag{1.9}$$

$$q_z = \frac{4eV}{mr_o^2\Omega^2} \tag{1.10}$$

Where a_z and q_z are the Mathieu parameters; r_o and Ω are the internal radius of the ring electrode and the angular frequency of the trapping signal, respectively. The solutions to the Mathieu equation define whether an ion has an unstable trajectory or if it oscillates indefinitely within the quadrupole ion trap. These solutions are used to generate a stability diagram (a plot of a_z versus q_z); Figure 1.5 (B) shows a small region of the stability diagram. Under normal operating conditions for ion trap/TOFMS, the stability diagram can be further simplified because a DC potential is not used. Thus, a_z is equal to zero and the ions possess values of q_z that lie along the q-axis. Figure 1.5 (B) shows that ions with q_z values of 0.908 or greater will have unstable trajectories within the ion trap. These ions accelerate and strike an electrode before the phase of the rf voltage changes, consequently, this leads to a well defined lower m/z limit given by:

$$\left(\frac{m}{z}\right)_{\text{min}} = \frac{4.4V}{(r_o^2\Omega^2)} \qquad \textbf{(1.11)}$$

As the value of q_z approaches zero, there is no well defined upper m/z limit for which ion trajectories become unstable. Instead, the upper m/z limit is described using the "pseudopotential well" model [41]. This model approximates the depth of a trapping well in terms of potential energy ($\bar{D}$) for a given m/z ion in both r and z dimensions:

$$\overline{D}_z = \frac{eV_o^2}{4mz_o^2\Omega_o^2} \qquad \textbf{(1.12)}$$

The geometry of the ion trap is such that $r_o^2 = 2z_o^2$, consequently:

$$\overline{D}_z = 2\overline{D}_r \qquad \textbf{(1.13)}$$

A schematic of the pseudopotential well for the z-dimension is shown in Figure 1.5 (C). For a fixed set of conditions, as the m/z values of the ions become increasingly larger, the potential energy well becomes increasing smaller thereby decreasing the trapping efficiency. Trapping efficiency decreases because of factors such as holes in the endcap electrodes (to allow ions in/out) and imperfections (i.e., sharp edges) in machining that lead to non ideal fields in commercial ion traps. Non ideal fields increase the probability of ion loss and become more significant as the potential energy well decreases [42].

For ions introduced into the quadrupole ion trap from an external ionisation source, additional factors further reduce the trapping efficiency. Externally generated ions, which are introduced through an opening in an endcap electrode, possess an initial kinetic energy. An ion entering the quadrupole ion trap at point 'a' in Figure 1.5 (C) is only trapped if it enters during the correct phase angle of the applied rf voltage. Furthermore, unless some of its energy is removed, the ion will pass straight through the quadrupole ion trap. The most common method of removing energy from ions entering the quadrupole ion trap involves the use of a low molecular weight gas (i.e., helium) [43]. Ions entering the quadrupole ion trap undergo collisions with the buffer gas effectively transferring some of their energy with each collision to the gas without significantly altering the ion trajectory. However, even when a buffer gas is used, the highest estimates of trapping efficiency are only ~10% [44]. Consequently, the low trapping efficiency for externally generated ions is the major factor that limits the duty cycle using an ion trap/TOFMS.

Mass analysis using the quadrupole ion trap is carried out using several different techniques. When a TOFMS is used for mass analysis, first, the rf voltage is shut off and allowed to decay. Subsequently, a voltage pulse is applied to at least one of the endcap electrodes to extract the stored ions. Traditional methods of mass analysis for the quadrupole ion trap include mass selective detection, mass selective storage, and mass selective ejection [45]. Note that mass selective ejection also operates under conditions in which a_z is zero. With this technique, mass analysis is carried out by ramping the value of V (see equation 1.10) to steadily increase q_z values. Once a q_z value of 0.908 is reached, ions are ejected from the ion trap to a detector and consequently a mass spectrum is generated.

The main advantage of using a quadrupole ion trap is that the combination of mass selective storage and mass selective ejection are used for tandem mass spectrometry [46]. Mass selective storage involves isolating a narrow m/z range of ions by operating along the dashed line shown in Figure 1.5 (B). When a collision gas is present in the ion trap, the selected ions are excited and undergo energetic collisions with the collision gas. A mass spectrum of the fragment ions produced from this process is observed using mass selective ejection. Note that unlike other tandem mass spectrometry techniques, the ion trap performs this operation 'n' times.

1.3.5 Other Methods

At the time this work was initiated, only the four methods listed above were reported for combining electrospray ionisation and TOFMS. Two other configurations, derived from the orthogonal geometry, have since been reported. Both of these configurations are capable of tandem mass spectrometry. The quadrupole/orthogonal TOFMS [47] has a quadrupole mass filter and a hexapole collision gas cell placed between the electrospray ionisation source and the ion extraction region of the orthogonal TOF. This combination is used either to focus the ions entering the TOF, or it is used for MS/MS analysis (i.e., tandem mass spectrometry). In the later mode, the quadrupole is used to select a precursor ion, which is transported to the hexapole collision gas cell. A similar version of the quadrupole/TOFMS was also reported by Shevchenko et al. [48]. The second configuration uses a magnetic sector in combination with a TOFMS [49]. This instrument was developed as a competitive technique for tandem mass spectrometry using a four-sector instrument.

1.4 Comparison of Ion Trap/TOFMS with Other Methods

The ion trap/TOFMS can be described as an alternative means of mass detection for a quadrupole ion trap, or as another method for temporarily storing ions for TOF mass analysis. For the analysis of ions produced by electrospray, the quadrupole ion trap, using traditional mass analysis methods, is an effective technique [42,50,51]. The main advantage of the ion trap/TOFMS, compared with traditional mass analysis techniques using an ion trap, is in the speed of mass analysis. Mass selective ejection requires a scan of the rf voltage, whereas the TOF mass analyser detects all ions simultaneously. Furthermore, removing higher m/z ions from the ion trap is more difficult with traditional mass analysis techniques. A technique called axial modulation was developed to scan out these ions, however, it does so at the expense of mass calibration accuracy [52]. Mass resolution is a major disadvantage of the ion trap/TOFMS compared with traditional mass analysis techniques using an ion trap. With reduced scan rates, mass resolution values greater than 30 000 fwhm at m/z 502 are obtainable using mass selective ejection [53]. These values are approximately an order of magnitude better than optimal mass resolution values achieved using an ion trap/TOFMS [54].

Duty cycle is reported as a main advantage of using an ion trap/TOFMS versus an orthogonal TOFMS [54]. Based on the argument that the time required for mass analysis is much shorter than the trapping time, a duty cycle of nearly 100 % has been reported for an electrospray ionisation ion trap/TOFMS [54]. However, duty cycle is not an advantage because the duty cycle using the ion trap/TOFMS is restricted by the trapping efficiency of the quadrupole ion trap. As discussed in section 1.3.4.1, the highest estimates of trapping efficiency for externally generated ions are only 10% [44]. However, when compared with orthogonal TOFMS, the ion trap/TOFMS does offer advantages. The use of an ion trap enables selective ion storage and MS^n analyses to be carried out. Furthermore, the ion trap/TOFMS can also be used to study gas phase chemistry; some examples are given in Chapter 4. A disadvantage of using the ion trap/TOFMS compared with the orthogonal TOFMS is that the quadrupole ion trap imposes both a lower and upper m/z limit on the mass spectrometer as was described in section 1.3.4.1. Consequently, there is no longer a theoretically unlimited m/z range. Furthermore, more m/z discrimination is expected due to the decreased trapping efficiency at higher m/z values.

1.5 Literature Cited

1. Fenn, J. B.; Mann, M.; Meng, C. K.; Wong, S. F.; Whitehouse, C. M. *Mass Spectrom. Rev.* **1990**, *9*, 37.
2. Karas, M.; Hillenkamp, F. *Anal. Chem.* **1988**, *60*, 2299.
3. Zeleny, J. *Phys. Rev.* **1917**, *10*, 1.

4. Dole, M.; Mack, L. L.; Hines, R. L. *J. Chem. Phys.* **1968**, *49*, 2240.

5. Mack, L. L.; Kralik, P.; Rheude, A.; Dole, M. *J. Chem. Phys.* **1970**, *52*, 4977.

6. Yamashita, M.; Fenn, J. B. *J. Phys. Chem.* **1984**, *88*, 4451.

7. Alexsandrov, M. L.; Gall, L. N.; Krasnov, V. N.; Nikolaev, V. I.; Pavelenko, V. A.; Shkurov, V. A. *Dokl. Akad. Nauk SSSR* **1984**, *277*, 379.

8. Meng, C. K.; Mann, M.; Fenn, J. B. in *Proceedings of the 36th Annual Conference on Mass Spectrometry and Allied Topics*, San Francisco, CA June 5-10, 1988, p. 771.

9. Kebarle, P; Tang, L. *Anal. Chem.* **1993**, *65*, 972A.

10. Taylor, G. I. *Proc. R. Soc. London A* **1964**, *A280*, 383.

11. Lord Rayleigh *Philos. Mag.* **1882**, *14*, 184.

12. Schmelzeisen-Redeker, G.; Bütfering, L.; Röllgen, F. W. *Int. J. Mass Spectrom. Ion. Proc.* **1989**, *90*, 139.

13. Iribarne, J. V.; Thomson, B. A. *J. Chem. Phys.* **1976**, *64*, 2287.

14. Thomson, B. A.; Iribarne, J. V. *J. Chem. Phys.* **1979**, *71*, 4451.

15. McLuckey, S. A.; Van Berkel, G. J. *Int. J. Mass Spectrom. Ion Proc.* **1997**, *162*, ix.

16. Przybylski, M.; Glocker, M. O. *Agnew. Chem. Int. Ed. Engl.* **1996**, *35*, 806.

17. Caldecourt, V. J.; Zakett, D.; Tou, J. C. *Int. J. Mass. Spectrom. Ion Phys.* **1983**, *49*, 233.

18. Gelpí, E. *J. Chromatogr. A* **1995**, *703*, 59.

19. Smith, R. D.; Loo, J. A.; Edmonds, C. G.; Barinaga, C. J.; Udseth, H. R. *Anal. Chem.* **1990**, *62*, 882.

20. Bruins, A. P.; Covey, T. R.; Henion, J. D. *Anal. Chem.* **1987**, *59*, 2642.

21. Blakley, C. R.; McAdams, M. J.; Vestal, M. L. *J. Chromatog.* **1978**, *158*, 261.

22. Blakley, C. R.; Carmody, J. J.; Vestal, M. L. *J. Am. Chem. Soc.* **1980**, *102*, 5933.

23. Stephens, W. E. *Phys. Rev.* **1946**, *69*, 691.

24. Wiley, W. C.; McLaren, I. H. *Rev. Sci. Instrum.* **1955**, *26*, 1150.

25. *Time-of-Flight Mass Spectrometry;* Cotter, R. J., Ed. (American Chemical Society, Washington, DC, 1997, Chapter 2).

26. *Time-of-Flight Mass Spectrometry;* Cotter, R. J., Ed. (American Chemical Society, Washington, DC, 1997, Chapter 3).

27. Verentchikov, A. N.; Ens, W.; Standing, K. G. *Anal. Chem.* **1994**, *66*, 126-133.

28. Dole, M.; Cox, H. L., Jr.; Gieniec, J. *Polym. Prepr., Amer. Chem. Soc., Div. Polym. Chem.* **1971**, *12*, 790.

29. Yefchak, G. E.; Schultz, G. A.; Allison, J.; Enke, C. G.; Holland, J. F. *J Am. Soc. Mass Spectrom.* **1990**, *1*, 440.

30. Ma, C.; Michael, S. M.; Chien, M.; Zhu, J.; Lubman, D. M. *Rev. Sci. Instrum.* **1992**, *63*, 139.

31. Boyle, J. G.; Whitehouse, C. M. *Rapid Commun. Mass Spectrom.* **1991**, *5*, 400.

32. Dodonov, A. F.; Chernushevich, I. V.; Laiko, V. V. *International Mass Spectrometry Conference; Amsterdam,* 1991; Extended Abstracts, p. 153.

33. Boyle, J. G.; Whitehouse, C. M. *Anal. Chem.* **1992**, *64*, 2084-2089.

34. Mirgorodskaya, O. A.; Shevchenko, A. A.; Chernushevich, I. V.; Dodonov, A. F.; Miroshnikov, A. I. *Anal. Chem.* **1994**, *66*, 99.

35. Douglas, D. J.; French, J. B. *J. Am. Soc. Mass Spectrom.* **1992**, *3*, 398-408.

36. Krutchinsky, A. N.; Chernushevich, I. V.; Spicer, V.; Ens, W.; Standing, K. G. *Proceedings of the 43rd ASMS Conference on Mass Spectrometry and Allied Topics*; Atlanta, Georgia; May 21-26, 1995; p 126.

37. Bondarenko, R. V.; Macfarlane, R. D. *Int. J. Mass Spectrom. Ion Proc.* **1997**, *160*, 241.

38. Michael, S. M.; Chien, B. M.; Lubman, D. M. *Anal. Chem.* **1993**, *65*, 2614-2620.

39. March, R. E.; Hughes, R. J. *Quadrupole Storage Mass Spectrometry*, John Wiley & Sons, New York, 1989, Chapter 2.

40. Mathieu, E. *J. Math. Pure Appl. (J. Liouville)* **1868**, *13*, 137.

41. Major, F. G.; Dehmelt, H. G. *Phys. Rev.* **1968**, *170*, 91-107.

42. McLuckey, S. A.; Van Berkel, G. J.; Goeringer, D. E.; Glish, G. L. *Anal. Chem.* **1994**, *66*, 689A-696A.

43. Stafford, G. C., Jr.; Kelley, P. E.; Syka, J. E. P.; Reynolds, W. E.; Todd, J. F. J. *Int. J. Mass Spectrom. Ion Proc.* **1984**, *60*, 85.

44. Nourse, B. D.; Cooks, R. G. Anal. Chim. Acta 1990, 228, 1-21.

45. Todd, J. F. J. *Mass Spectrom. Rev.* **1991**, *10*, 3.

46. Louris, J. N.; Cooks, R. G.; Syka, J. E. P.; Kelley, P.E.; Stafford, G. C., Jr.; Todd, J. F. J. *Anal. Chem.* **1987**, *59*, 1677.

47. Morris, H. R.; Paxton, T.; Dell, A.; Langhorne, J.; Berg, M.; Bordoli, R .S.; Hoyes, J.; Bateman, R. H. *Rapid Commun Mass Spectrom.* **1996**, *10*, 889.

48. Shevchenko, A.; Chernushevich, I.; Ens, W.; Standing, K. G.; Thomson, B.; Wilm, M.; Mann, M. *Rapid Commun Mass Spectrom.* **1997**, *11*, 1015.

49. Bateman, R. H.; Green, M. R.; Scott, G. *Rapid Commun. Mass Spectrom.* **1995**, *9*,

1227.

50. Van Berkel, G. J.; Glish, G.; McLuckey, S. *Anal. Chem.* **1990**, *62*, 1284-1295.

51. McLuckey, S. A.; Van Berkel, G. J.; Goeringer, D. E.; Glish, G. L. *Anal. Chem.* **1994**, *66*, 737A-743A.

52. Kaiser, R. E., Jr.; Cooks, R. G.; Stafford, G. C., Jr.; Syka, J. E. P.; Hemberger, P. E. *Int. J. Mass Spectrom. Ion Proc.* **1991**, *106*, 79.

53. Schwartz, J. C.; Syka, J. E. P.; and Jardine, I. *J. Am. Soc. Mass Spectrom.* **1991**, *2*, 198.

54. Chien, B. M.; Michael, S. M.; Lubman, D. M. *Int. J. Mass Spectrom. Ion Proc.* **1994**, *131*, 149.

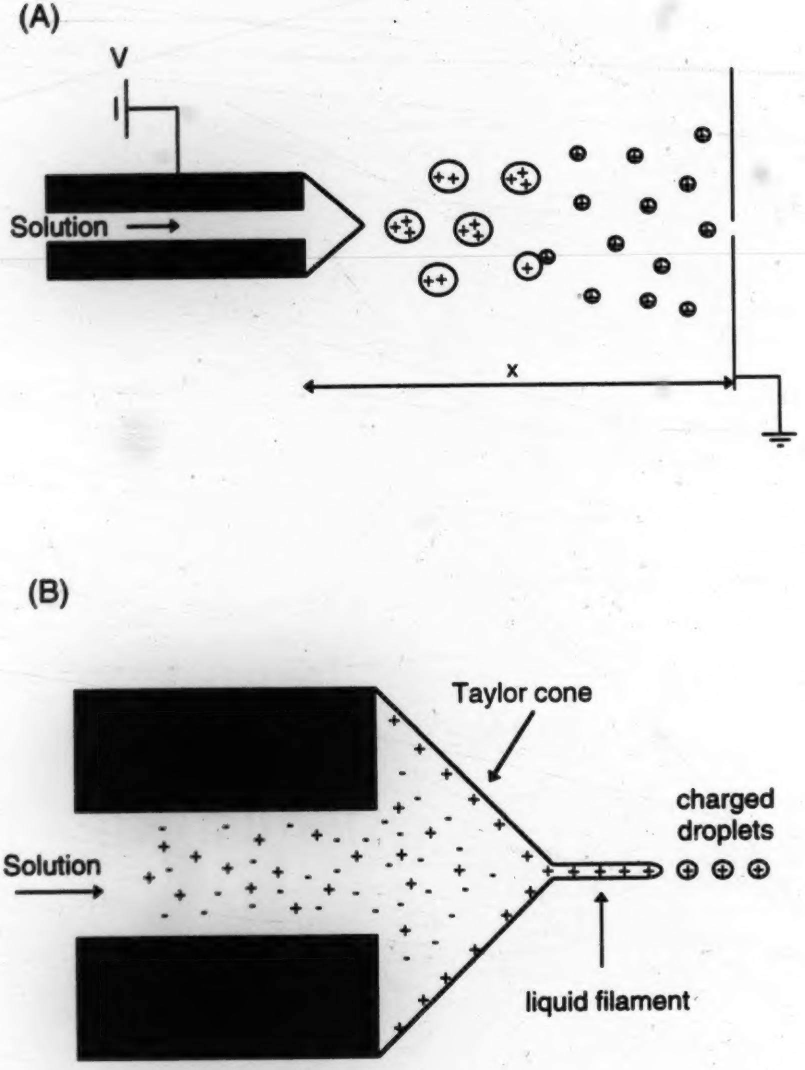
(A)
V
Solution
x
(B)
Taylor cone
charged droplets
Solution
liquid filament

Figure 1.1 (A) Schematic of the electrospray ionisation process. (B) Close up of the Taylor cone, liquid filament and droplet formation.

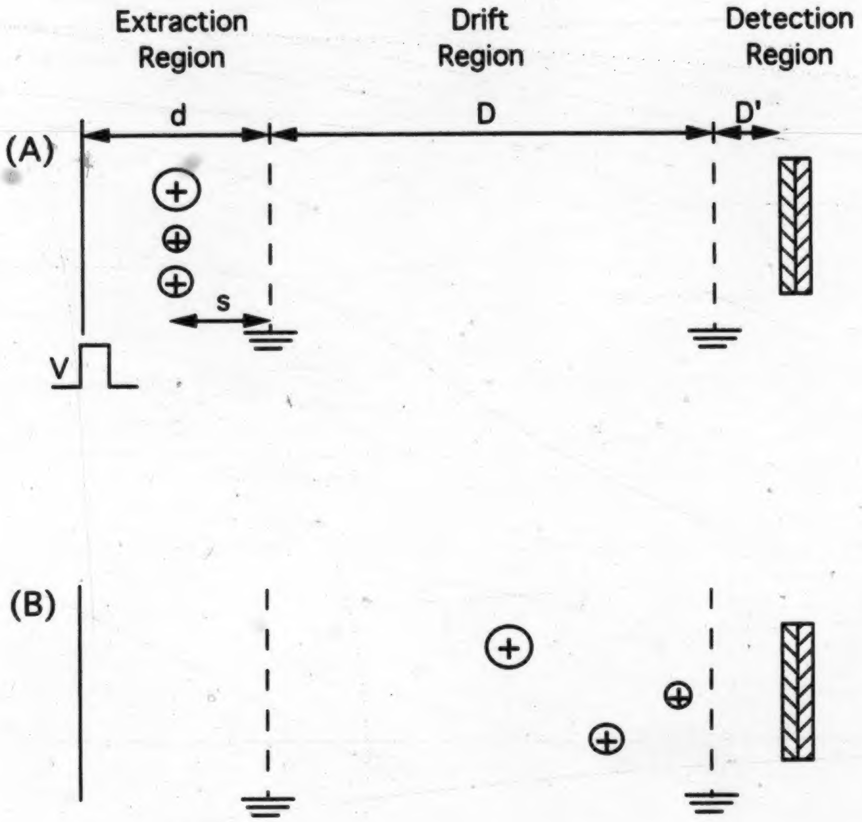
Extraction Region
Drift Region
Detection Region
d
D
D'
(A)
s
V
(B)

Figure 1.2 Schematic of a time-of-flight mass analyser. (A) At time zero, (B) during mass analysis. See text for details.

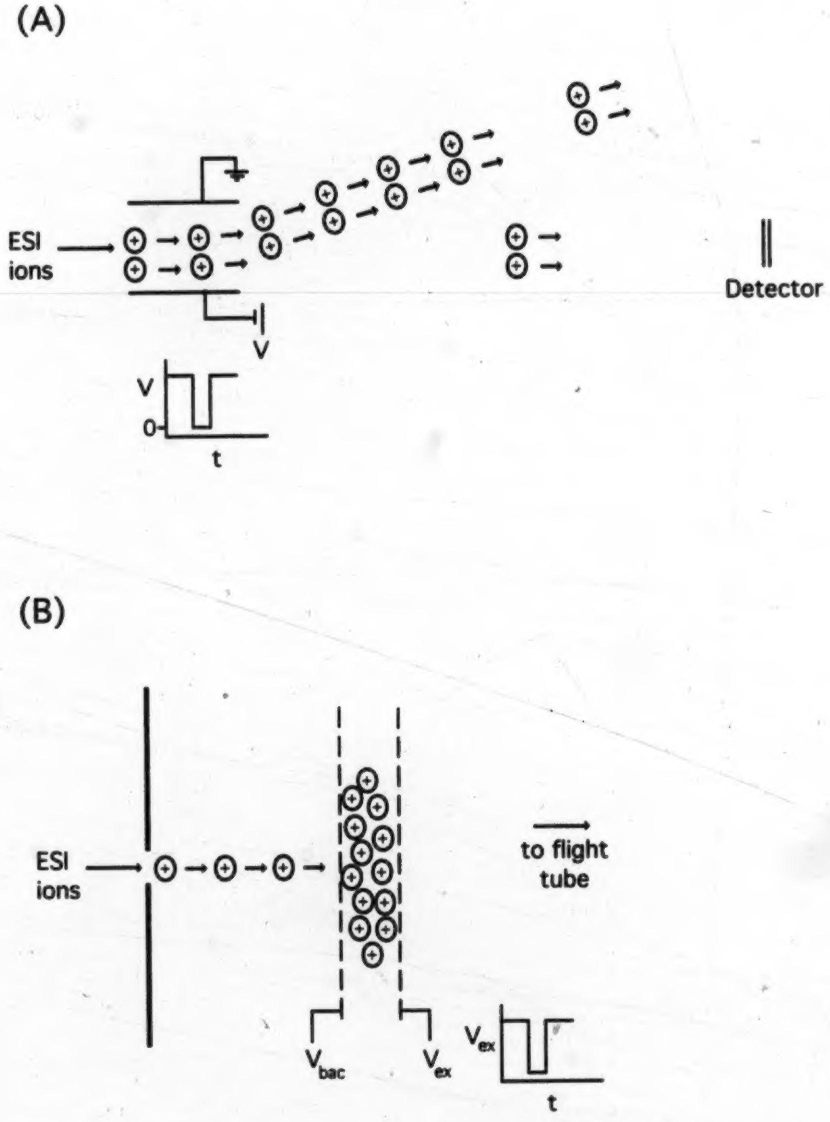
(A)
ESI ions
V
V
0
t
Detector
(B)
ESI ions
to flight tube
V_bac
V_ex
V_ex
t

Figure 1.3 Two of the earlier methods used to combine electrospray ionisation and TOFMS. (A) Beam deflection using the gate model and (B) "ion storage" TOF. See text for details.

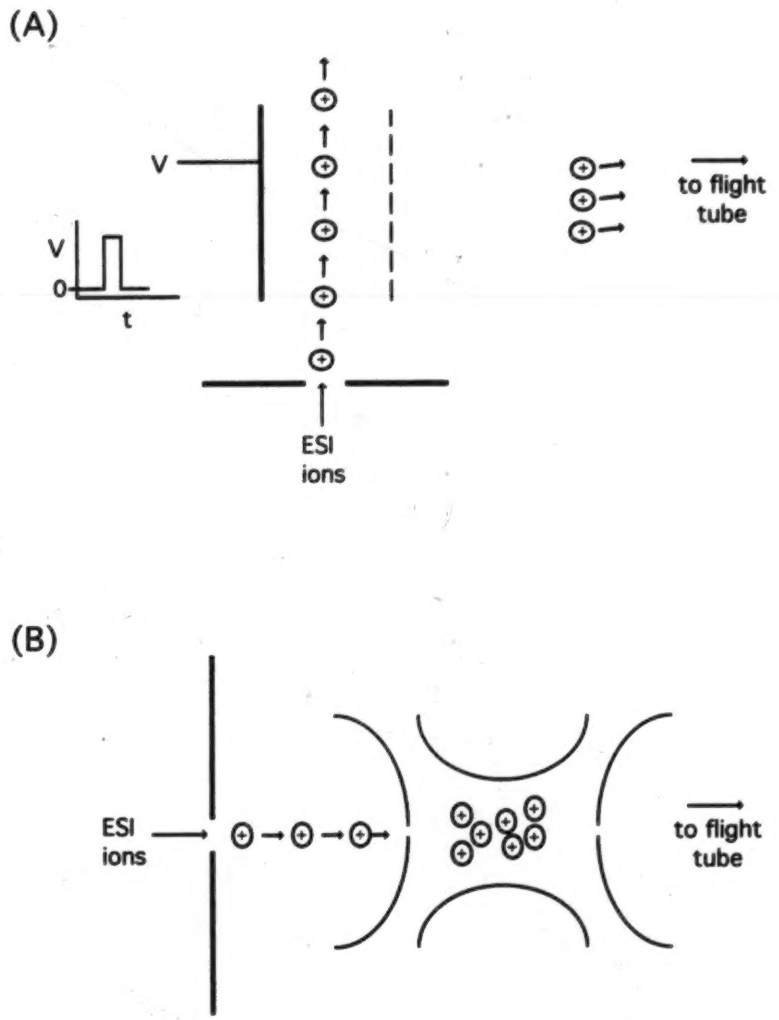
(A)
V
V
0
t
ESI
ions
to flight
tube
(B)
ESI
ions
to flight
tube

Figure 1.4 A schematic of two commonly used methods for coupling electrospray ionisation and TOF. (A) Orthogonal extraction and (B) ion trap/TOF. A description is given in the text.

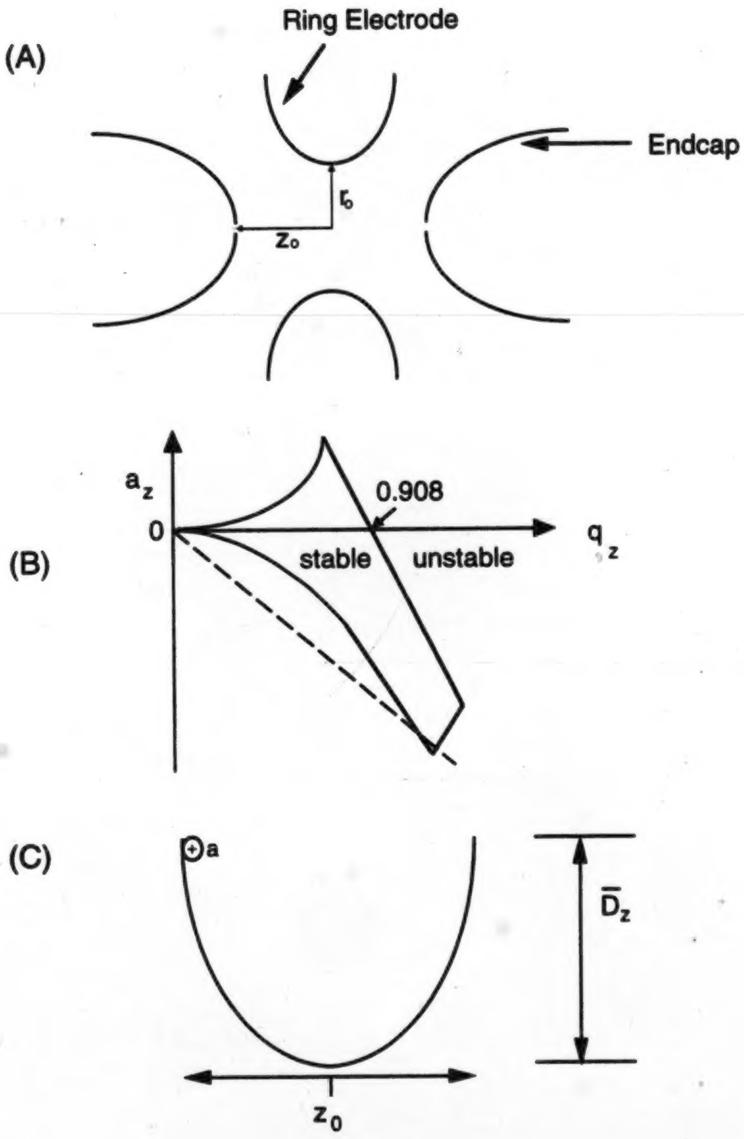
(A)
Ring Electrode
Endcap
r₀
z₀
(B)
a_z
0
0.908
q_z
stable
unstable
(C)
a
D̄_z
z₀

Figure 1.5 The quadrupole ion trap. (A) A schematic of the various components of the ion trap. (B) A part of the a versus q stability diagram. The dashed line indicates the mass-selective storage mode of operation. (C) A representation of the depth of the trapping well in the z-direction; point 'a' represents an ion entering the ion trap from an external source. See text for details.

Chapter 2

Development of Instrumentation for Atmospheric Pressure Ionisation/Time-of-Flight Mass Spectrometry

2.1 Introduction

The origins of atmospheric pressure ionisation (API) mass spectrometry date back to the work of Knewstubb and Sugden who studied the combustion chemistry of flames produced at atmospheric pressure using a magnetic deflection mass spectrometer in the late 1950's [1, 2]. In the 1960's, ions produced from atmospheric pressure sources, alpha particle radiation [3] and corona discharge [4], were studied using mass spectrometry. Horning et al. introduced API for biomedical analysis when they used a ^{63}Ni ionisation source to rapidly detect drugs in unpurified biological extracts [5,6]. A detailed review by Carroll et al. discusses the early developments of API [7], however, it is only recently that interest in API sources has greatly increased. The reason is largely due to the success of electrospray and ionspray for analysing large molecular weight proteins [8].

API sources are broadly divided into either gas phase or liquid phase ionisation [9]. Gas phase ionisation occurs through the same reaction pathways as chemical ionisation sources [9]. The most common atmospheric pressure chemical ionisation sources are electrons emitted by a ^{63}Ni foil and corona discharge [10]. Liquid phase ionisation transports analyte ions from solution to the gas phase without the addition of heat. Electrospray and ionspray, described in Chapter 1 [11], are two common examples of liquid phase ionisation.

In designing instrumentation for combining API sources with mass spectrometry, Bruins recognises two main problems [9]. The first is transporting ions from atmosphere into the vacuum system of the mass spectrometer. The second problem, cluster formation, is a result of the strong cooling of a mixture of gas and ions that occurs when expanding into vacuum.

2.1.1 Ion Transport and Cluster Formation

Gas expansion into a lower pressure region through a small orifice has been described qualitatively [12]. Gas molecules entering a low-pressure region through an orifice acquire high velocities. These molecules continue to move at the same speed and in the same direction (undergoing strong and rapid cooling) until they reach a certain point far away from the orifice (here the gas is being pumped away) where the gas molecules are moving at random. The transition from the region of directed motion (known as the silent zone) to the region where random movement occurs produces shock waves where ions and gas molecules undergo numerous collisions. Consequently, when designing an interface for an API source, the distance of the sampling plate from the orifice is a critical parameter as it is desirable to sample ions in the silent zone. The location of the Mach disk, χ_M, which represents the distance from the orifice where this transition occurs, is given by [12]:

$$\chi_M = 0.67 D_o (P_o/P_1)^{1/2} \tag{2.1}$$

Where D_o is the diameter of the orifice, P_o is atmospheric pressure, and P_1 is the downstream pressure in the lower pressure region.

Due to the strong and rapid cooling that occurs during expansion into the lower pressure region, condensation of polar neutrals (i.e., water or solvents) on the analyte ion results in the formation of cluster ions. Preventing the formation of cluster ions is achieved by continuously flushing the API source region with dry nitrogen gas [13]. Nitrogen gas flushes water and other neutrals away from the orifice while at the same time, due to its inability to form hydrogen bond bridges, it does not form cluster ions itself. Declustering is achieved between the nozzle and sampling plate (discussed below) using collision induced dissociation (CID) [4,14]. The ions in this region are accelerated causing collisions to occur with neutral gas molecules that are present. As the collision energy in this region is increased, not only is declustering achieved, but eventually covalent bonds are also ruptured leading to fragmentation of the analyte [15].

2.2 Experimental

An instrument was constructed at the University of Alberta for combining an API source with a time-of-flight mass spectrometer (TOFMS). This instrument was based on the orthogonal geometry described in Chapter 1 [16]. A discussion of the design and function of the various components of this instrument, as well as the motivation behind the design, is given.

2.2.1 Interface

Coupling an API source with a mass spectrometer is carried out using either a single-stage or a multiple-stage interface. The main advantage of using multiple-stage interfaces is that larger orifice sizes are used. This enables a larger gas throughput and also reduces the tendency of the orifice to plug [9]. A two-stage interface was constructed at the University of Alberta for the purpose of introducing externally generated ions into a TOFMS. After initial construction, testing and further optimization of the interface were carried out by maximizing ion current values obtained using a corona discharge ionisation source (see also section 2.2.4). A PAR model 135 electrometer (Princeton Applied Research, Princeton, NJ) was used to measure the current values. Corona discharge was used since it is a relatively simple API source to construct and it is also very stable. The interface has undergone several modifications since it was first constructed in 1993. A schematic of the two-stage interface in its present form, is shown in Figure 2.1.

The interface was constructed from stainless steel, its circular shell actually consists of two parts, x and y shown in the figure, 10.0 cm and 5.0 cm long, respectively. The outer diameter (OD) and wall thickness of the shell were 12.5 cm and 0.4 cm, respectively. The two shaded regions in the figure represent metal rings (1.2 cm thick) that were vacuum sealed to the shell using O-rings. These metal rings were used to isolate the various stages of the interface. A cylindrical tube, the nozzle support (5.4 cm long, 2.5 cm OD, and a wall thickness of 0.7 cm), was used to adjust the spacing between the nozzle and the sampling plate. A second stainless steel cylindrical tube (2.2 cm OD, 24.0 cm long, and a wall thickness of 2.0 mm) directly attached to the mechanical pumps that were used to evacuate the first stage. The interface was attached to the mass spectrometer using an assembly that enabled the position of the interface to be adjusted with respect to the acceleration region of the mass spectrometer. Teflon was used for electrically isolating various components of the interface. Two, four-pin feedthroughs were used to apply voltages to the various components of the interface.

The orifice sizes of both the nozzle and the sampling plate were optimized experimentally. Although skimmer cones have certain advantages [17], a thin flat steel disk (0.6 mm thick), similar to one used by Caldecourt [15], was used for the sampling plate in this interface. Flat steel disks were decided upon initially mainly because of their ease of machining in a reproducible manner compared with skimmer cones. Note that later on, several skimmer cones were also constructed at the University of Alberta for use with the interface. However, the results obtained using these cones were not significantly better than the results obtained with the flat plates, likely due to the difficulties in machining (i.e., rough edges).

The diameter of the nozzle orifice was set to 120 μm as this was experimentally the best trade off between allowing too many neutrals into the vacuum (resulting in high pressure), and maximizing ion current. At this time, the interface was modified (alteration of the nozzle support) to extend the sampling plate inside the Mach disk region (placed 4.1 mm away), as calculated by equation 2.1 to be ~ 4.9 mm. After a series of experiments, the diameter of the orifice of the sampling plate was set to 230 μm.

Two different designs for the ion optics were tested to determine which would provide better focussing of the ions as they entered the ion extraction region. The first design used a beam guide, based on the work by Boyle and Whitehouse [18]. The second method involved a set of focussing plates, similar to the set-up used by Whitehouse et al. [19]. A metal plate, connected to an electrometer, was placed 1 mm from the end of either focussing apparatus. The larger ion current was detected when the set of three focussing plates was used, consequently, this method of focussing was decided upon for the interface. The spacing between these circular plates (2.8 cm in diameter, 0.6 mm thick, and an opening of ~7 mm in the centre) was 4 mm.

2.2.2 Vacuum System and Orthogonal TOFMS

Figure 2.2 shows a schematic of the hardware that was constructed for the orthogonal linear TOFMS. The TOFMS consisted of two differentially pumped regions, the ion extraction region and the flight tube. The ion extraction region, contained in a 20 cm × 20 cm × 20 cm cubic stainless steel vacuum chamber, was modelled primarily based on the work by Standing and coworkers [20]. This region consisted of four plates that were 44 mm × 44 mm × 0.6 mm wide. With the exception of VA1, which was solid, all of the plates had 25 mm diameter circular holes in their centres that were covered by a stainless steel mesh (90% transmission). The spacings between the plates were as follows: VA1 and VA2 were 5 mm apart VA2 and VA3 were 5 mm apart, and VA3 and the acceleration grid were 20 mm apart. When VA1 and VA2, were set to ground potential, a continuous stream of ions from the interface filled the region between them. Due to the large negative voltage of the liner, ions could potentially leak out from the temporary ion storage region and into the flight tube before the extraction event. To prevent leakage, VA3 was set to a slightly positive voltage when VA1 and VA2 were grounded [20]. The ions were extracted from the space between VA1 and VA2 by simultaneously applying a positive voltage pulse to VA1 and a negative voltage pulse to VA3. An Einzel lens assembly (each of the three electrodes in the assembly was 25 mm long; the separation between plates was 2 mm) was placed after the acceleration grid to aid in focussing the ions in the flight tube. The initial kinetic energies of the ions as they entered the ion extraction region gave the ions a velocity component in the direction normal to the flight tube. A deflector plate [18] (5.0 cm long, 4.4 cm wide) was used in the instrument to compensate for this natural drift. The acceleration grid was the only opening between the two differentially pumped regions. Inside the flight tube was an electrically isolated mesh liner (26 mm in diameter, ~80 cm long) that extended from the acceleration grid to 5 mm in front of the first plate of a dual multichannel plate (MCP) detector (Galileo Electro-Optics Corp., Sturbridge, MA). Note that a reflectron is used to improve the mass resolution of a TOFMS [21]. However, ion losses in the ion mirror can become significant thereby reducing sensitivity, thus, a reflectron was not used in this instrument.

An important feature to the set-up was the ability to "float the detector." Under normal operating conditions, the maximum voltages applied to the plates of a dual MCP detector are -2.2 kV and -200 V (maximum voltage change across a dual MCP detector is 2 kV). Consequently, the voltage applied to the liner is limited to -2.2 kV and therefore the total accelerating voltage is also limited. If a larger voltage is applied to the liner than the detector, a defocussing of the ion beam in the detector region results. This defocussing is undesirable as it results in peak broadening and decreased sensitivity in the mass spectra. If the distance between the anode of the detector (grounded) and the second MCP plate is increased (normal separation distance is approximately 100 to 200 μm), this enables larger voltages to be applied to both MCP plates. With a separation distance of 2.0 mm, a voltage of -3 kV can be applied to the second MCP plate. Further increases in sensitivity might be possible with smaller separation distances. However, due to the possibility of high voltage arcing damaging the detector, smaller distances were not investigated. The modification greatly improved the sensitivity; this is shown in section 2.3.1 below. Note that an attempt was made to float the entire detector assembly, including the anode (without moving its position), however, this method was abandoned when mass spectral quality was reduced due to problems with impedance matching (detector ringing).

The ion extraction region was pumped by a 15-cm diffusion pump (~1100 L/s with a cold trap) and the flight tube was pumped by a 10-cm diffusion pump (~500 L/s with a cold trap). The interface was pumped by two Varian SD-450 (500 L/min) mechanical pumps. After 48 hours of operating the diffusion pumps, the pressures were ~27 Pa (interface region), $\sim 4 \times 10^{-4}$ Pa (extraction region), and $\sim 5 \times 10^{-5}$ Pa (flight tube).

2.2.3 Data Collection

At the end of the flight tube, the signal captured by the dual MCP detector was amplified using a 500 MHz (3dB), 20 dB amplifier (CLC 100, Comlinear Corporation). A LeCroy 9310M or 9350M digital oscilloscope was used to capture the signal. The major difference between the two oscilloscopes is the sampling rate. The maximum sampling rate of the 9350M oscilloscope is 1×10^9 samples/s, or a time resolution of 1 ns/pt, whereas the maximum sampling rate of the 9310M oscilloscope is 1×10^8 samples/s or a time resolution of 10 ns/pt. Mass spectra were continuously summed using the oscilloscope without selective averaging. Since the longest flight times were $< 50\ \mu$s, the maximum ion extraction rate was theoretically ~20 kHz. Due to electronic limitations in trying to store mass spectra at fast rates (i.e., the digital oscilloscope only sums mass spectra at a rate of approximately 13 Hz), extraction rates of less than one thousandth of this were used. Unless otherwise stated, the mass spectra presented in this chapter are representative of 150 ion extraction events. The final mass spectra were stored to an IBM 386 PC.

2.2.4 Ionisation Sources

Corona discharge and electrospray were the two ionisation sources used. The corona discharge source itself was a slightly modified sewing needle, 9 cm long and 1 mm wide, that was placed 3 mm in front of the nozzle orifice. The electrospray ionisation needle was constructed from two stainless steel capillaries. The first capillary (250 µm inner diameter (ID), 1.59 mm OD, and 10 cm long), was used only for mechanical support and to provide a means for electrical contact. A smaller capillary (100 µm ID, 225 µm OD, and ~ 1 cm long), which was the actual electrospray ionisation needle, was slid into the mechanical support until only ~3 mm of this capillary was exposed. The two capillaries were soldered together to fix this position and to prevent leakage of the analyte solution.

2.2.5 Sample Preparation

Tributylamine was purchased from Matheson, Coleman & Bell (East Rutherford, NJ). Kyotorphin, bradykinin and equine cytochrome c were all purchased from Sigma (St. Louis, MO) without further purification. Synthetic peptides are gifts from the Center of Excellence in Protein Engineering at the University of Alberta. Methanol was purchased from BDH Laboratories Inc. (Toronto, ON). The water was obtained from a NANOpure water system (Barnstead/Thermolyne). Trifluoroacetic acid was purchased from Caledon Laboratories (Georgetown, ON).

For studying analytes using corona discharge, first a small amount of the analyte was dissolved in water and placed into a sealed container. A low flow rate of N_2 (1 to 2 mL/min) was passed over the surface of the analyte solution and the analyte enriched N_2 flowed to within 5 mm of the corona discharge needle tip. For electrospray ionisation, analytes were dissolved in a solvent combination consisting of methanol, water and trifluoroacetic acid (TFA). Peptides were dissolved in 10% water, 90% methanol and 0.01% TFA (v/v) while proteins were dissolved in 50% water, 50% methanol and 0.1 to 1% TFA (v/v).

2.2.6 Operating Conditions

When the corona discharge source was used, the needle was positioned ~ 3 mm in front of the nozzle orifice, and a potential of between 3.0 and 3.4 kV was applied to the needle. The voltages applied to the nozzle and sampling plates were 100 - 150 V and 8 V, respectively. The first and third focussing plates were set to 15 V while the second was set to ~ -250 V.

When the electrospray ionisation source was used, the needle was positioned 10 to 12 mm from the nozzle (slightly off-axis), and a voltage of 3.4 to 4.4 kV was applied. An analyte solution was placed in a Hamilton syringe (gas tight # 1002) and a model 55-1111 syringe pump (Harvard Apparatus) was used to continuously deliver the solution to the electrospray needle tip at a flow rate of 1.5 μL/min. Nitrogen was passed into the region between the electrospray ionisation source and the nozzle at a flow rate of 1 to 1.6 L/min. The voltages applied to the nozzle and sampling plate ranged from 60 to 120 V and 6 to 45 V, respectively.

Independent of the type of ionisation source used, the extraction region and flight tube were operated as follows. During ion storage, VA1 and VA2 were grounded while VA3 was set to 18 V. During extraction, VA1 was pulsed to 230 V (50 μs duration) and VA3 was pulsed to −380 V (50 μs duration) simultaneously while VA2 remained at 0 V. Both high voltage pulse generators were developed at the University of Alberta. The positive pulse generator had a maximum output of +500 V and a rise time of 150 ns at this voltage, while the negative pulse generator had a maximum output of −380 V with a fall time of 125 ns at this voltage. The rise and fall times both decreased with decreasing pulse amplitude.

Unless otherwise noted, the acceleration grid as well as the first and third electrodes in the Einzel lens assembly were all operated at −4000 V. The voltages applied to the second electrode in the Einzel lens assembly and the deflector plate were −3950 to −4000 V and −3800 V to −3900 V, respectively. The voltage applied to the first plate of the dual MCP detector was −4900 V.

2.3 Results

2.3.1 Corona Discharge

Corona discharge was used as the ionisation source for initial optimization of the instrument. Figures 2.3 (A) and (B) show mass spectra of water clusters that illustrate the improvement that results from "floating the detector"; the inset represents an expanded view from m/z 210 to 310. Figure 2.3 (A) shows a mass spectrum obtained using the normal operating conditions for the dual MCP detector. Figure 2.3 (B) shows a dramatic increase in sensitivity that was observed when the voltages on both the detector and the liner were increased. The reason for this improvement is largely due to the increased energy with which the ions impact the multichannel plates. The detection probability of low mass ions is shown to increase as the acceleration potential increases [22]. Furthermore, for the acceleration potentials used in Figure 2.3, the increase in detection probability is expected to be greater for higher mass ions [22]. This is consistent with the figure as the improvement in the signal-to-noise (S/N) ratio for the smallest m/z ions is only a factor of between 2 and 7 comparing Figures 2.3 (A) and (B). However, for the larger m/z ions shown in the inset, the increase in the S/N ratio is more than an order of magnitude.

The corona discharge source was also briefly used to examine some analytes, including various amines. Figure 2.4 presents the results that were obtained using a solution of tributylamine. With this crude method of analyte introduction, the corresponding mass spectra are complicated by the presence of background water clusters. However, protonated molecule peaks are observed for both tributylamine and dibutylamine, the later is a decomposition product of tributylamine.

Water clusters were used to assist in optimizing the sensitivity and mass resolution of the instrument over a large m/z range. This was carried out by dramatically increasing (a factor of 10) the flow rate of nitrogen gas over water. By increasing the flow rate, the extent of the formation of water clusters (i.e., $(H_2O)_nH^+$) was also increased. Figure 2.5 shows a mass spectrum in which clusters with 'n' values of 1 to 62 were observed. The mass resolution values over this region (calculated using the full width of the peak at half maximum) were limited by the sampling rate of the digital oscilloscope. However, values of ~700 fwhm were typical for water clusters containing at least 35 water molecules. The mass resolution for the cluster with an 'n' value of 38, shown in the inset of Figure 2.5, is ~710 fwhm.

2.3.2 Electrospray ionisation

Once the interface and instrumental parameters had been optimized, an electrospray ionisation source was implemented. Compared with the set-up for the corona discharge source, one change was made. The line that was used to introduce sample vapour (1.6 mm ID tubing) was changed to a larger line (6.4 mm ID tubing) and used for the introduction of dry nitrogen gas necessary for desolvation. For the initial studies, an analyte solution was continuously introduced to the electrospray needle tip. Figure 2.6 shows mass spectra for two peptides, kyotorphin (amino acid sequence is YR) and bradykinin. The concentration of sample that was being continually infused was ~ 2 mM in Figure 2.6 (A), and ~0.4 mM in Figure 2.6 (B). In Figure 2.6 (A), both the singly and doubly charged molecular ion peaks are observed as well as a small peak corresponding to the dimer. Shown in the inset is an expanded view of the singly charged peak in which the isotope is resolved and the mass resolution of the monoisotopic peak is ~ 800 fwhm. In Figure 2.6 (B), the peak corresponding to the doubly charged molecular ion is almost exclusively observed. Shown in the inset is an expanded view of this peak with a mass resolution of ~ 600 fwhm.

Figures 2.7 (A) and (B) show typical mass spectra for two of the larger analytes, a synthetic peptide (Ac-DIKHLEAEYRFLDTEVKSLEDEIRALDADVKACES-Amide) and equine cytochrome c, respectively. The concentrations that were directly infused were 30 μM in Figure 2.7 (A) and 25 μM in Figure 2.7 (B). In both mass spectra, a distribution of multiply charged molecular ion peaks were observed. For equine cytochrome c, the quality of the mass spectrum is poor as the signal corresponding to the analyte is barely discernable from the background noise. Note that species larger than equine cytochrome c were not observed using the orthogonal TOFMS.

2.3.3 Limitations

The major problem with this orthogonal TOFMS was the lack of sensitivity. A major cause of this problem was that the data acquisition system was far too slow thereby resulting in a poor duty cycle for the instrument. Since maximizing sensitivity was the most important consideration in the development of this instrument, a low duty cycle was unacceptable. Another problem with the instrument was that a large deflection voltage was required. At the time of this work, deflection voltages were shown to drastically reduce the mass resolution achievable with orthogonal extraction instruments [23]. Mass resolution is reduced because the flight paths of the ions with the same m/z values become variable when a deflection voltage is used (i.e., some ions are deflected more than others). In an attempt to overcome this problem, a flexible bellows was used to replace part of the flight tube. This enabled the angle of the flight tube to be changed and theoretically allowed for the natural drift of the ions in direction perpendicular to the flight tube without the application of a deflection voltage. When compensating for the natural drift of the ions in this manner, the mass resolution is expected to vastly improve. However when the bellows was used with this instrument, only angles less than 6° were used because angles larger than 6° decreased the signal intensity even further. With these small angles, a deflection voltage was still required, consequently, the optimal mass resolution was still being limited by the deflector plate.

Due to the many difficulties, the most important of which being the lack of sensitivity due to the slow data acquisition system, work with the orthogonal TOFMS was terminated.

However, the problems associated with this instrument are NOT representative of orthogonal TOFMS instruments in general. Furthermore, at the time when this data was collected, both the instrumental parameters and the solution chemistry were not optimized. In terms of instrumental parameters, besides the slow speed of the data collection system, their was a problem related to the kinetic energy of the ions entering the ion extraction region. The interface parameters were not optimized in the aforementioned experiments, and in retrospect, the energies of ions entering this region were far too large. This point is illustrated by the relatively large deflection voltages that were required in comparison with other orthogonal instruments that used deflection plates [18]. In the time since this configuration was used, several changes have been made to both the instrumental parameters and the solution chemistry. With these changes, an improvement in the performance of the orthogonal configuration would be expected.

Although at the time it was thought that the performance of the instrument in the orthogonal configuration could be significant improved, it was decided to investigate a different type of configuration for coupling electrospray and TOFMS. This combination uses an ion trap as a means to temporarily store the ions as was discussed in Chapter 1. A main reason for switching the current instrument to this type of instrument was that sensitivity was expected to improve for several reasons. Most important, the requirements of the data acquisition system for this type of instrument were compatible with the data acquisition system currently being used. Thus, the duty cycle with this configuration is expected to dramatically improve. Furthermore, the ion trap/TOFMS uses a buffer gas to slow down the ions, therefore, detection of ions with large kinetic energies should be facilitated with this system. Also, improvements in mass resolution are expected since a deflection plate is no longer required as ion introduction is on-axis to the flight tube. In addition, there were other advantages of using an ion trap such as the ability to carry out selective ion monitoring as well as perform tandem mass spectrometry. Consequently, the instrument was modified for this configuration as is described in the next chapter.

2.4 Literature Cited

1. Knewstubb, P. F.; Sugden, T. M. *Nature* **1958**, *181*, 474.
2. Knewstubb, P. F.; Sugden, T. M. *Nature* **1958**, *181*, 1261.
3. Kebarle, P.; Hogg, A. M. *J. Chem. Phys.* **1965**, *42*, 668.
4. Shahin, M. M. *J. Chem. Phys.* **1966**, *45*, 2600.
5. Horning, E. C.; Horning, M. G.; Carroll; D. I., Dzidic, I.; Stillwell, R. N. *Anal. Chem.* **1973**, *45*, 936.
6. Carroll, D. I.; Dzidic, I.; Stillwell, R. N.; Horning, M. G.; Horning, E. C. *Anal. Chem.* **1974**, *46*, 706.
7. Carroll, D. I.; Dzidic, I.; Horning, E. C.; Stillwell, R. N. *Appl. Spectrosc. Rev.* **1981**, *17*, 337.
8. Fenn, J. B.; Mann, M.; Meng, C. K.; Wong, S. F.; Whitehouse, C. M. *Science* **1989**, *246*, 64.
9. Bruins, A. P. *Mass Spectrom. Rev.* **1991**, *10*, 53.
10. Dzidic, I.; Carroll, D. I.; Stillwell, R. N.; Horning, E. C. *Anal. Chem.* **1976**, *48*, 1763.

11. Kebarle, P.; Tang, L. *Anal. Chem.* **1993**, *65*, 972A.

12. Campargue, R. *J., Phys. Chem.* **1984**, *88*, 4466.

13. see for example, Yamashita, M.; Fenn, J. B. *J. Phys. Chem.* **1984**, *88*, 4451.

14. Kambara, H.; Kanomata, I. *Anal. Chem.* **1977**, *49*, 270.

15. Caldecourt, V. J.; Zakett, D.; Tou, J. C. *Int. J. Mass. Spectrom. Ion Phys.* **1983**, *49*, 233.

16. Dodonov, A. F.; Chernushevich, I. V.; Laiko, V. V. *In International Mass Spectrometry Conference; Amsterdam,* 1991; Extended Abstracts, p. 153.

17. Anderson, J. B.; Andres, R. P.; Fenn, J. B. *Molecular Beams*; Ross, J., Ed. (Interscience Publishers, New York, 1966, chapter 8).

18. Boyle, J. G.; Whitehouse, C. M. *Anal. Chem.* **1992**, *64*, 2084.

19. Whitehouse, C. M.; Dreyer, R. N.; Yamashita, M.; Fenn, J. B. *Anal. Chem.* **1985**, *57*, 675.

20. Verentchikov, A. N.; Ens, W.; Standing, K. G. *Anal. Chem.* **1994**, *66*, 126.

21. see for example, *Time-of-Flight Mass Spectrometry;* Cotter, R. J., Ed. (American Chemical Society, Washington, DC, 1997, chapter 3).

22. Geno, P.W.; Macfarlane, R. D. *Int. J. Mass Spectrom. Ion Phys.* **1989**, *49*, 233.

23. Guilhaus, M. *J. Am. Soc. Mass Spectrom.* **1994**, *5*, 588.

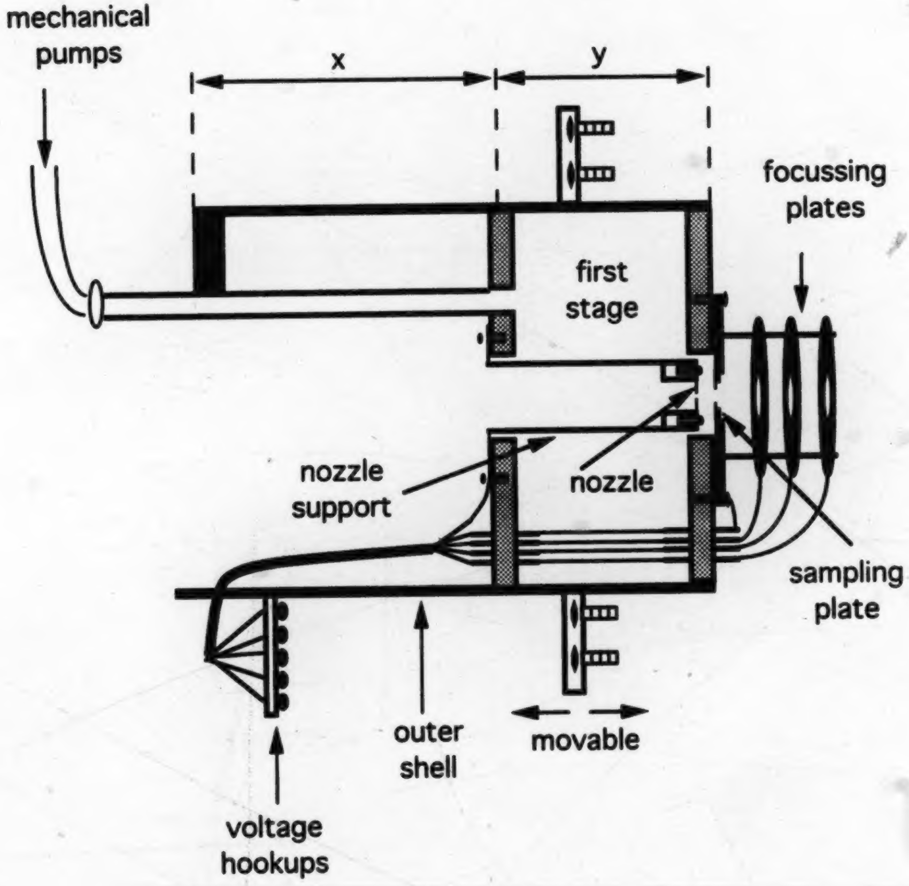
mechanical pumps
x
y
focussing plates
first stage
nozzle support
nozzle
sampling plate
outer shell
movable
voltage hookups

Figure 2.1 Schematic of the two-stage interface constructed at the University of Alberta. Drawing is not to scale, dimensions are given in the text.

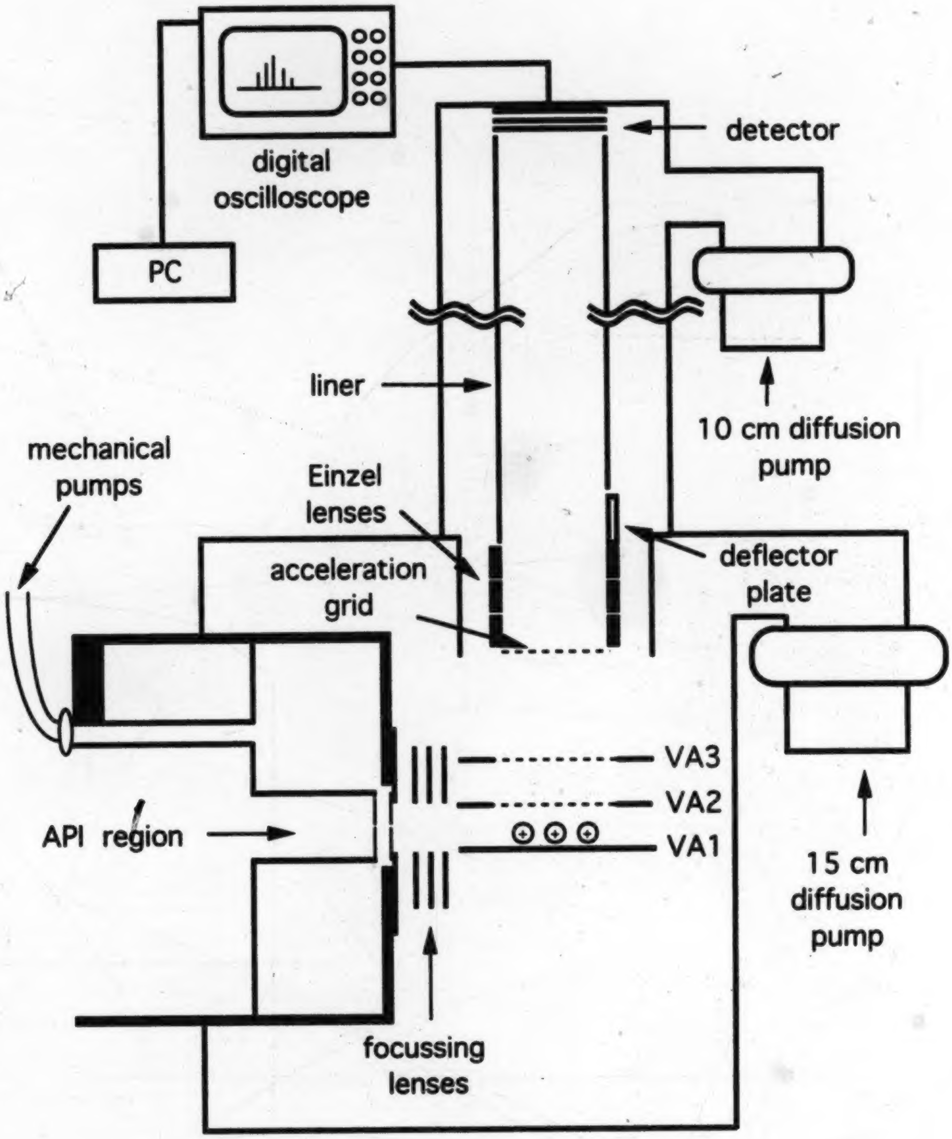
digital oscilloscope
PC
detector
liner
10 cm diffusion pump
mechanical pumps
Einzel lenses
acceleration grid
deflector plate
VA3
VA2
VA1
API region
15 cm diffusion pump
focussing lenses

Figure 2.2 Schematic of the electrospray ionisation/linear TOFMS in the orthogonal configuration. Drawing is not to scale, a description of the instrument is given in the text.

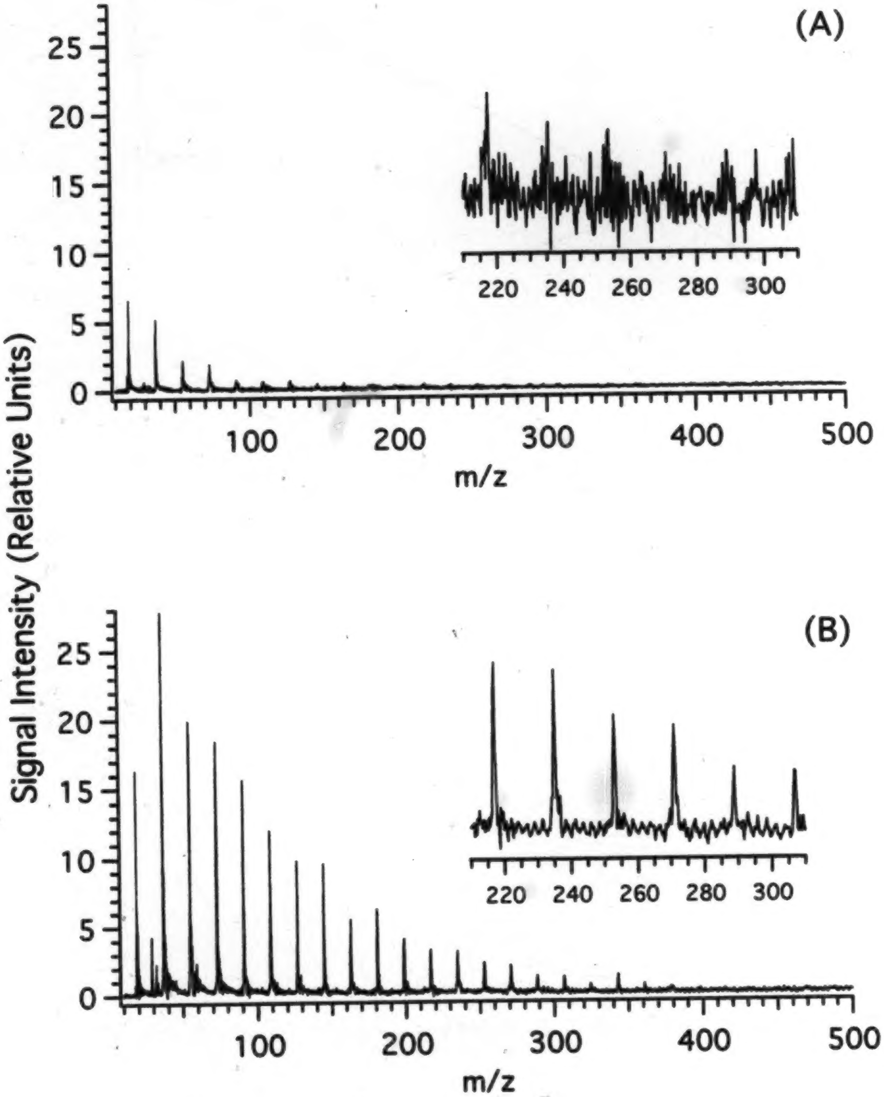

Figure 2.3 The effect of floating the detector on the quality of the mass spectra for background water clusters. (A) Normal MCP operation, detector voltage = −2170 V, liner = −2100 V. (B) Detector voltage = −4800 V, liner= −4000 V.

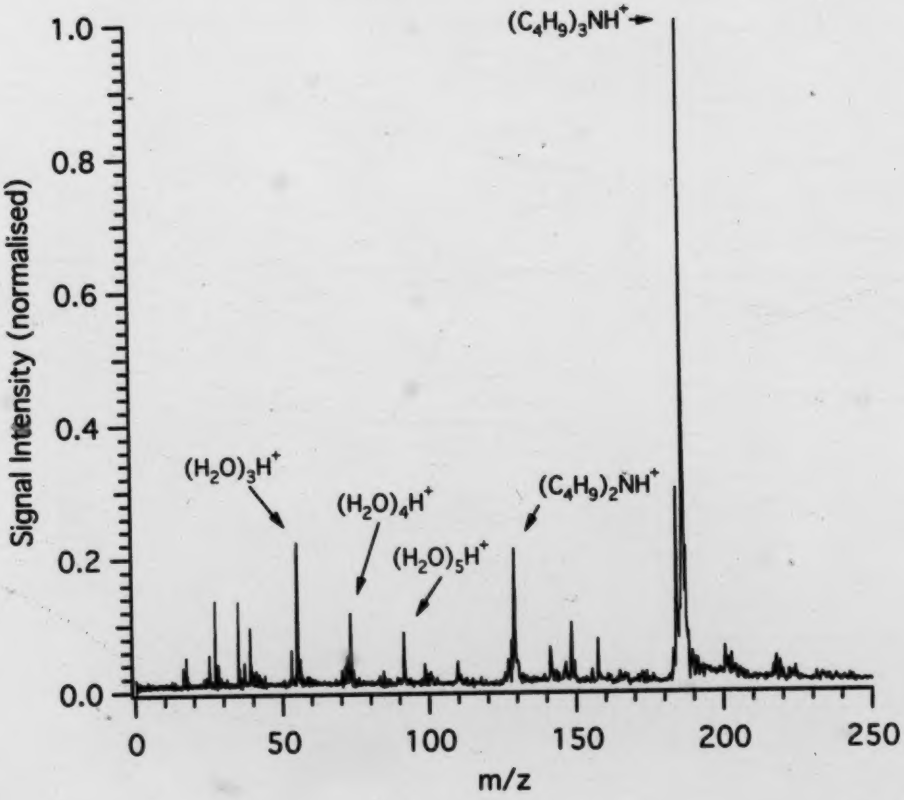

Figure 2.4 Mass spectrum of tributylamine obtained using a corona discharge source. Operating conditions are given in the text.

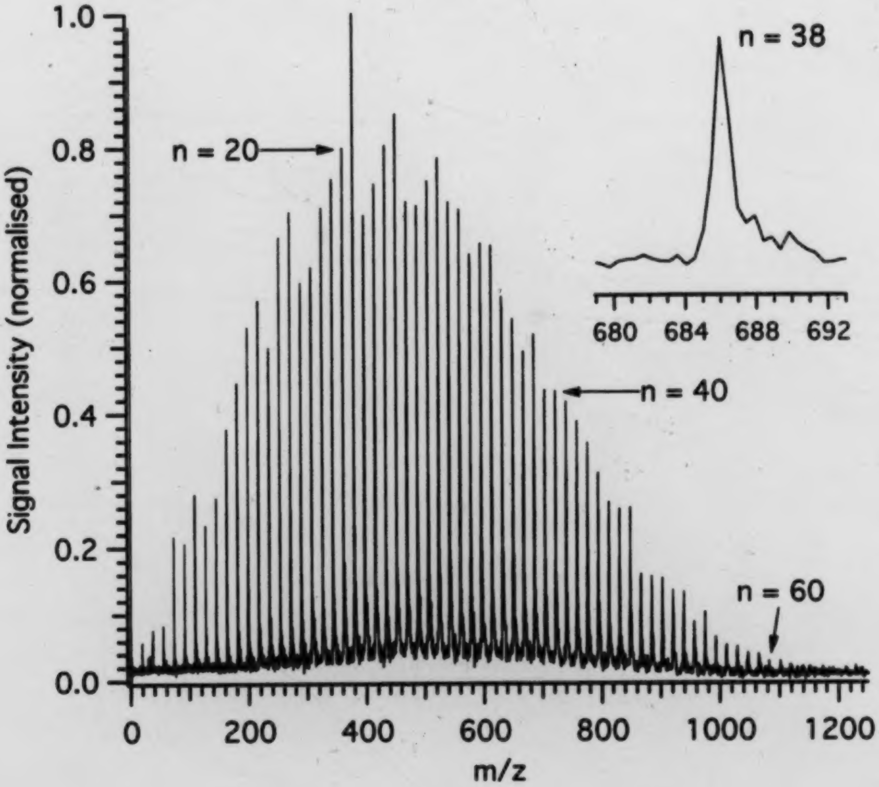

Figure 2.5 Corona discharge mass spectrum obtained from water vapour. The result was the extensive formation of $(H_2O)_nH^+$ clusters with n = 1 to 62 observed. Shown in the inset is the expanded view of the n = 38 water cluster with a mass resolution of ~ 710 fwhm.

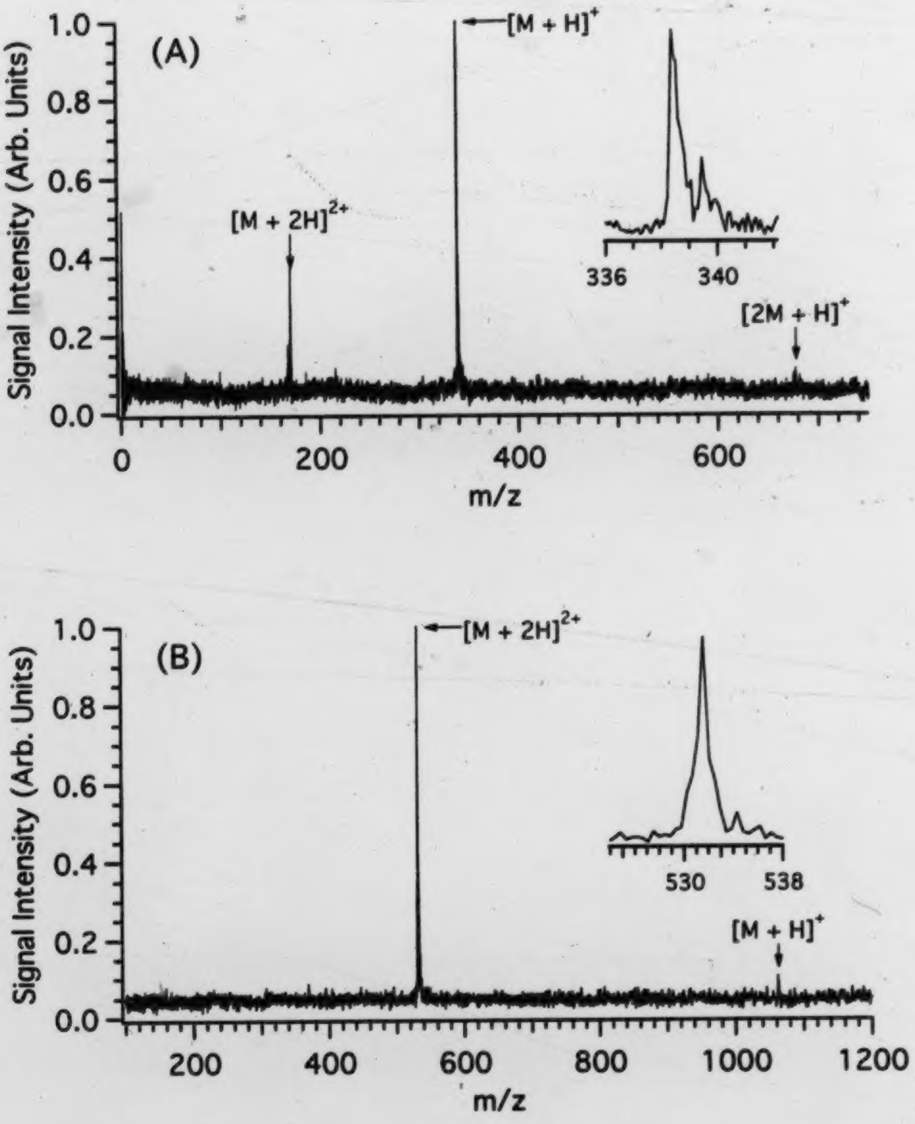

Figure 2.6 Electrospray ionisation mass spectra of (A) kyotorphin (YR) with isotopic resolution of the $[M + H]^+$ peak (inset) and (B) bradykinin with mass resolution of ~ 600 fwhm for the $[M + 2H]^{2+}$ peak (inset).

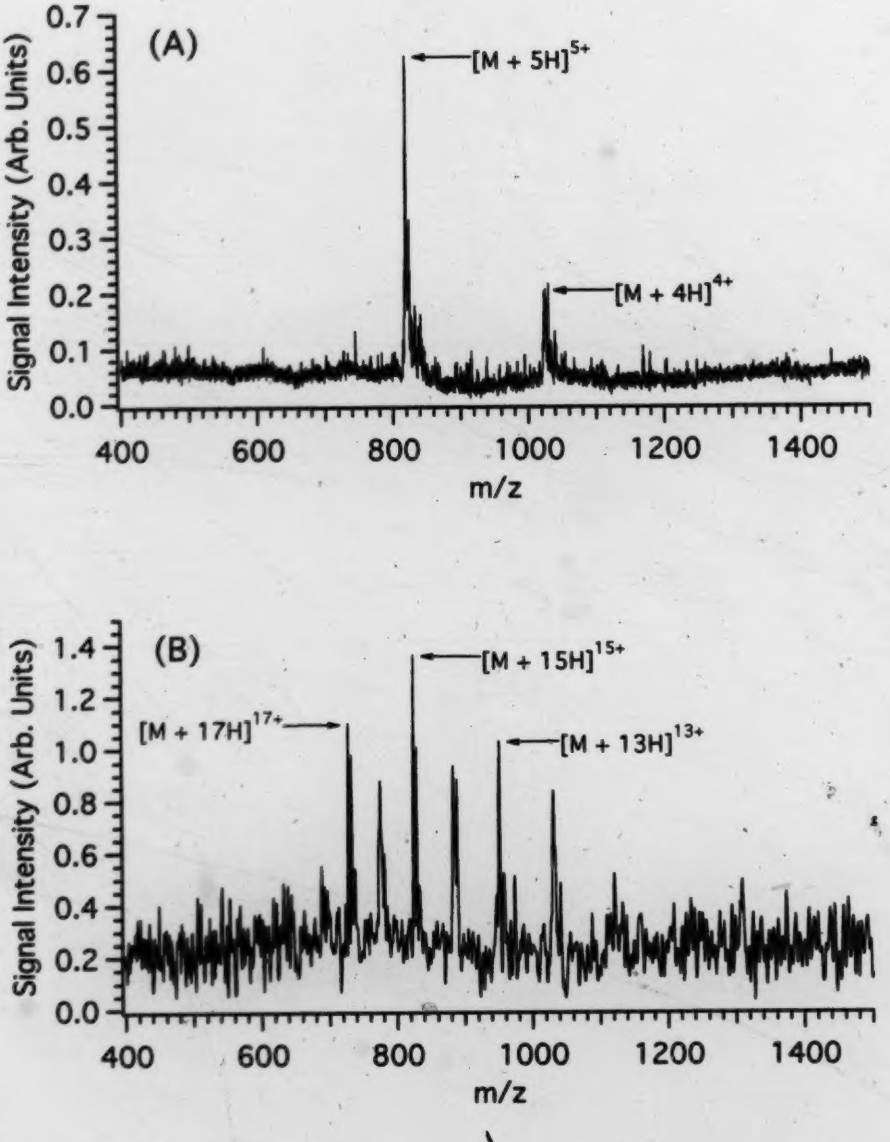

Figure 2.7 Electrospray ionisation mass spectra of (A) a synthetic peptide (Ac-DIKHLEAEYRFLDTEVKSLEDEIRALDADVKACES-Amide) and (B) equine cytochrome c. Operating conditions are given in the text.

Chapter 3

Development of an Electrospray Ionisation Ion Trap/Linear Time-of-Flight Mass Spectrometer for Micro-Column Liquid Chromatography Detection[a]

3.1 Introduction

Electrospray ionisation has become an increasingly important technique for molecular ion generation in mass spectrometry [1,2]. Electrospray ionisation is particularly applicable to the analysis of polar and ionic species, including peptides and proteins [2]. Separation techniques, such as liquid chromatography (LC), are readily combined with electrospray ionisation for on-line chemical identification and structural analysis [3]. Combining electrospray ionisation with a time-of-flight mass spectrometer (TOFMS) offers several advantages [4]. These advantages include the speed of mass analysis, sensitivity, and a theoretically unlimited mass-to-charge ratio detection range. Speed of analysis is especially important for fast separation techniques, such as capillary electrophoresis, where the peak widths during elution of the analyte are short [5]. Several methods of coupling electrospray ionisation to a TOFMS were presented in Chapter 1 [6-11].

---

[a] A form of this chapter has been published as: R. W. Purves, L. Li "Development of an Ion Trap/Linear Time-of-Flight Mass Spectrometer with Electrospray Ionization for Micro-Column Liquid Chromatography Detection", *J. Microcolumn Separations* **1995**, 7, 603.

In this chapter, the use of an electrospray ionisation ion trap/TOFMS for on-line analysis of biochemical samples is explored. The idea of using an ion trap for converting a continuous electrospray ion beam into an ion packet for TOF mass analysis was developed by Lubman and coworkers [9,12-14]. In brief, electrosprayed ions enter the ion trap where a rf voltage is applied to the ring electrode of the ion trap to store and accumulate the ions. After a predetermined trapping time, the rf voltage is shut off and a high voltage pulse is applied to the exit endcap electrode to extract the ions into the flight tube for mass analysis. Note that to correct for the initial kinetic energy spread of the electrosprayed ions, and thereby improve mass resolution, a reflectron TOFMS is commonly used instead of a linear TOFMS [9-11]. However, the use of a reflectron can also result in reduced ion transmission efficiency due to losses in the ion mirror. Consequently, to maximize sensitivity, a linear TOFMS is used in this study. The emphasis of this initial study is to determine the capability of this system, regarding variables such as detection limits and mass resolution, using flow injection analyses. On-line micro-column LC detection is also demonstrated for a simple mixture of proteins.

3.2 Experimental

3.2.1 Ion Trap/Linear TOFMS

Figure 3.1 shows a schematic of the electrospray ionisation ion trap/linear TOFMS.

Except for the ion trap, all hardware was designed and constructed at the University of Alberta. The ion trap and its power supply were purchased from R. M. Jordan Co. (Grass Valley, CA). The internal radius of the ring electrode was 1.0 cm and both endcap electrodes had a 3 mm opening in the centre. The opening of the exit endcap was covered by a 90% transmission stainless steel grid. A circular ceramic ring (47 mm ID, 9.4 mm wide, and 1 mm thick) was placed between each endcap and the ring electrode to enclose the ion trap. A small circular hole in one of these ceramic rings (1.6 mm) allowed buffer gas (helium) to be added inside the ion trap. The exit endcap was separated from the acceleration grid (25 mm opening) by 5 mm. The design and operation of the TOFMS were described in Chapter 2. In this configuration, two changes were made to the design of the TOFMS. The ion trap was used in place of the three plates in the ion extraction region and the orientation of the interface with respect to the flight tube was changed by 90°. The distance between the front plate of the ion focussing plates and the opening of the entrance endcap was fixed at 4 mm. Note that the length of the flight tube was changed to 87 cm for this, and future studies.

Although vacuum hardware was unchanged from the apparatus described in Chapter 2, the pressure in the two high vacuum regions varied as a function of the amount of buffer gas introduced into the ion trap. Consequently, the pressure in the ion extraction region ranged from ~4 - 7 × 10^{-4} Pa, while the pressure in the flight tube ranged from ~0.5 - 1.2 × 10^{-4} Pa.

The electrospray needle was positioned slightly off-axis to maximize the electrospray current [15]. The spraying was carried out in a region that was being constantly flushed with heated (~ 80 °C) dry nitrogen at a rate of ~ 4 L/min. The voltage applied to the needle tip was between 2.8 and 4.2 kV and it was optimized for each particular solvent mixture. Typical voltages applied to the nozzle and sampling plate ranged from 20 - 75 V, and 1.0 - 7.0 V, respectively. The first and third focussing plates were operated at 0 V, while the second focussing plate was varied from −30 to −150 V.

3.2.2 Ion Trap Operation and Ion Extraction.

A timing diagram for one ion extraction event is shown in Figure 3.2. Ions were trapped by applying a rf voltage to the ring electrode of the ion trap while the two endcap electrodes were operated at ground potential. The rf frequency was fixed at 765 kHz and the rf voltage was optimized for each sample (1000 V_{p-p} to 2000 V_{p-p}). After accumulating the ions for a specific time (~100 ms was used unless otherwise noted), the rf voltage was turned off. A short delay time (1.2 μs) between shutting off the rf voltage and extracting the ions enabled the rf voltage to decay. Ions were extracted into the flight tube by applying a voltage pulse (−500 V for 30 μs) to the exit endcap. Before the start of the next ion extraction event, approximately 0.5 ms were required for the rf voltage to recover to its trapping potential.

The negative high voltage pulse generator was developed at the University of Alberta and had a fall time of 150 ns at −500 V. The acceleration grid and mesh liner were operated at −3500 V. Post acceleration of the ions was achieved by applying −4100 V to the first plate of the dual MCP detector. Note that a protection circuit was placed after the detector and before the amplifier to prevent high voltage arcs from damaging the amplifier and digital oscilloscope. The design and operation of this circuit are described in Appendix A.

3.2.3 Data Collection and Analysis.

Data collection was previously described in Chapter 2. For the purposes of this study, the mass spectra were stored directly from the digital oscilloscope to a PC using a data acquisition system that was developed at the University of Alberta [16]. Flow injection profiles were constructed in the following manner. First, the analyte was injected and simultaneously the software started to collect mass spectra at a given data acquisition rate (i.e., 10 spectra/s). A small mass range, corresponding to where the analyte was observed in the mass spectrum, was selected for analysis. For each mass spectrum collected during an injection, the total peak area of this mass range was calculated. The contribution to the total peak area from the chemical background noise, which was calculated using the mass spectra preceding elution of the analyte, was subtracted from each of these total peak area measurements. The flow injection profile was a plot of this corrected peak area measurement as a function of time.

3.2.4 Sample Injections.

Injections were carried out both with and without a LC column present. Two different injectors were used, a Rheodyne model 7520 injector (Chromatographic Specialties Inc., Brockville, ON) that had a sample loop size of 0.5 μL, and a Valco model C14W injector (Chromatographic Specialties) that had a sample loop size of 60 nL. For all of the injections, a model 55-1111 Harvard Apparatus syringe pump (South Natick, MA) was used to deliver the solvent at a flow rate of 4 μL/min. For the flow injection analyses (i.e., no column present), one end of a piece of fused silica capillary tubing (100 μm ID × 360 μm × 15 cm long; Polymicro Technologies Inc., Phoenix, AZ) was connected to the injector. The other end of the capillary tubing was attached to the electrospray needle using a Valco zero dead volume connector. For actual separations, a Fusica C_{18}, 320 μm ID × 5 cm micro-column (spherical particles, 3 μm; LC Packings, San Francisco, CA), was connected directly to the sample injector. A small piece of capillary tubing (100μm ID × 360 μm × 10 cm) extended from the end of this micro-column and was attached to the electrospray needle using a Valco zero dead volume connector. To obtain a UV chromatogram, one end of a piece of capillary tubing (100 μm ID × 360 μm OD × 20 cm) was connected to the outlet of the micro-column. The other end of the capillary tubing was positioned into a holder for detection using a 214 nm UV detector (Waters Quanta 4000 capillary electrophoresis). At a point 4 cm from the end of the capillary, a 1 cm portion of the polyimide coating was burnt away. This produced a clear quartz surface for the UV radiation to pass through.

3.2.5 Chemicals and Solutions.

Bradykinin was electrosprayed in a solution containing 90% methanol, 10% water and 0.01 % TFA while the protein samples were electrosprayed in 20 - 45% acetonitrile, 55 - 80% water and 0.1% TFA. The solvent combination used for separations with the column was an isocratic mixture of 57% water, 43% acetonitrile and 0.1% TFA.

3.3 Results and Discussion

3.3.1 Evaluation of Linear TOFMS

The first study carried out was to evaluate the mass resolution of the instrument since a potential concern of using electrospray ionisation with linear TOFMS is the relatively low mass resolution values compared with reflectron systems. Figures 3.3 (A) and (B) show the mass spectra of two proteins, equine cytochrome c and equine apomyoglobin, obtained using the ion trap/linear TOFMS. In each case, 6 pmol of analyte were injected and during elution, a mass spectrum representing a continuous average of 50 ion extraction events was collected. An expanded view of the most intense peak in each mass spectrum is shown in the inset. Figure 3.3 (A) shows a mass spectrum of equine cytochrome c in which the peak width and flight time of the $[M + 16H]^{16+}$ peak are 15.9 ns and 29.31 μs, respectively. Consequently, the mass resolution of this peak is 920 fwhm. The mass resolution of the $[M + 22H]^{22+}$ peak in the mass spectrum of equine apomyoglobin, shown in Figure 3.3 (B), is 750 fwhm. The mass resolution values of the other peaks in the mass spectra are slightly less, however, most of these peaks still have mass resolution values that are greater than 600 fwhm. Several experimental parameters affected the mass resolution values obtained using the ion trap/linear TOFMS, these are investigated in detail in Chapter 5. The mass resolution is significantly improved compared with previous optimal mass resolution values of 300 to 500 fwhm that were obtained using electrospray ionisation and linear TOF instruments [8,11]. Note that the optimal mass resolution that is obtainable for these proteins when using a TOF is effectively limited by the isotopic distribution of the protein. For example, the mass resolution of equine cytochrome c, based on the isotopic distribution, is calculated to be ~ 1500 fwhm. For these samples, only a relatively small enhancement in mass resolution is achieved when using a reflectron compared with this linear system. This point is further elaborated on in the summary at the end of this chapter.

3.3.2 Detection Limits

With multiple ion detection and high ion transmission, a TOFMS is expected to provide high sensitivity. A preliminary study of the detection limits of the instrument was carried out using bradykinin (MW = 1061.2). Figure 3.4 shows flow injection profiles, calculated using the $[M + 2H]^{2+}$ peak (mass range was from 529.0 u to 534.0 u), for four injections of bradykinin ranging from 75 fmol to 3 pmol. The flow injection profiles were smoothed using a Savitzky-Golay 2nd order algorithm (15 points). The corresponding mass spectra, obtained during elution of bradykinin, are presented in Figure 3.5. For the injection of 75 fmol, Figure 3.5 (D), the doubly charged molecular ion peak has a signal to background noise (S/N) ratio of approximately 8. The singly charged peak was not observed in Figure 3.5 as the conditions were optimized to favour the detection of the doubly charged species.

A major factor affecting the detection limit is the chemical background noise. Many background ions at low mass-to-charge ratio values observed in Figure 3.5 are a consequence of the solvent mixture being used. The noisy baseline is largely due to inadequately desolvated species that contain several charges and various numbers of solvent molecules and also impurities that are present in the samples or solvents. The level of the background noise in Figure 3.5 (D) is approximately 4 mV_{p-p}. The contribution by the chemical background noise to the total noise observed in this mass spectrum is removed by turning off the voltage applied to the electrospray needle. When the needle is turned off and all other conditions remain unchanged, the level of the background noise from the remaining sources was observed to account for only 0.15 mV_{p-p}. Thus, potentially, greater than an order of magnitude increase in the S/N ratio is possible through a reduction in the chemical background noise. Note that this large background is not unique to this instrument, Smith et al. have also observed substantial chemical background noise, which was attributed to the electrospray process, in their quadrupole instrument [2].

3.3.3 On-line Separations

An on-line separation of a simple protein mixture was carried out. Figures 3.6 (A) and 3.6 (B) show the extracted ion chromatograms resulting from the isocratic separation of 4 pmol each of equine cytochrome c and equine apomyoglobin. The curve for equine cytochrome c, shown in Figure 3.6 (A), was calculated using the $[M + 17H]^{17+}$ peak, while the curve for equine apomyoglobin, shown in Figure 3.6 (B), was determined using the $[M + 21H]^{21+}$ peak. Note that in this experiment an ion extraction rate of 5 Hz (trapping time ~200 ms) was used. For comparison, a UV chromatogram of the same mixture is shown in Figure 3.6 (C). The conditions used to generate these figures did not allow for complete separation of these two proteins. Furthermore, the UV chromatogram was not obtained on-line with the ion trap/TOFMS, thus a strict comparison cannot be made. Nevertheless, for this simple experiment, this figure shows that the electrospray ionisation ion trap/linear TOFMS can be used for LC detection of proteins present in low pmol levels.

3.3.4 Summary

The preliminary results presented in this chapter have illustrated the potential of using an electrospray ionisation ion trap/linear TOFMS as a detector for fast separation techniques. Future studies will also use a linear TOFMS since the unprecedented mass resolution values were determined to be acceptable for most separations. A comparison of the detection limits of this instrument to an ion trap/reflectron TOFMS is difficult because reported detection limits for the reflectron system were calculated based on the amount of sample consumed during continuous infusion of the analyte. Nonetheless, the detection limits of the ion trap/linear TOFMS are at least comparable with the lower detection limit of 20 - 80 fmol (S/N = 3) reported by Lubman and coworkers using an ion trap/reflectron TOFMS [9,13]. Since several variables affected the performance of the electrospray ionisation ion trap/linear TOFMS, a detailed characterization of the instrument was initiated. The results from this characterization are the focus of the next two chapters.

3.4 Literature Cited

1. Fenn, J. B.; Mann, M.; Meng, C. K.; Wong, S. F.; Whitehouse, C. M. *Science*, **1989**, *246*, 64.
2. Smith, R. D.; Loo, J. A.; Edmonds, C. G.; Barinaga, C. J.; Udseth, H. R. *Anal. Chem.* **1990**, *62*, 882.
3. Gelpi, E., *J. Chromatogr. A* **1995**, *703*, 59.
4. see for example, *Time-of-Flight Mass Spectrometry*; R.J. Cotter, Ed., American Chemical Society, Washington DC, **1994**.
5. Fang, L.; Zhang, R.; Williams, E. R.; and Zare, R. N.; *Anal. Chem.* **1994**, *66*, 3696.
6. Boyle, J. G.; Whitehouse, C. M. *Rapid Commun. Mass Spectrom.* **1991**, *5*, 400.
7. Dodonov, A. F.; Chernushevich, I. V.; Laiko, V. V. *International Mass Spectrometry Conference; Amsterdam,* 1991; Extended Abstracts, p. 153.
8. Boyle, J. G.; Whitehouse, C. M. *Anal. Chem.* **1992,** *64*, 2084.
9. Michael, S. M.; Chien, B. M.; Lubman, D. M. *Anal. Chem.* **1993**, *65*, 2614-2620.
10. Mirgorodskaya, O. A.; Shevchenko, A. A.; Chernushevich, I. V.; Dodonov, A. F.;

Miroshnikov, A. I. *Anal. Chem.* **1994**, *66*, 99.

11. Verentchikov, A. N.; Ens, W.; Standing, K. G. *Anal. Chem.* **1994**, *66*, 126-133.
12. Michael, S. M.; Chien, B. M.; Lubman, D. M. *Rev. Sci. Instrum,* **1992**, *63*, 4277.
13. Chien, B. M.; Michael, S. M.; Lubman, D. M. *Int. J. Mass Spectrom. Ion Proc.* **1994**, *131*, 149.
14. Qian, M. G.; Lubman, D. M. *Anal. Chem.* **1995**, *67*, 234A.
15. Agnes, G.; Horlick, G. *Appl. Spectrosc.*, **1992**, *46*, 401.
16. Coulson, L. D.; Nagra, D. S.; Guo, X.; Whittal, R. M.; Li, L. *Appl. Spectrosc.*, **1994**, *48*, 1125.

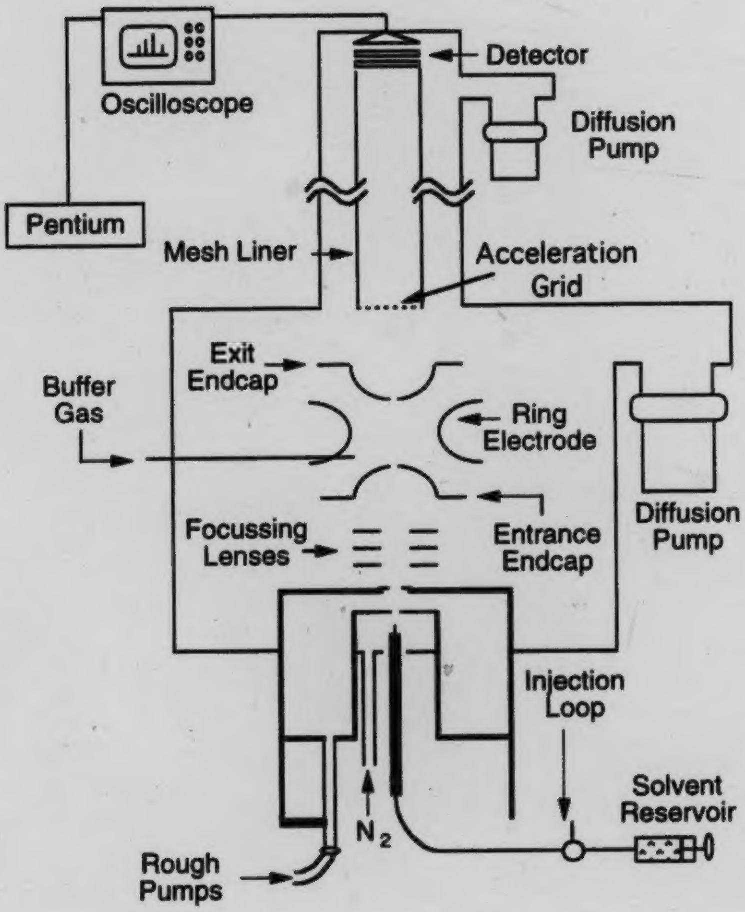
Detector
Oscilloscope
Diffusion Pump
Pentium
Mesh Liner
Acceleration Grid
Exit Endcap
Buffer Gas
Ring Electrode
Focussing Lenses
Entrance Endcap
Diffusion Pump
Injection Loop
Solvent Reservoir
N_2
Rough Pumps

Figure 3.1 Schematic of the electrospray ionisation ion trap/linear time-of-flight mass spectrometer. Drawing is not to scale, dimensions are given in the text.

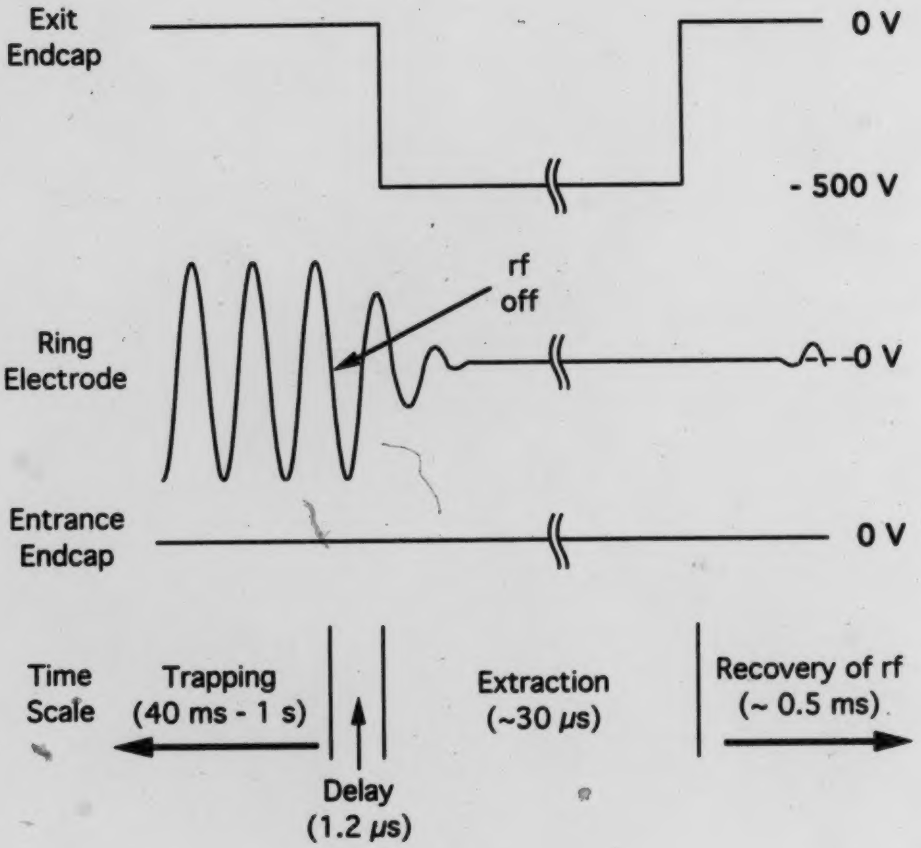
Exit
Endcap
0 V
- 500 V
rf
off
Ring
Electrode
0 V
Entrance
Endcap
0 V
Time
Scale
Trapping
(40 ms - 1 s)
Delay
(1.2 μs)
Extraction
(~30 μs)
Recovery of rf
(~ 0.5 ms)

Figure 3.2 Timing diagram for one ion extraction event using an ion trap/linear time-of-flight mass spectrometer.

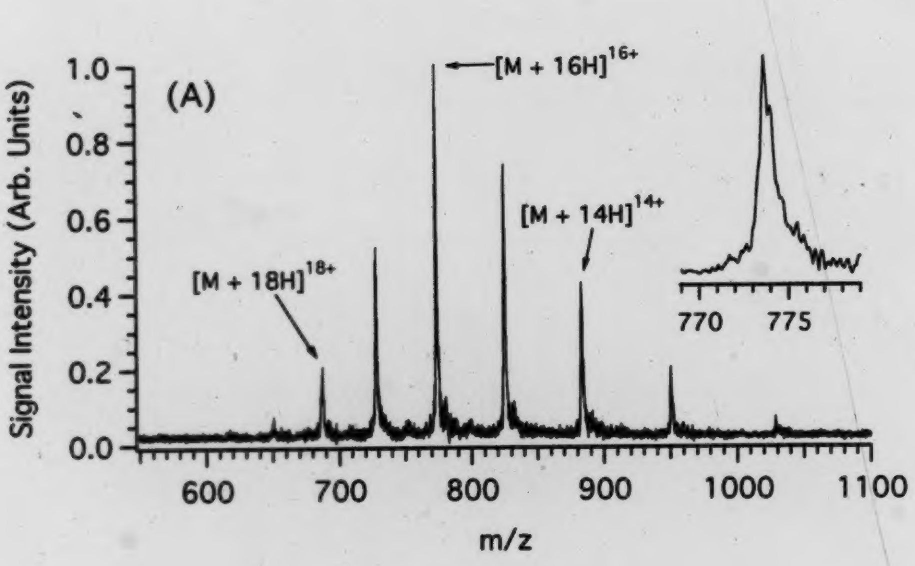

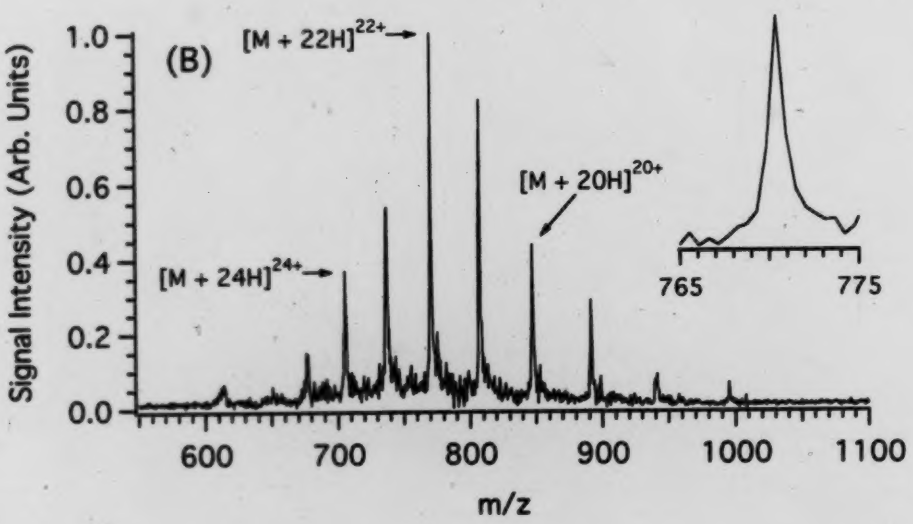

Figure 3.3 Electrospray ionisation mass spectra of (A) equine cytochrome c and (B) equine apomyoglobin obtained using an electrospray ionisation ion trap/linear TOFMS. An expanded view of the most intense peak in each mass spectrum is shown in the inset.

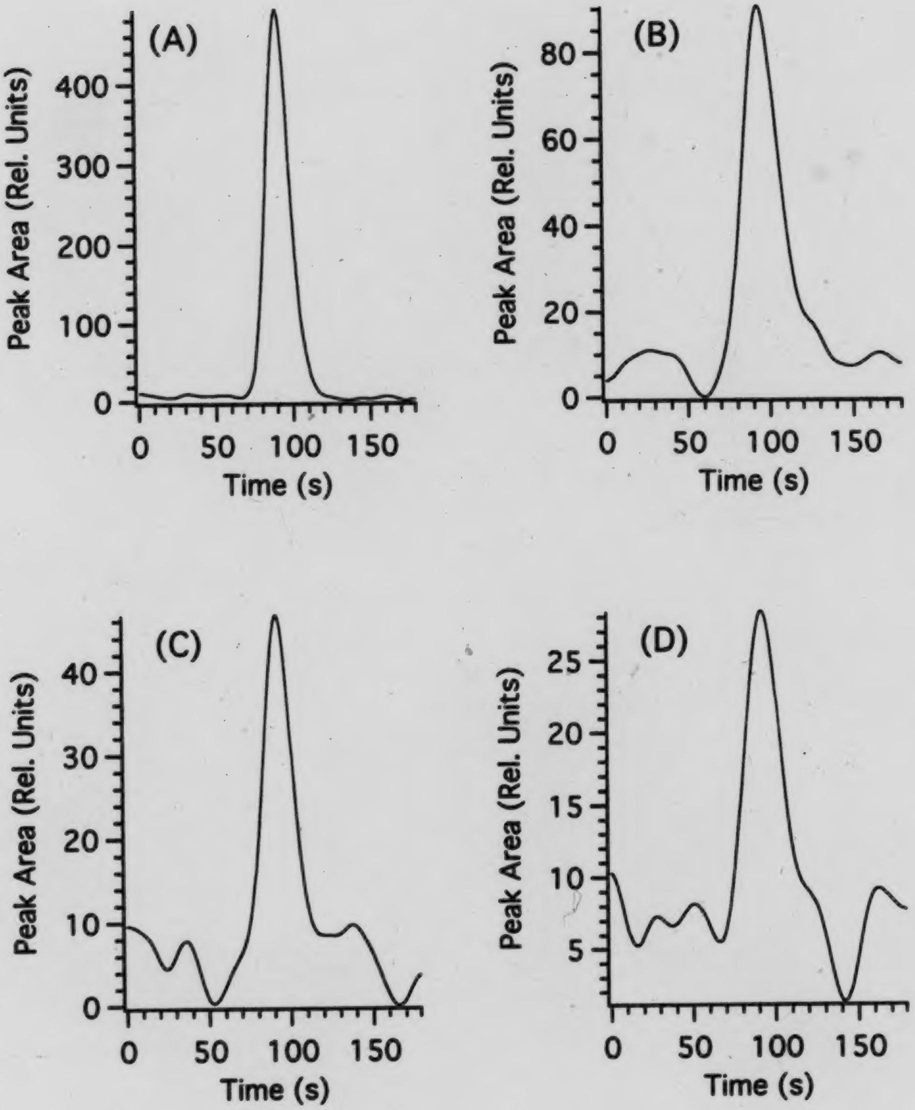

Figure 3.4 Flow injection profiles for four different amounts of bradykinin injected. (A) 3 pmol, (B) 300 fmol, (C) 150 fmol, and (D) 75 fmol. A Savitzky-Golay 2nd order algorithm (15 points) was used to smooth the data.

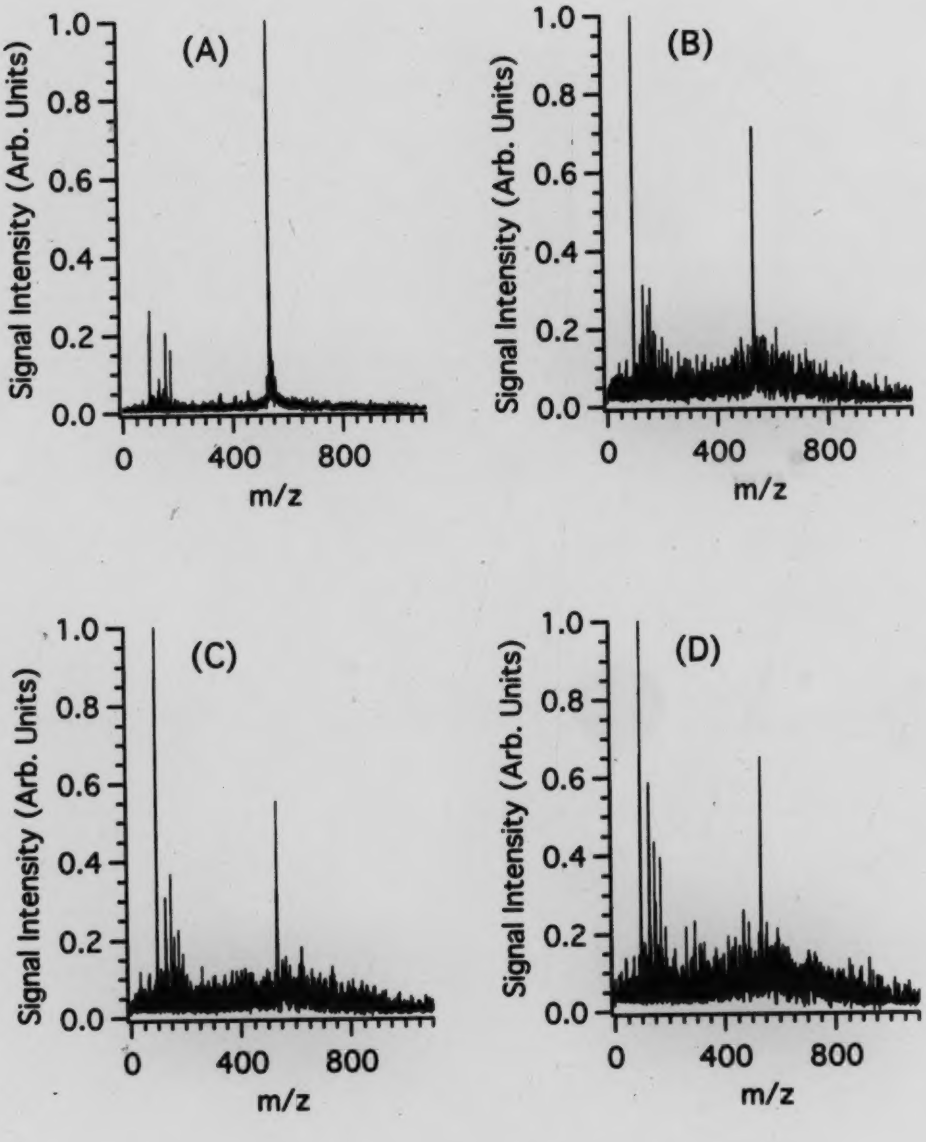

Figure 3.5 Mass spectra of bradykinin for four different amounts injected using the electrospray ionisation ion trap/linear TOFMS. (A) 3 pmol, (B) 300 fmol, (C) 150 fmol, and (D) 75 fmol.

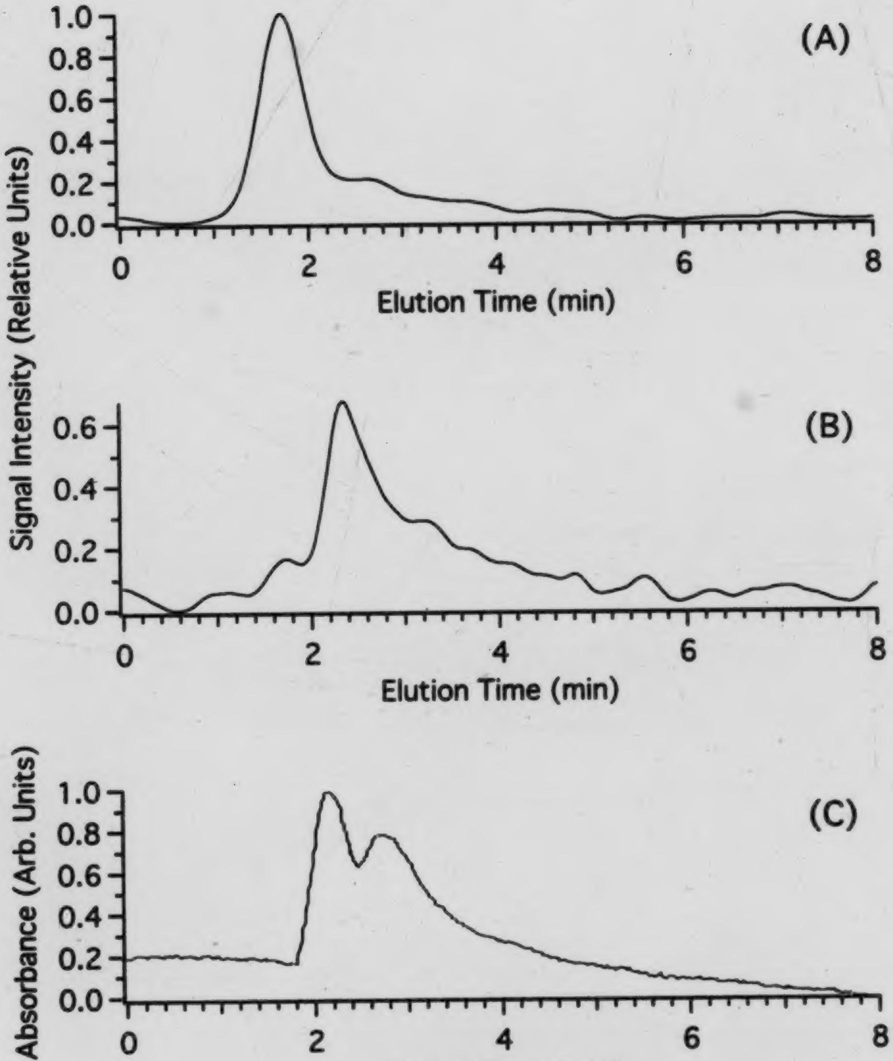

Figure 3.6 Extracted ion chromatogram of (A) equine cytochrome c and (B) equine apomyoglobin obtained using micro-LC electrospray ionisation ion trap/linear TOFMS and (C) a UV chromatogram of the same mixture. The chromatographic conditions are given in the text. A Savitzky-Golay 2nd order algorithm (15 points) was used to smooth the data in (A) and (B).

Chapter 4

Adduct Formation in an Electrospray Ionisation Ion Trap/Time-of-Flight Mass Spectrometer[a]

4.1 Introduction

Since its introduction in the 1950's [1], the quadrupole ion trap has undergone extensive development as researchers attempt to exploit many of its unique characteristics for use with mass spectrometry [2]. The ion trap confines ions, with a wide mass range, for an extended time [3]. Consequently, the ion trap is used for temporarily storing electrosprayed ions prior to time-of-flight (TOF) mass analysis [4,5]. Another advantage of using the ion trap is the ability to study gas-phase ion chemistry [6-8]. However, this advantage becomes a serious complication when unexpected gas-phase reactions occur during the ion storage event. The formation of interfering adduct peaks in the ion trap was observed using an ion trap/linear TOFMS. The cause of the adduct peaks and their subsequent removal from the system is described. This discussion is particularly relevant to any ion trap instrument that uses diffusion pumps to create high vacuum.

---

[a] A form of this chapter has been published as: R. W. Purves, W. Gabryelski, L. Li "The Effect of Using Silicon Based Diffusion Pump Fluid on Spectral Quality in an Electrospray Ionization Ion Trap/Time-of-Flight Mass Spectrometer", *Rev. Sci. Instrum.* **1997**, *68*, 3252. W. Gabryelski developed the cleaning procedure for the ion trap/linear time-of-flight mass spectrometer.

The formation of adduct peaks arising from interactions in solution is also briefly examined. These adduct peaks, well documented in the literature [9], can assist in the analysis (e.g., structure elucidation [10]), or they reduce the effectiveness of the analysis (e.g., reduced sensitivity [9]). A simple example is given to illustrate some difficulties that can arise when electrospray ionisation mass spectrometry is used for quantitative analysis. The use of instrumental variables to control the formation of adduct peaks is also addressed. In particular, examples shown are used for the discussion of ion energies and trapping efficiency presented in Chapter 5.

4.2 Experimental

The design of the ion trap/linear TOFMS has been previously described in detail in Chapters 2 and 3 [11]. The data presented in this chapter was collected by continuously introducing analyte to the electrospray needle tip as was described in Chapter 2. A few changes were made to the operation of the instrument compared with the previous chapter. The frequency of the rf generator was changed to 1 MHz and the voltage of the acceleration grid and mesh liner were changed to −4100 V. Furthermore, a new negative high voltage pulse generator was developed to surpass the −500 V maximum output of the previous voltage pulse generator. When this new pulse generator was used, the rf voltage applied to the ring electrode was also being induced on the exit endcap resulting in decreased signal intensity. To overcome this problem, a circuit, adapted from previous work by Baker and Johnson [12], was developed to ground the induced rf noise during the ion storage event. The design and function of this circuit are briefly described in Appendix A. The new negative high voltage pulse generator, including the additional circuitry, delivered up to - 1000 V with a rise time of 44 ns. Importantly, when the rf voltage applied to the ring electrode was 2000 V_{p-p}, the induced noise level was ~4 V_{p-p} compared with ~150 V_{p-p} without the additional circuitry. The extraction voltage used for all the mass spectra shown in this chapter was - 800 V. Note that all of the figures presented in this chapter represent consecutive sums of 100 ion trap ejections.

One other important change was made concerning the preparation of the analyte solutions. The use of trifluoroacetic acid (TFA) is shown to cause signal suppression for basic compounds when analysed by electrospray ionisation mass spectrometry due to the strong ion pairing property of TFA [13]. The detection limits are about 10 times larger than those obtained using 1% acetic acid [13]. Consequently, to acidify the samples, 0.1% (v/v) acetic acid was used for peptides and 1% acetic acid (v/v) was used for proteins.

4.3 Results and Discussion

4.3.1 Adducts From Silicon-Based Diffusion Pump Fluid

A characterization of the ion trap/linear TOF mass spectrometer was initiated and during this process, characteristic adduct peaks were observed. These peaks were detected during a study of the effect of trapping time on the mass spectral quality of large analytes (i.e., proteins). The adduct peaks were observed for even the smallest of the proteins studied (bovine insulin, MW = 5733.6), but were not usually present when low molecular weight compounds, such as small peptides with molecular weights less than 2000, were studied. In general, the number and intensity of the adduct peaks increased as the mass of the protein increased. Furthermore, trapping time was the only instrumental variable that appeared to affect the degree of adduct formation. Therefore, it was concluded that the adduct forming reaction was occurring in the ion trap.

An example of the adduct formation is illustrated in Figure 4.1 using equine cytochrome c. Figure 4.1 (A) shows the complexity of a mass spectrum containing several adduct peaks. In Figure 4.1 (B), three adduct peaks of the $[M + 16H]^{16+}$ ion are observed. The exact mass of these adducts was difficult to determine from this mass spectrum because not only is it harder to calculate a small mass change at high mass values accurately, but also because the mass resolution degraded with the onset of these peaks. The mass of each adduct in this mass spectrum was estimated to be ~485 u. A more accurate determination of the mass of these adducts is presented in Figure 4.2. This mass spectrum was generated from a solution of 2 mM ammonium acetate in 80% acetonitrile and 20% water (v/v). When the drying gas was removed from the desolvation region during the electrospray process, an extremely intense background resulted. A peak at m/z 502, which corresponds to $[NH_4 + \text{adduct}]^+$, was also observed. Consequently, the mass shift corresponding to each adduct peak was calculated to be 484 u. A probable source of the adducts, based on this mass, is the silicon-based diffusion pump fluid, namely tetraphenyl tetramethyl trisiloxane (DC 7040 from Dow Corning, MW = 484).

A series of mass spectra collected for equine apomyoglobin over the trapping range from 50 - 500 ms illustrates the effect of the adducts on mass spectral quality. Figure 4.3 (A) shows the intensity of the $[M + 21H]^{21+}$ and the $[M + 21H + 484]^{21+}$ peaks as a function of trapping time. Figure 4.3 (B) shows the corresponding peak width (fwhm) of the $[M + 21H]^{21+}$ peak. The onset of the $[M + 21H + 484]^{21+}$ peak in Figure 4.3 (A) was observed to occur after a trapping time of ~100 ms. For longer trapping times, the analyte signal intensity reached a plateau (peak area was still increasing) while the intensity of the adduct peak continued to increase. What is not shown in Figure 4.3 (A), is the intensity of the other adduct peaks (i.e., $[M + 21H + x(484)]^{21+}$) as a function of the trapping time. The intensities of these peaks were not recorded during this study, however, Figure 4.1 clearly shows that multiple adduct peaks are also formed. In addition, Figure 4.3 (B) shows that as the intensity of the $[M + 21H + 484]^{21+}$ peak increases, a noticeable degradation in mass resolution is observed. The behaviour depicted in Figure 4.3 is typical of all the charge states observed for apomyoglobin, and qualitatively, it applies to all the proteins studied. Note that for trapping times greater than 1 s, mass spectra were dominated by the adduct peaks resulting in many overlapping peaks and therefore very poor mass resolution. Consequently, before the characterization of the ion trap/linear TOFMS could continue, it was imperative that the source of the adduct peaks be removed from the instrument.

Liquid nitrogen was added to the cold traps of the diffusion pumps to reduce residual gases from the diffusion pump fluid. However, this was insufficient as the intensities of the adduct ions were only reduced about 50%. To remove background fluid that may have built up inside the instrument, the stainless steel casing of the instrument was heated to ~100 °C overnight. The next day a build-up of an oily liquid was observed on the quartz windows of the instrument (not heated). Consequently, the entire instrument was dismantled and cleaned using a combination of solvents (mainly methanol, acetonitrile, acetone, and n-hexane). The diffusion pump fluid was changed to pentaphenyl trimethyl trisiloxane (DC 7050), which has a vapour pressure of over an order of magnitude less than DC 7040 (5×10^{-10} torr compared with 1×10^{-8} torr [14]). These steps appeared to have no effect as the mass spectra were still dominated by the presence of adducts from DC 7040. Apparently, cleaning with solvents alone was not sufficient in removing DC 7040 still present in the instrument.

Subsequently, a more rigorous cleaning procedure was employed. The first step involved the electrolytic anodization of metallic components in an acid bath containing 56% glycerol, 37% phosphoric acid, and 7% water (v/v). This was followed by cleaning with a detergent (Sparkleen) to remove any remaining contaminants from the metal surfaces. Ceramic components were cleaned using a 3:1 mixture of sulphuric acid and 30% hydrogen peroxide, followed by heating to ~400 °C in a muffle furnace overnight. This procedure virtually eliminated adduct peaks corresponding to DC 7040 from the mass spectra; however, new adduct peaks were observed. Figure 4.4 (A) shows a mass spectrum of equine cytochrome c that was obtained using the same experimental conditions as Figure 4.1 except that the trapping time was increased from ~330 to ~500 ms. Figures 4.4 (B) and (C) show expanded views of the adducts of the $[M + 17H]^{17+}$ and $[M + 15H]^{15+}$ ions, respectively. Note that the adduct peaks corresponding to mass shifts of 92 u were only observed for charge states 13^+ through 16^+, while adducts corresponding to mass shifts of 131 u were only observed for charge states 17^+ and 18^+. The adduct peak resulting from an addition of 92 u was from glycerol present in the acid bath and the peak corresponding to a mass shift of 131 u was likely from the detergent. It is clear both glycerol and the detergent contaminate the ion trap resulting in the formation of adduct ions. The peaks with the mass shifts of 273 u and 546 u are likely adducts caused from the DC 7050 diffusion pump fluid (MW = 546).

As a result, the instrument was dismantled, cleaned, and the diffusion pump fluid was changed to a mixed five-ring polyphenyl ether (Santovac 5). Although Santovac 5 has a higher vapour pressure (1.3×10^{-9} torr [14]) than DC 7050, it is the diffusion pump fluid generally recommended for mass spectrometry [14]. The cleaning procedure was modified to exclude the use of the detergent and the composition of the acid bath was changed to a 1:1 mixture of 85% phosphoric acid and water (v/v). Figure 4.5 shows a mass spectrum of equine cytochrome c acquired after a trapping time of 1 s; the adduct peaks are not observed.

Consequently, although ion traps can tolerate high pressures, it does not mean that considerations of vacuum quality can be ignored. Silicon-based pumping fluids cause the formation of interfering adduct peaks and their use in an electrospray ionisation ion trap/TOFMS, or in any instrument that uses an ion trap, is not recommended. The use of Santovac 5 as the diffusion pump fluid does not result in the formation of adduct peaks and is therefore recommended for this type of application. In addition, the aforementioned cleaning procedure provides an effective means for removing contaminants that deposit on the ion trap over time.

4.3.2 Solution Adduct Formation

Adducts formed in solution are readily examined using electrospray ionisation mass spectrometry [10]. Figure 4.6 (A) shows an example of adduct formation using equine cytochrome c. This mass spectrum was collected using typical operating conditions and the appearance of multiple adduct peaks was an unexpected result at the time. Figure 4.6 (B) shows an expanded view of the adducts of the $[M + 14H]^{14+}$ ion. The mass shift for each adduct corresponds to 62 u, a consequence of Cu (I) present in the solution. The copper was originating from rust inside an older Hamilton syringe that was being temporarily used to deliver the analyte solution. Acetonitrile dissolved the copper from the needle thereby resulting in the formation of copper adduct peaks in the mass spectrum (note that methanol/water did not produce adduct peaks). The formation of multiple copper adduct peaks was also observed by Jiao et al. when they added Cu (I) to a solution of ubiquitin [15]. For purposes of quantitation, keeping as much of the analyte as possible in the $[M + xH]^{x+}$ form is crucial. Otherwise, changes in the solution matrix composition can affect the distribution of the various forms of the analyte thereby making quantitative data unreliable. This concern is addressed in Chapter 6.

As the size of the analyte increases, the peak width also increases as adducts become increasingly more difficult to remove [9]. Adduct formation is illustrated using equine apomyoglobin in Figure 4.7 and bovine trypsinogen in Figure 4.8. In Figures 4.7 (A), (B), and (C), the voltage drops between the nozzle and sampling plate in the interfacial region are 13 V, 18 V, and 23 V, respectively. An expanded view of the $[M + 19H]^{19+}$ peak is shown in the inset for each mass spectrum. The adduct peaks in Figure 4.7 correspond to a mass shift of 96, which is likely due to the presence of sulphate present in the original protein sample. The figure shows that by increasing the voltage in the interfacial region, these adduct peaks are effectively removed. Furthermore, the noisy baseline, due in part to partially solvated analyte peaks, is also reduced. Note that in the inset of Figure 4.7 (C), a shoulder is observed on the low mass side of the $[M + 19H]^{19+}$ peak. This is likely a result of fragmentation that was caused by the large voltage drop.

In Figures 4.8 (A), (B), and (C), the voltage drops in the interfacial region were 40 V, 50 V, and 60 V, respectively. Increasing this voltage drop improves the mass spectral quality as the peak width of the $[M + 16H]^{16+}$ peak (shown in the inset) decreases. A contributing source to the peak broadening at the lower voltage drops is attributed to solvent adducts. Note that by increasing the voltage drop, the kinetic energies of the bovine trypsinogen ions were also increased, thereby the signal intensity was decreased (i.e., decreased trapping efficiency). Consequently, unlike equine apomyoglobin, the adduct peaks cannot be effectively removed from the mass spectrum without sacrificing signal intensity. The significance of this observation is discussed in the next chapter.

4.4 Literature Cited

1. Paul, W.; Steinwedel, H., *U.S. Patent 2,939,952* **1960**.
2. Todd, J. F. J. *Mass Spectrom. Rev.* **1991**, *10*, 3.
3. March, R. E., *J. Mass Spectrom.* **1997**, *32*, 351.
4. Michael, S. M.; Chien, B. M.; Lubman, D. M. *Anal. Chem.* **1993**, *65*, 2614.
5. Chien, B. M.; Michael S. M.; Lubman, D. M. *Int. J. Mass Spectrom. Ion Proc.* **1994**, *131*, 149.

6. Pachuta, R. R.; Kenttämaa, H. I.; Cooks, R. G.; Zennie, T. M.; Ping, C.; Chang, C.; Cassady, J. M. *Org. Mass Spectrom.* **1988**, *23*, 10.

7. Brodbelt, J. S.; Wysocki, V. H.; Cooks, R. G. *Org. Mass Spectrom.* **1988**, *23*, 54.

8. Brodbelt-Lustig, J. S.; Cooks, R. G. *Int. J. Mass Spectrom. Ion Proc.* **1988**, *86*,253.

9. Smith, R. D.; Loo, J. A.; Edmonds, C. G.; Barinaga, C. J.; Udseth, H. R. *Anal. Chem.* **1990**, *62*, 882.

10. Przybylski, M.; Glocker, M. O. *Agnew. Chem. Int. Ed. Engl.* **1996**, *35*, 806.

11. Purves, R. W.; Li, L. *J. Microcolumn Separations* **1995**, *7*, 603.

12. Baker, R. J.; Johnson, B. P. *Rev. Sci. Instrum.* **1993**, *64*, 1655.

13. Kuhlmann, F. E.; Apffel, A.; Fischer, S. M.; Goldberg, G.; Goodley, P. C. *J. Am. Soc. Mass Spectrom.* **1995**, *6*, 1221.

14. *High Vacuum Technology, a Practical Guide;* Hablanian, M. H. (Marcel Dekker, Inc., New York, 1990, p. 174).

15. Jiao, C. Q.; Freiser, B. S.; Carr, S. R.; Cassady, C. J. *J. Am. Soc. Mass Spectrom.* **1995**, *6*, 521.

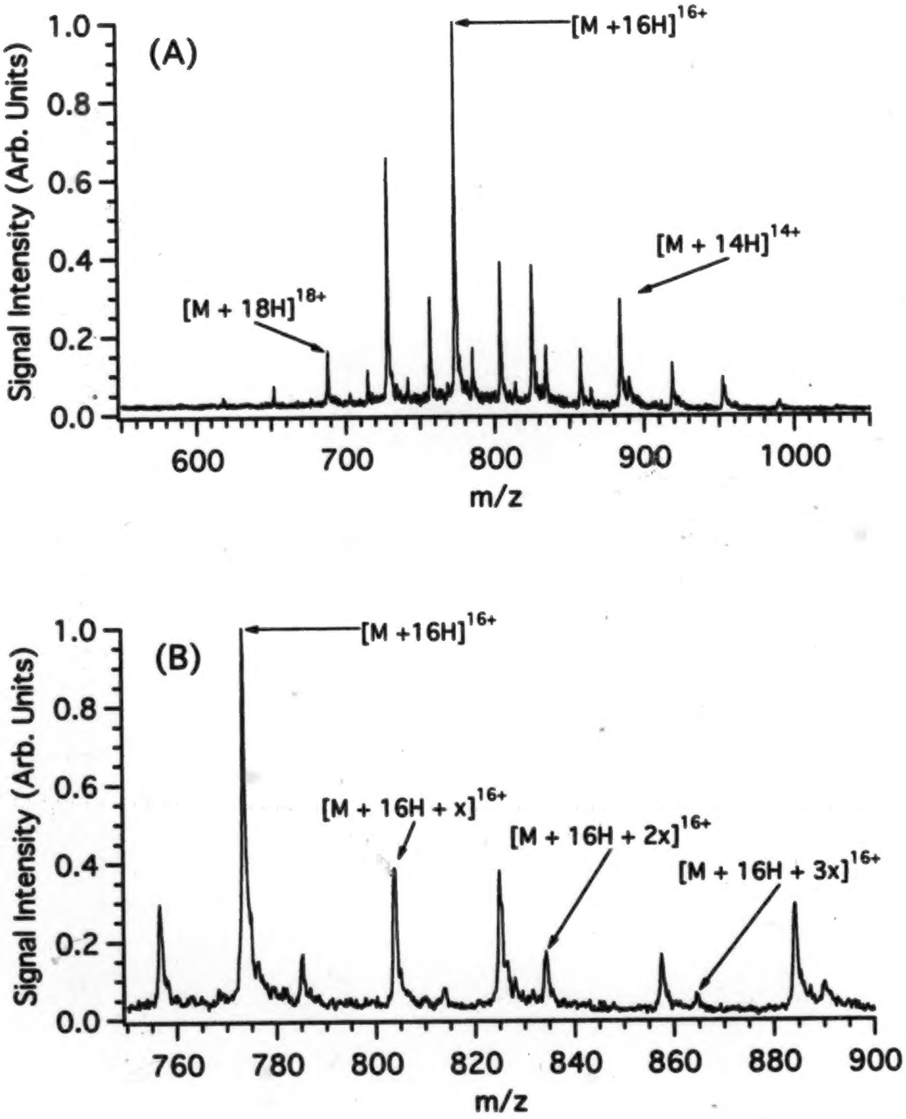

Figure 4.1 (A) Mass spectrum of equine cytochrome c obtained using DC 7040 diffusion pump fluid and a trapping time of 330 ms. (B) Expanded view of the adducts of the $[M + 16H]^{16+}$ ion.

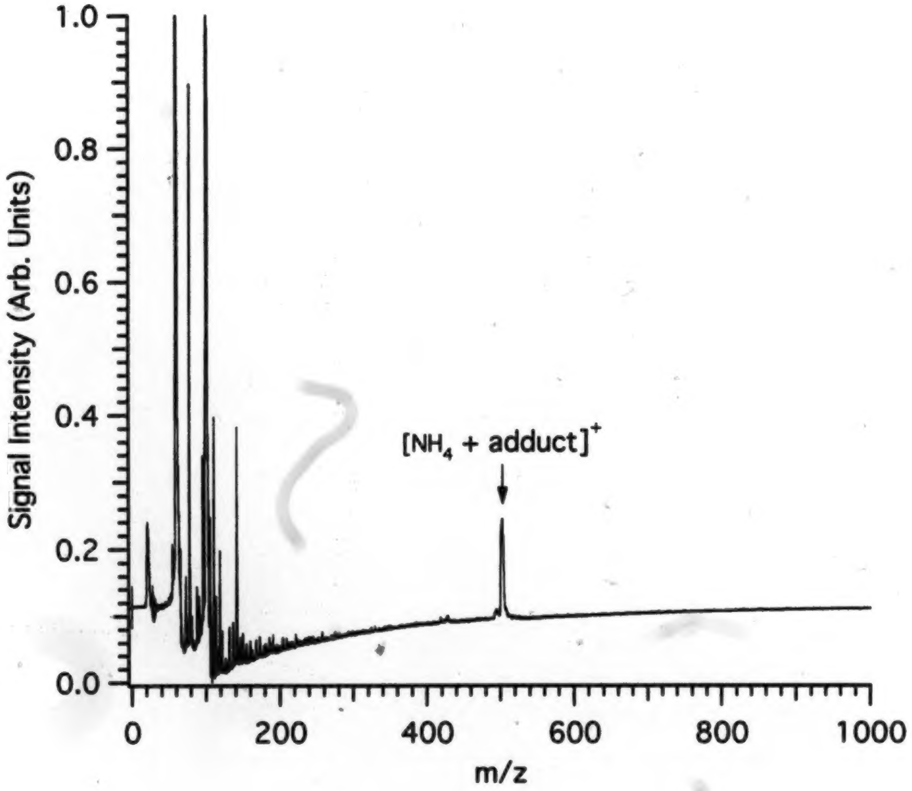

Figure 4.2 Mass spectrum of a solution of 2 mM ammonium acetate in 80% acetonitrile and 20% water with no bath gas in the desolvation region. The diffusion pump fluid was DC 7040.

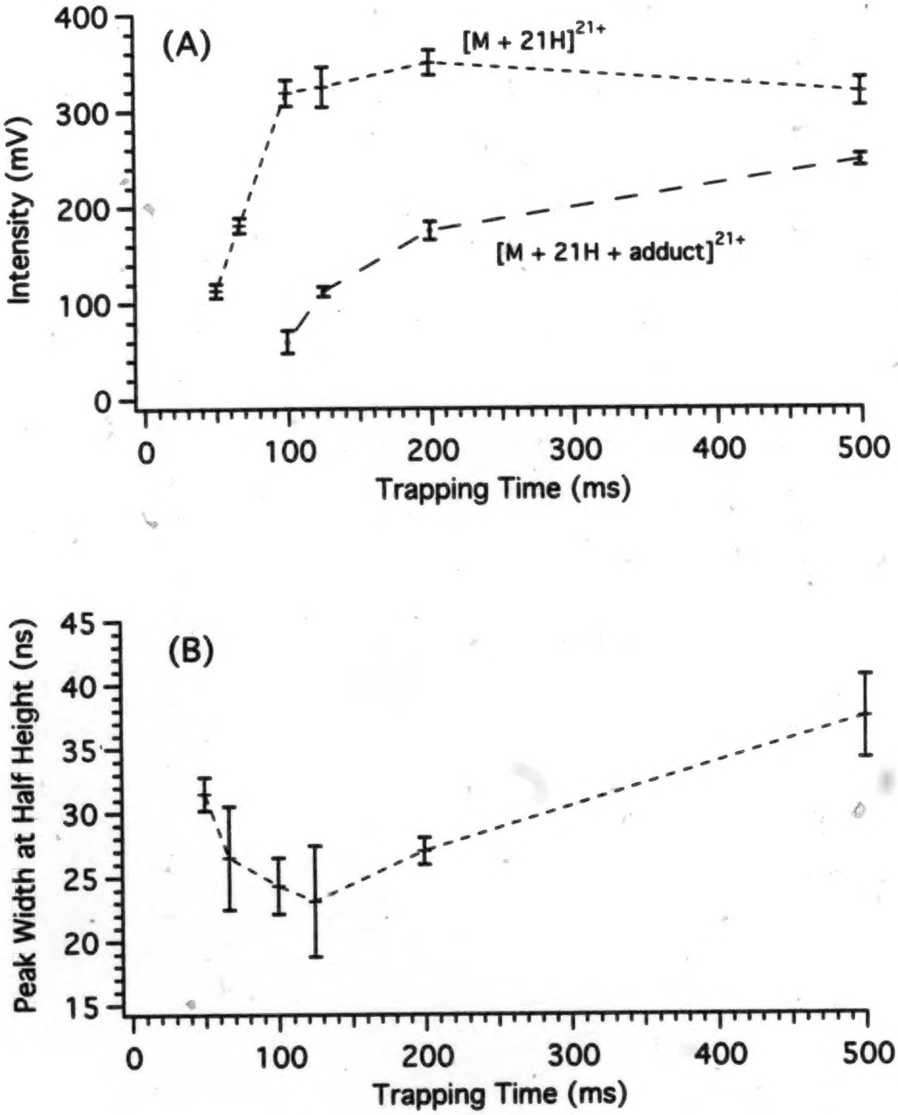

Figure 4.3 (A) Plot of the intensity of the [M + 21H]$^{21+}$ and the [M + 21H + 484]$^{21+}$ peaks for equine apomyoglobin as a function of trapping time; DC 7040 diffusion pump fluid was present in the instrument. (B) Plot of the peak width (ns) of the [M + 21H]$^{21+}$ peak for the same experiment.

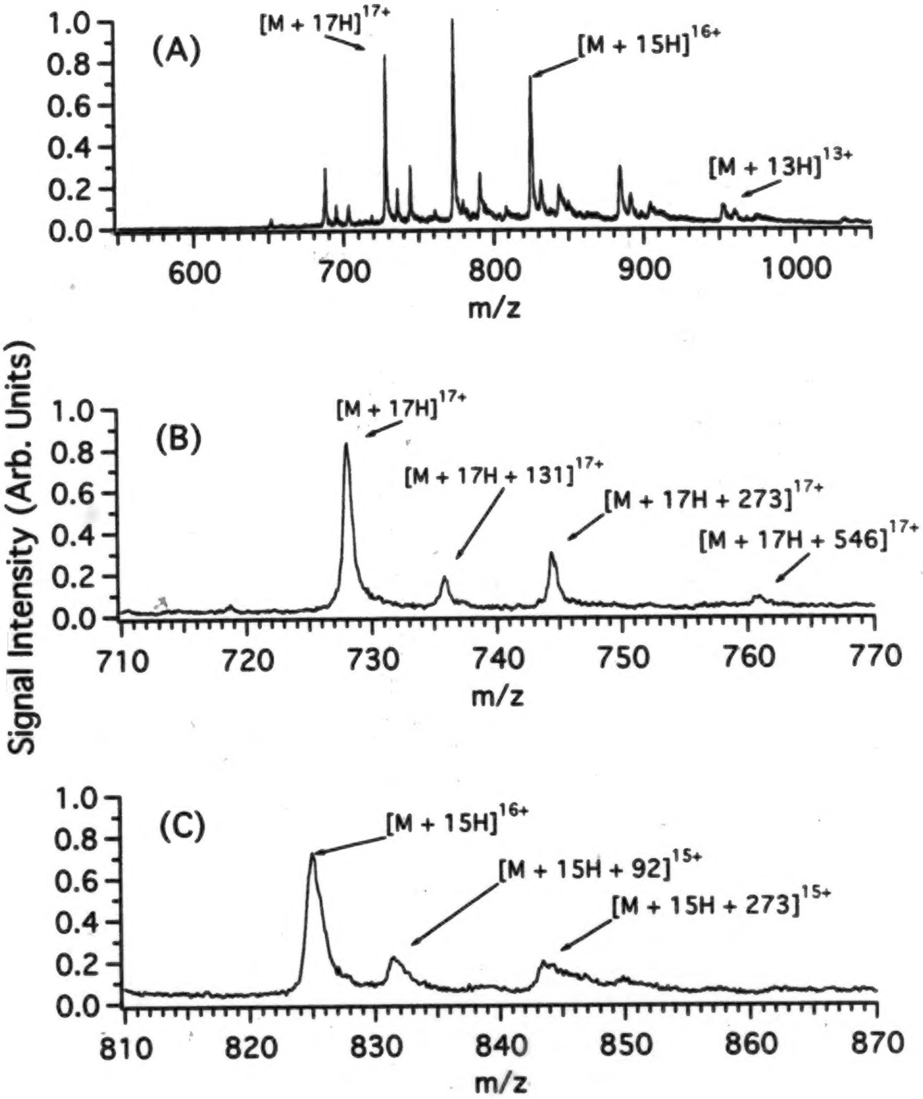

Figure 4.4 (A) Mass spectrum of equine cytochrome c obtained using a detergent in the cleaning procedure and changing the diffusion pump fluid to DC 7050. The trapping time used was 500 ms. (B) Expanded view of the 17^+ charge state and its adducts. (C) Expanded view of the 15^+ charge state and its adducts.

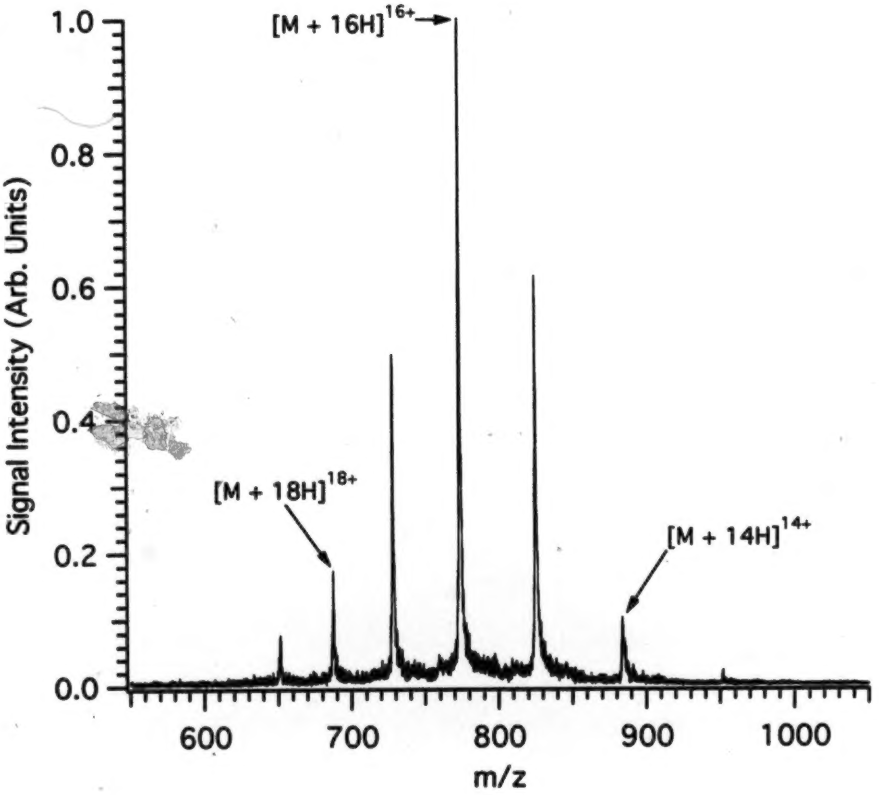

Figure 4.5 Mass spectrum of equine cytochrome c obtained using Santovac 5 diffusion pump fluid and a trapping time of 1 s.

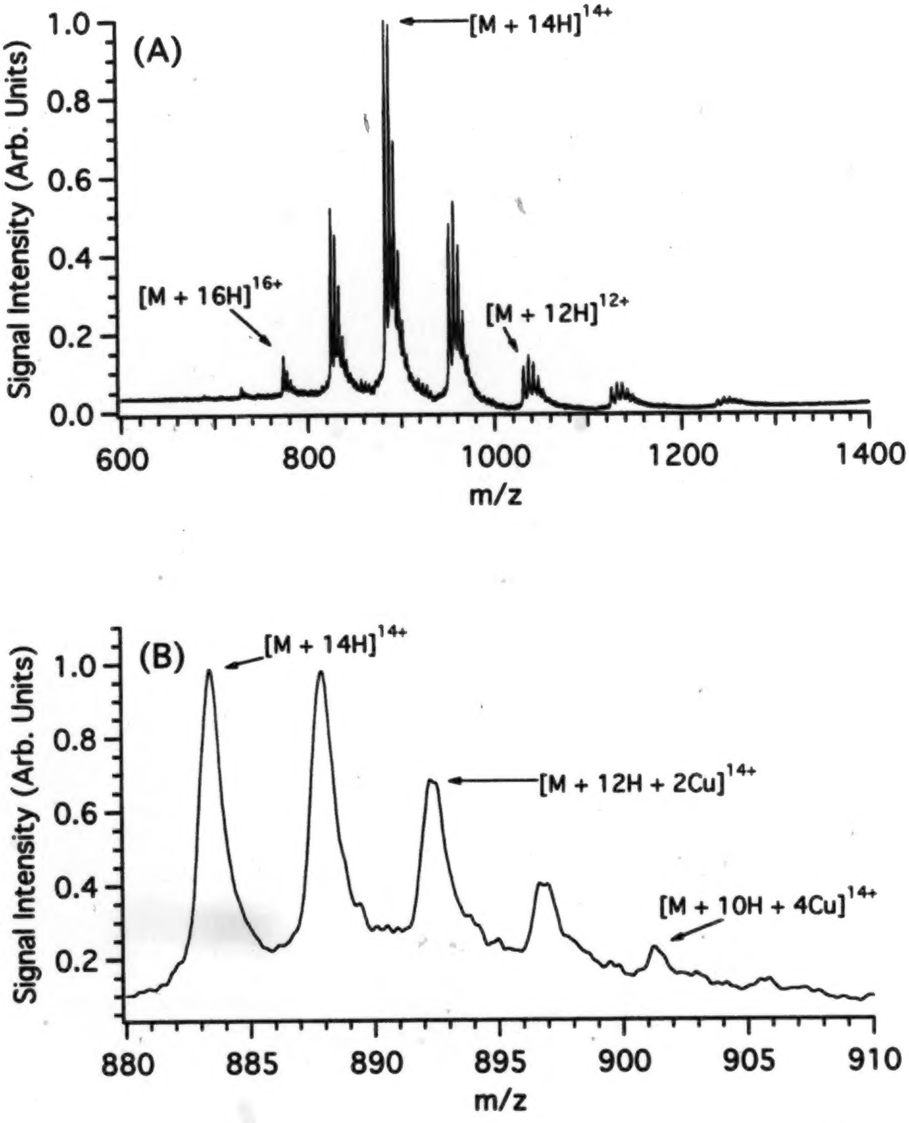

Figure 4.6 (A) Mass spectrum of a solution of equine cytochrome c containing Cu(I). (B) Expanded view of the 14^+ charge state and its corresponding adducts.

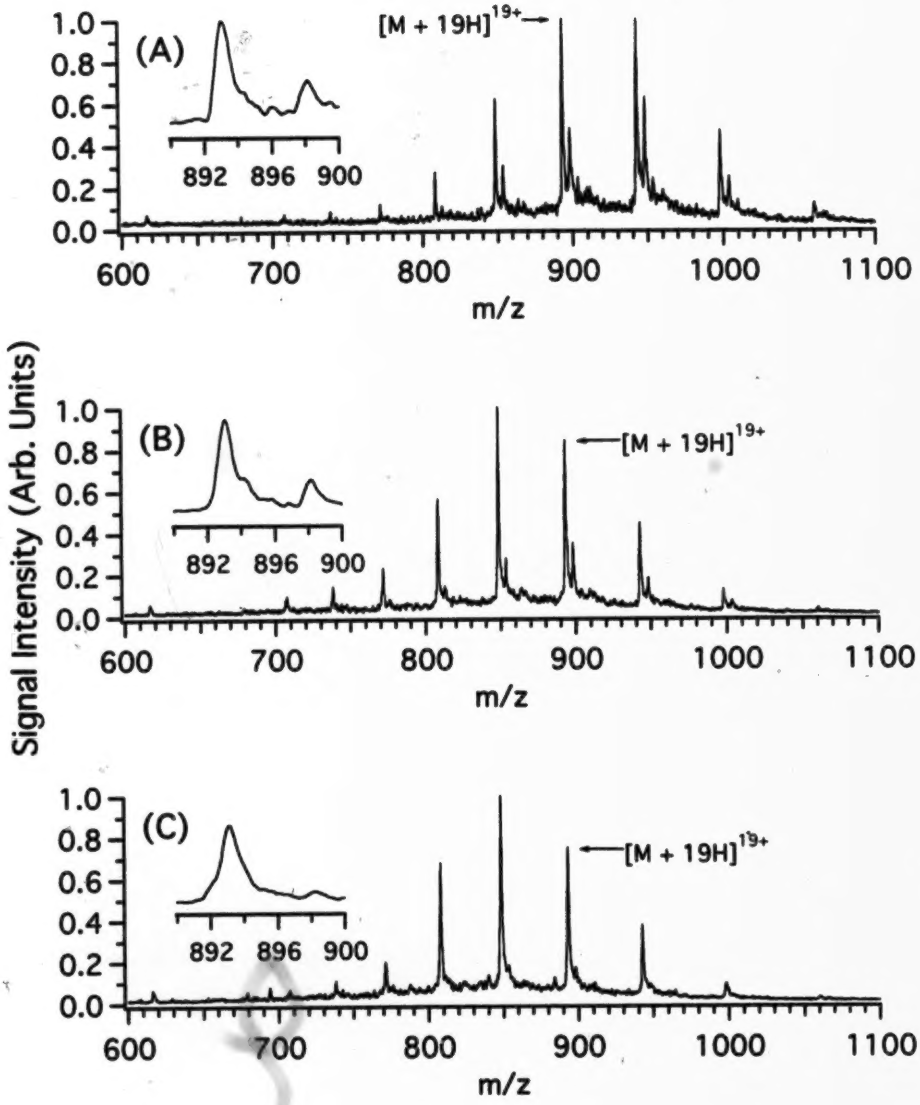

Figure 4.7 Reduction of adduct peaks in a mass spectrum of equine apomyoglobin by changing the voltage drop between the nozzle and sampling plate in the interfacial region. (A) $\Delta V = 13$ V, (B) $\Delta V = 18$ V, and (C) $\Delta V = 23$ V.

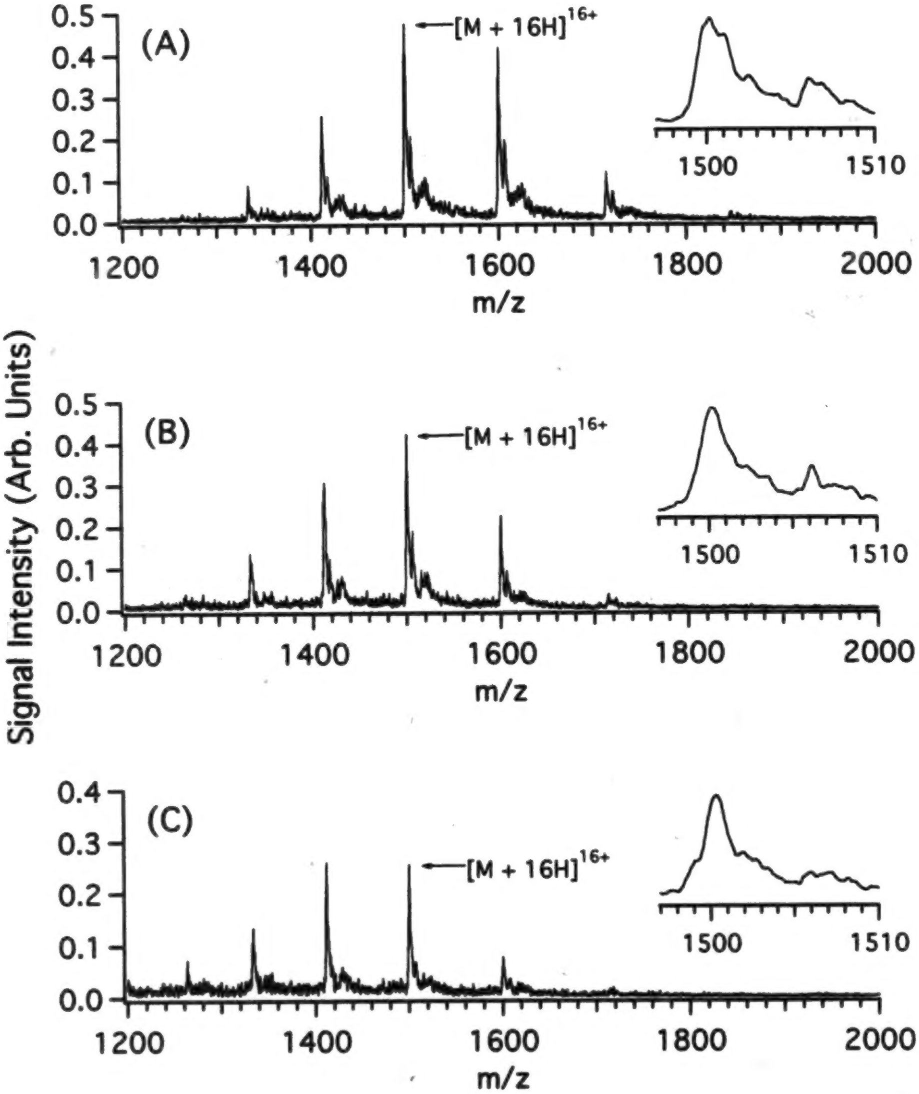

Figure 4.8 Reduction of adduct peaks in a mass spectrum of bovine trypsinogen by changing the voltage drop between the nozzle and sampling plate in the interfacial region. (A) ΔV = 40 V, (B) ΔV = 50 V, and (C) ΔV = 60 V.

Chapter 5

Characterization of an Electrospray Ionisation Ion Trap/Linear Time-of-Flight Mass Spectrometer[a]

5.1 Introduction

An ion trap/time-of-flight mass spectrometer (TOFMS) combines the desirable properties of a TOF mass analyser [1] with the ion storage and tandem mass spectrometry capabilities of an ion trap [2]. In Chapter 3, a preliminary study investigated the potential of using an electrospray ionisation ion trap/linear TOFMS as a detector for micro-column liquid chromatography [3]. Currently, the advantages and limitations of this type of instrument have not been thoroughly investigated in the literature. Various studies using electrospray ionisation ion trap/TOF mass spectrometry have not fully explored considerations such as mass accuracy, mass-to-charge ratio discrimination, and detection mass range [3-7]. In this chapter, several variables that effect the analytical capabilities of an electrospray ionisation ion trap/linear TOFMS are investigated. Variables relating to ion focussing, ion trapping, ion extraction, and ion detection are characterized to understand how the overall performance of the system is affected. The limitations of the electrospray ionisation ion trap/linear TOFMS are discussed and suggested modifications for improving this combination are also presented.

---

[a] A form of this chapter was accepted for publication as: R. W. Purves, L. Li "Development and Characterization of an Electrospray Ionization Ion Trap/Linear Time-of-Flight Mass Spectrometer", *J. Am. Soc. Mass Spectrom.*, *in press*.

In addition part of this chapter is in preparation for publication as: R. W. Purves, L. Li "Mass Accuracy Measurements in an Electrospray Ionization Ion Trap/Linear Time-of-Flight Mass Spectrometer".

5.2 Experimental Section

The design and operation of this instrument were previously described in detail in the preceding chapters [3]. Again, the analyte was continuously introduced to the electrospray needle tip.

Depending upon the analyte studied, the voltages applied to the nozzle and sampling plate were 20 - 60 V and 0 - 8 V, respectively. The first and third focussing plates were operated at 0 V, while the second plate was operated between -50 V and -200 V. There were also changes made to the ion extraction procedure compared with the previous chapter. The delay time between shutting off the rf voltage and the application of the high voltage pulse was increased to 4 μs. Furthermore, the negative voltage pulse generator was operated at −960 V and the ion extraction time was reduced from 30 μs to 10 μs.

5.2.1 Calibration of Helium Flow Rate Into the Ion Trap

The flow rate of helium gas into the ion trap was calibrated using the following procedure. The needle valve was closed and the main valve on the helium tank was opened briefly to allow the pressure in the first stage of the regulator to exceed 2000 psi. The pressure in the first stage of the regulator was adjusted to 2000 psi by bleeding off some of the helium using the needle valve. The needle valve was used to set the flight tube pressure and the time that it took for the regulator pressure to drop from 2000 to 1900 psi was recorded. Three trials for five different flight tube pressures were recorded. Later, the helium line was removed from the system and placed inside of an inverted Burette filled with water. Using a similar procedure as described above, the time necessary for the regulator pressure to drop from 2000 to 1900 psi was recorded for different helium flow rates into the Burette. Consequently, by comparing the times for the 100 psi pressure drops, the flight tube pressure could be directly related to the flow rate of helium. A graph of the flow rate of helium, F, into the ion trap as a function of the change in pressure, ΔP, in the flight tube is shown in Figure 5.1. An exponential curve, given by the dashed line, was fit to this data. The equation for this curve, given in equation 5.1, is used to calculate the flow of helium into the ion trap.

$$F = 1.123 - 1.167 \cdot \exp(-3.446 \cdot \Delta P) \tag{5.1}$$

Where F and ΔP are in units of mL/min and μtorr, respectively. Note that a pressure of 0.4 μtorr is used as the baseline pressure (i.e., $\Delta P = P_{observed} - 0.4\ \mu$torr)

5.2.2 Bipolar Extraction

To carry out the bipolar extraction experiments, a positive high voltage pulse generator is required for the entrance endcap and a negative high voltage pulse generator is required for the exit endcap. Ideally, the internal delays and rise/fall times of the pulse generators would be identical. Unfortunately, the two high voltage pulse generators developed at the University of Alberta did not meet these requirements. The negative high voltage pulse generator, which was described in Chapter 4, had a rise time of 44 ns and a maximum output of − 1000 V. The positive high voltage pulse generator, based on the design of Bernius et al. [8], had a rise time of 20 ns at 1000 V. Unlike the negative high voltage pulse generator, the positive high voltage pulse generator grounds the induced rf voltage from the ring electrode between pulses and therefore did not require any modification (0.4 V_{p-p} induced rf noise at 2000 V_{p-p}). A delay circuit was used to synchronize the internal delays of the high voltage pulse generators. The experiment was designed so that the high voltage pulse generators would be at half their respective output voltages simultaneously (i.e., the negative pulse generator started 12 ns earlier and reached its voltage 12 ns later compared with the positive pulse generator). The only difference between the bipolar extraction experiments and the unipolar (i.e., normal operating conditions) extraction experiments was that during ion extraction, the voltage of the entrance endcap was 400 V and the voltage of the exit endcap was −400 V.

5.3 Results and Discussion

5.3.1 Mass Resolution

Several variables influence the mass resolution observed for a given analyte using an electrospray ionisation ion trap/linear TOFMS. One of the most important of these variables is trapping time. Mass resolution is shown to improve with increased trapping time using an ion trap/reflectron TOFMS [6]. Since the operation of the ion trap/linear TOFMS is most suited to high speed applications, such as separations using capillary electrophoresis [9], the minimum data acquisition rate considered in this study was 4 Hz (i.e., a maximum trapping time of ~250 ms). The mass resolution values, calculated using the full width at half maximum (fwhm), reported herein were obtained using 250 ms trapping times unless otherwise noted. For analytes with molecular weights up to ~20 000 u, typical mass resolution values were between 800 and 1200 fwhm, unless otherwise limited by the isotopic distribution of the analyte (e.g., see bradykinin below).

Studies were carried out using poly(ethylene glycol) monomethyl ether (PEG) to determine the optimum mass resolution values over the mass-to-charge ratio range of the instrument. For mass-to-charge ratios of less than 400, optimum mass resolution values were greater than 1100 fwhm. The optimal mass resolution value was noticed to decrease as the mass-to-charge ratio increased until a mass-to-charge ratio of approximately 700 was reached. For mass-to-charge ratios in excess of 700, optimum mass resolution values appeared to stabilize around 1000 fwhm. Note that optimal mass resolution values were not measured for mass-to-charge ratios greater than ~1000 because of the inability to resolve isotopes. Figure 5.2 shows two examples of the mass resolution capabilities of this instrument using two peptides. Figure 5.2 (A) shows isotopic resolution of the $[M + 2H]^{2+}$ peak for a small peptide with the sequence FIPK. The mass resolution of the monoisotopic peak, shown in the inset, is 1125 fwhm. Figure 5.2 (B) shows a mass spectrum for bradykinin in which the mass resolution is only 560 fwhm by definition. However, the various isotopes of the peptide are clearly distinguishable in this figure. Consequently, although the instrumental mass resolution for each isotope is approximately 1000 fwhm, the width of the isotopes causes this overlap thereby degrading the observed mass resolution. Note that this is not a typical mass spectrum of bradykinin; the conditions used in Figure 5.2 were manipulated to produce this peak preferentially.

The mass resolution capabilities of this instrument for larger analytes are illustrated in Figure 5.3 using equine cytochrome c and bovine serum albumin. Figure 5.3 (A) shows a typical mass spectrum observed for a smaller protein, equine cytochrome c, in which the mass resolution of the $[M + 16H]^{16+}$ peak, shown in the inset, is 1020 fwhm. Note that the mass resolution values of most of the other major peaks in the equine cytochrome c mass spectrum were also ~1000 fwhm. For proteins larger than ~20 000 u, the optimal mass resolution values decrease. For example, optimal mass resolution values of bovine trypsinogen (MW 23 981.0) and bovine carbonic anhydrase II (MW 29 023.7) were only approximately 600 and 400 fwhm, respectively. Shown in Figure 5.3 (B) is a smoothed mass spectrum of bovine serum albumin (MW ~ 66 430) in which the charge states are no longer baseline resolved (mass resolution is 53 fwhm for the $[M + 35H]^{35+}$ peak). One reason the degradation of mass resolution occurs was that these ions had higher initial kinetic energies as they entered the ion trap and therefore it was harder to trap and cool them [10]. The situation was further complicated by space charge effects, discussed in section 5.3.4. Figure 5.4 shows that the degradation of the mass resolution for these larger analytes is not due to a mass-to-charge ratio trapping limit of the ion trap itself. In this figure, the mass spectrum of chicken lysozyme, Figure 5.4 (A), occurs at higher mass-to-charge ratio values than the mass spectrum shown for bovine carbonic anhydrase II, Figure 5.4 (B). For chicken lysozyme, the mass resolution of the most intense peak, shown in the inset, is ~980 fwhm. However, for bovine carbonic anhydrase II, the mass resolution for the $[M + 34H]^{34+}$ peak, shown in the inset, is only ~400 fwhm. Note that the situation for the larger proteins was further complicated because of adduct formation (discussed in Chapter 4 [11]). When compared with smaller analytes, the larger proteins formed adducts more readily and if they were not removed, these adducts degraded the quality of the mass spectrum. To dissociate these adducts, larger voltage drops between the nozzle and sampling plate were often required. Unfortunately, this voltage increase also resulted in an increase in ion kinetic energy, consequently, ion trapping efficiency was reduced.

5.3.2 Mass Range.

Large proteins, such as anti-bovine IgG (antibody developed in rabbit, ~150 000 u), have been detected using the electrospray ionisation ion trap/TOFMS with the highest mass-to-charge ratios approaching ~ 5500. Unfortunately, a dramatic decrease in mass resolution for these analytes was observed, as was discussed above, and therefore the analytical utility of this instrument for these high mass analytes was compromised. Potentially, by addressing some important concerns (see section 5.3.8), the usable mass range could be significantly increased.

The maximum mass-to-charge ratio values observed using the ion trap/linear TOFMS were limited by the rf generator. The range of frequencies that the rf generator delivered were restricted between about 0.7 and 1.1 MHz, and the maximum output voltage was approximately 3 kV_{p-p}. Note that although the maximum output of the rf generator is 5 kV_{p-p}, it was not used above 3 kV_{p-p} because above this voltage the rf cannot be shut off during the ion extraction event. Inevitably, this would lead to erroneous mass assignments as is discussed in section 5.3.6.

The upper mass-to-charge ratio limit in the ion trap is extended by decreasing the rf trapping frequency. This observation was derived from the "pseudopotential well" model, discussed in Chapter 1 [12]. This model, approximates the depth, in terms of potential energy, of a trapping well in both r and z-dimensions for a given m/z ion under specific conditions. From this model, the well depth is directly related to the square of the amplitude of the trapping voltage and inversely related to the square of the trapping frequency. It follows that reducing the trapping frequency increases the depth of the trapping well and therefore increases the upper mass-to-charge ratio limit, if all other variables remain unchanged. Qualitatively, this was observed for anti-bovine IgG because at the maximum rf output, changing the trapping frequency from 960 kHz to 760 kHz resulted in a shift of the upper mass-to-charge ratio limit from ~4000 to ~5500 for this analyte. Thus, using a rf generator with a lower frequency range could enable larger mass-to-charge ratio ions to be effectively trapped and therefore observed in the final mass spectrum.

Another important observation relevant to extending the mass-to-charge ratio limit of the system is related to the kinetic energy of the ions as they enter the ion trap. Drastically changing the ion optics, by applying a slightly negative voltage to the sampling plate, changed the range of the mass-to-charge ratios observed. This occurred because trapping of an ion is easier when its initial kinetic energy entering the ion trap is low (this was achieved here through a reduction in ion velocity). Trapping ions in this manner is particularly useful for ions with large mass-to-charge ratios when the rf generator is already near or at its maximum output. Unfortunately, the major problem with applying a negative voltage to the sampling plate was that the signal intensity was also dramatically reduced due to a defocussing of the ion beam. The importance of this observation will become apparent when the proposed use of a rf-only quadrupole to control the kinetic energy of the ions is discussed in section 5.3.8.

5.3.3 Effect of the Buffer Gas and Trapping Time.

The effect of trapping time was examined, at different buffer gas flow rates, for many analytes. In this experiment, four mass spectra representing 250 consecutive ion trap extraction events were collected for each set of conditions. From these mass spectra, both the mass resolution (fwhm) and the peak area of the analyte were determined. The error bars in the subsequent figures represent one standard deviation from the mean of the four mass spectra. Note that in all figures in which gas was not present, the gas line was physically disconnected to preclude the possibility of gas leaking into the ion trap through the needle valve. Based on mass considerations, the behaviour of all the analytes studied was broadly classified into one of two groups.

The behaviour of analytes with masses up to approximately 1000 u was extensively studied and the important points are illustrated below using a small peptide, FIPK. Figures 5.5 (A) - (F) show the effect of changing the trapping time, for different flow rates of the helium buffer gas, on the peak area of FIPK. Figures 5.6 (A) - (F) show the subsequent effects on the peak width and hence mass resolution. The figures show that the addition of even a small amount of buffer gas significantly affects the mass spectra. This is not surprising since the addition of buffer gas to the ion trap has been shown to significantly increase both the sensitivity and mass resolution of an analyte using both conventional [13] and TOF mass analysers [6]. Helium gas removes kinetic energy from ions entering the ion trap (improved trapping efficiency) and cools the ions to the centre of the ion trap at a much faster rate (improved mass resolution). Furthermore, Figure 5.6 shows that the presence of buffer gas is more critical when shorter trapping times (< 100 ms) are used. It is important to emphasize that at typical operating conditions (trapping times of 250 ms), increasing the buffer gas flow rate, up to 0.54 mL/min, resulted in significant improvements in peak area without significantly increasing the peak width. Further increasing the helium flow rate to 0.72 mL/min resulted in even larger peak areas, however this slight improvement was overshadowed by the resulting detrimental effect on the peak width.

The behaviour of larger analytes was considerably different from the above discussion of the low mass analytes. Equine cytochrome c was used as an example of this type of analyte. Figures 5.7 (A) - (E) show the effect on the area of the $[M + 16H]^{16+}$ peak as a function of the trapping time, for five different helium flow rates. Figures 5.8 (A) - (E) show the subsequent effects on the width of the $[M + 16H]^{16+}$ peak and therefore mass resolution also. Other charge states of equine cytochrome c were also examined and qualitatively, the behaviour for the most intense charge states was similar to what is observed in Figures 5.7 and 5.8. For the larger analytes, the addition of buffer gas does not offer the same advantages that it did for the low mass analytes. Figure 5.7 illustrates that, when longer trapping times are used (i.e., times greater than 100 ms), the increase in peak area from the addition of buffer gas is considerably less than what was observed for the low mass analytes. Furthermore, for these longer trapping times, the peak widths, shown in Figure 5.8, significantly increase when modest buffer gas flow rates are used (i.e., flow rates greater than 0.20 mL/min). In fact, the optimal flow rate for simultaneously optimizing peak area and peak width for typical operating conditions is only 0.03 - 0.07 mL/min. Note that only for the shortest trapping times is the addition of larger flow rates of helium to the ion trap advantageous.

This limitation is thought to be a result of the effect of pressure on a TOF mass analyser. Since the ion trap serves not only as an ion storage device, but also as the extraction region for the TOF, a conflict arises with this combination because higher vacuum pressures degrade the quality of a TOF mass spectrum [14]. The higher pressure in the ion extraction region inevitably causes collisions between the buffer gas and analyte during the extraction event. For linear TOF instruments, deterioration of mass resolution is the major effect observed with high pressure [14]. Consequently, for trapping times longer than ~ 100 ms, a dramatic increase in the peak width was observed for larger analytes (i.e., small proteins) once a small flow rate of helium into the trap was surpassed (> 0.07 mL/min). The reason that the effect is observed with larger analytes, and not with smaller analytes, is likely due to the larger cross sectional area of the protein. Note that for proteins larger than equine cytochrome c, such as bovine trypsinogen and bovine carbonic anhydrase II, these effects were even more pronounced using this instrument. Based on the above discussion, it is expected that the mass spectra obtained could be significantly improved by using a more effective way of controlling the kinetic energy of ions entering the trap in combination with a cooling method that does not involve a buffer gas (see section 5.3.8).

5.3.4 Space Charge Effects.

High number densities of ions in the ion trap have adverse effects on mass resolution [10]. Space charge effects in the ion trap/linear TOFMS were studied by varying the concentration of an analyte for a given set of conditions. For this study, the optimum helium flow rate for each analyte was used, and the trapping time was 250 ms. The results for four different analytes are summarized in Table 5.1. Note that every point in the table represents a statistical analysis of nine mass spectra (each mass spectrum is a sum of 500 consecutive ion extraction events).

Table 5.1 Effect of concentration on the observed peak width for various analytes.

	Peak Width (ns)			
Analyte Concentration (μM)	FIPK $[M + 2H]^{2+}$	Bovine Insulin $[M + 6H]^{6+}$	Equine Cytochrome c $[M + 16H]^{16+}$	Equine Apomyoglobin $[M + 19H]^{19+}$
2.0	11.2 ± 0.2	22.1 ± 0.2	18.5 ± 0.5	28.7 ± 1.5
1.0	-	21.5 ± 0.3	17.6 ± 0.2	24.1 ± 1.1
0.4	11.2 ± 0.2	20.9 ± 0.3	16.2 ± 0.2	19.7 ± 1.0

Small analytes, represented by FIPK in the table, do not show a dependence on concentration over the range studied. However, for all the proteins examined, the peak widths increase with increasing concentration. This effect was consistently observed for all charge states of all of the proteins. Furthermore, the effect is the most dramatic for the largest of the three proteins in the table, equine apomyoglobin, as the peak width increases by ~ 50% over the narrow concentration range studied. Unlike the smaller analytes, proteins contain more charges, thereby the repulsion by the like charges becomes more significant in the ion trap. Note that at higher buffer gas pressures (0.20 mL/min and 0.40 mL/min), this effect was not observed presumably because collisions during the extraction event limited the mass resolution.

5.3.5 Mass-to-Charge Ratio Discrimination.

One major advantage of using a TOF mass analyser is the ability to collect a complete mass spectrum with every ion extraction event. Consequently, any effect that leads to mass-to-charge ratio discrimination would greatly reduce the effectiveness of using the TOF mass analyser and limit the utility of this instrument. Figures 5.9 and 5.10 illustrate some problems associated with mass-to-charge ratio discrimination encountered using this instrument.

Figures 5.9 (A) - (D) show four mass spectra of equine apomyoglobin that were sequentially obtained while only changing the rf voltage. Figure 5.9 illustrates that at different rf voltages, the apparent distribution of this protein markedly changes. This type of mass-to-charge ratio discrimination is a limitation of the instrument as the ability of the TOF to collect a complete mass spectrum with each ion extraction event is compromised. Figures 5.10 (A) and (B) show two mass spectra of equine cytochrome c that bring up an important point concerning mass-to-charge ratio discrimination. The two figures were obtained using identical conditions, except in Figure 5.10 (A) the flow rate of helium gas into the ion trap was 0.03 mL/min, while in Figure 5.10 (B) the flow rate was 0.32 mL/min. The figures show that there are significantly more charge states when the buffer gas flow rate is increased. In particular, the ions with the most charges show the largest improvements in signal intensity. This occurs since the kinetic energy (E_K) is directly proportional to the charge (z) on the ion (i.e., $E_K = zeV$). This result emphasizes the importance of reducing the kinetic energies of the ions entering the ion trap and implies that the degree of mass-to-charge ratio discrimination is greatly influenced by this variable. However, the mass resolution of the mass spectrum shown in Figure 5.10 (B) was significantly reduced due to the presence of the buffer gas. Again, the need for a more effective way of controlling the kinetic energy of the ions before they enter the ion trap along with a cooling method that does not degrade the quality of a TOF mass spectrum is required.

5.3.6 Mass Accuracy

5.3.6.1 Considerations for Ion Trap/TOFMS

At the time this set of experiments was carried out, this important issue had not yet been fully addressed for an ion trap/TOFMS. With this type of instrument, mass accuracy was highly dependent upon the delay time used. The reason for this is that if extraction is initiated before the rf voltage has decayed to 0 V, then the field between the exit endcap and the ring electrode becomes variable with time (see Figure 3.2). Consequently, ions with different mass-to-charge ratio values exit the ion trap at different times and experience different fields during ion extraction leading to an incorrect assignment of mass values. As the rf trapping voltage is increased, the decay time also increases, consequently, errors in mass accuracy become more pronounced. If the delay only affected mass accuracy, then using a long delay would provide a simple solution. However, when typical operating conditions are used, longer delays also have an adverse effect on the peak area of the analyte.

A study was carried out to illustrate these effects using equine cytochrome c. Two different delays were examined, for each delay, 10 mass spectra representing 500 ion extraction events each, were collected. One delay, 230 ns, represented the delay when the peak area of the analyte was at a maximum, while the other delay, 4 μs, represented the delay necessary for the rf to decay to 0 V. For purposes of the following discussion they are referred to as short and long delay, respectively. Peak area, mass resolution (peak widths), and mass accuracy were examined in this study. Table 5.2 shows a comparison of these parameters obtained using the different delay times. Note that in this table, peak areas and peak widths are shown for the most intense peak, $[M + 16H]^{16+}$, only.

Table 5.2 Comparison of peak area, peak width, and mass accuracy at different delay times of ion extraction after the rf voltage is turned off.

		Short Delay (0.23 μs)	Long Delay (4 μs)
Peak Area (Relative Units)		50 800 ± 1700	36 000 ± 1000
Peak Width (ns)		17.2 ± 0.3	16.7 ± 0.3
Mass Accuracy (error in ppm)	$[M + 18H]^{18+}$	−360	−39
	$[M + 17H]^{17+}$	−530	9
	$[M + 16H]^{16+}$	−600	25
	$[M + 15H]^{15+}$	−525	42
	$[M + 14H]^{14+}$	−340	32

Note that the mass accuracy values were calculated using internal standards ([M + 13H]$^{13+}$ and [M + 19H]$^{19+}$) and a two-point linear calibration. The standard deviation of the mass accuracy error values were, on average, ±60 ppm for the long delay and ±75 ppm for the short delay. Table 5.2 shows that a long delay gives the best mass accuracy values. However, the peak area is less using this delay.

A recent development using fast rf clamping [15] suggests that mass accuracy with this instrument at short delay times can be potentially improved. The rf clamping concept, introduced by Chambers et al. [15], involves an immediate drop of the rf voltage to ground potential after shutting off the rf voltage. This clamp allows extraction of the ions to occur almost immediately after termination of the rf voltage without causing changes in the acceleration voltage during extraction that will adversely affect the mass accuracy. Improvements in sensitivity and mass resolution have been demonstrated for a small analyte (m/z = 69) using this "clamping circuit" compared with a circuit that allows the rf to decay [15].

5.3.6.2 Mass Accuracy Values for Electrospray Ion Trap/TOFMS

This section explores the mass accuracy values that were obtained using the ion trap/linear TOFMS. Four different types of analyses were considered, namely internal standard (both with and without isotopic resolution), and external standard (both with and without isotopic resolution).

The use of an internal standard with isotopic resolution represents the best situation for mass accuracy measurements using this instrument. A solution of Poly (ethylene glycol) monomethyl ether (PEG) was used as the analyte for this type of analysis. The structure of PEG along with a typical mass spectrum are presented in Figure 5.11. Three distributions were present in this mass spectrum, an expanded version of the oligomer with 12 repeat units is shown in the inset in the figure. The major distribution was a result of a sodiated molecular ion peak, $[M + Na]^+$, while the secondary distribution represented $[M + K]^+$. The smallest distribution, labelled $[M' + Na]^+$ represented a contaminant (i.e., PEG without the terminal methyl group). The oligomers corresponding to x values of 8 and 15 were used as the internal standards. Ten mass spectra (each was a sum of 500 consecutive ion extraction events) were collected. The mass accuracy of the 6 oligomers between the two calibrant ions was determined. Note that a shift in the peak position by one point (1 ns) on the digital oscilloscope, at a mass-to-charge ratio of ~ 500, corresponded to a change in mass of ~ 0.04 u. Since this represents a mass accuracy error of 80 ppm, an interpolation function was used to increase the number of points by a factor of 10, thereby reducing the error associated with sampling. Table 5.3 gives a summary of the mass accuracy information obtained from this experiment.

Note that the average error corresponds to approximately 1 point (8 ppm) in the interpolated mass spectrum. Further improvements may be expected by using a larger number of points in the interpolation function. However, this could not be tested because interpolation functions larger than '10 points/data point' required more computer memory than was available.

Table 5.3 Mass accuracy obtained using an internal standard with isotopic resolution.

Mass spectrum	x = 9	10	11	12	13	14
1	451.248	495.281	539.305	583.326	627.357	671.379
2	451.248	495.282	539.308	583.338	627.361	671.393
3	451.248	495.277	539.310	583.332	627.361	671.392
4	451.248	495.280	539.317	583.339	627.375	671.403
5	451.256	495.283	539.314	583.334	627.368	671.399
6	451.242	495.274	539.307	583.328	627.350	671.385
7	451.241	495.277	539.308	583.334	627.357	671.382
8	451.241	495.281	539.310	583.334	627.357	671.392
9	451.251	495.290	539.320	583.344	627.379	671.406
10	451.251	495.291	539.307	583.331	627.358	671.375
mean ($\bar{x}$)	451.247	495.282	539.310	583.333	627.362	671.391
s	0.005	0.005	0.005	0.005	0.009	0.010
error (ppm)	-10	7	11	6	9	11

The use of an external standard with isotopic resolution was carried out using PEG as the analyte and polypropylene glycol as the calibrant. In particular, the oligomers with 7 repeat units (MW = 447.293) and 11 repeat units (MW =679.461) were used as the calibrant ions. The mass accuracy results obtained for the PEG oligomers with 9 through 14 repeat units are presented in Table 5.4.

Table 5.4 Mass accuracy obtained using an external standard (isotopic resolution).

Mass spectrum	x = 9	10	11	12	13	14
1	451.249	495.292	539.314	583.336	627.343	671.371
2	451.260	495.288	539.310	583.336	627.357	671.385
3	451.264	495.288	539.319	583.336	627.357	671.380
4	451.252	495.292	539.310	583.318	627.357	671.371
5	451.256	495.292	539.314	583.336	627.348	671.375
6	451.260	495.292	539.319	583.327	627.357	671.385
7	451.256	495.292	539.314	583.331	627.353	671.380
8	451.256	495.292	539.314	583.331	627.353	671.385
9	451.260	495.296	539.319	583.331	627.353	671.380
10	451.264	495.292	539.310	583.345	627.348	671.371
mean ($\bar{x}$)	451.258	495.292	539.314	583.333	627.353	671.378
s	0.005	0.001	0.003	0.007	0.005	0.006
error (ppm)	13	28	18	4	−7	−7

The use of an internal standard without isotopic resolution is illustrated using a 1 μM solution of equine cytochrome c. The $[M + 13H]^{13+}$ and $[M + 19H]^{19+}$ ions were used as the calibrants, the results are presented in Table 5.5.

Table 5.5 Mass accuracy obtained using an internal standard (non isotopic resolution).

Mass spectrum	$[M + 18H]^{18+}$	$[M + 17H]^{17+}$	$[M + 16H]^{16+}$	$[M + 15H]^{15+}$	$[M + 14H]^{14+}$
1	687.661	728.059	773.521	825.128	883.897
2	687.580	727.983	773.446	824.996	883.891
3	687.648	728.055	773.490	825.013	883.768
4	687.651	728.088	773.583	825.044	883.938
5	687.658	728.093	773.533	825.042	883.927
6	687.621	728.108	773.580	825.136	883.987
7	687.659	728.068	773.507	825.025	883.924
8	687.702	728.123	773.577	825.041	883.919
9	687.671	728.075	773.506	824.972	883.798
10	687.662	728.116	773.572	825.081	883.944
mean ($\bar{x}$)	687.651	728.077	773.532	825.048	883.899
s	0.032	0.040	0.046	0.053	0.067
error (ppm)	-39	9	25	42	32

For mass accuracy measurements of proteins that are not isotopically resolved, a limiting factor is due to variations in the isotopic distribution of the analyte. Based on the terrestrial average of the $^{13}C/^{12}C$ ratio, the molecular mass of a protein can be calculated only to within ± 40 ppm [16].

The use of an external standard when isotopic resolution cannot be achieved represents the worst situation for mass accuracy measurements. An example of this type of analysis was carried out using equine apomyoglobin as the analyte. The $[M + 12H]^{12+}$ and $[M + 18H]^{18+}$ ions of equine cytochrome c were used for calibration. The masses of five different charge states of equine apomyoglobin based on this calibration are presented in Table 5.6.

Table 5.6 Mass accuracy values obtained using an external standard (non isotopic resolution).

Mass spectrum	$[M + 22H]^{22+}$	$[M + 21H]^{21+}$	$[M + 20H]^{20+}$	$[M + 19H]^{19+}$	$[M + 18H]^{18+}$
1	771.573	808.288	848.671	893.244	942.739
2	771.615	808.285	848.638	893.211	942.778
3	771.467	808.279	848.612	893.255	942.699
4	771.651	808.222	848.601	893.249	942.835
5	771.426	808.196	848.638	893.304	942.739
6	771.661	808.243	848.628	893.238	942.711
7	771.656	808.285	848.606	893.211	942.812
8	771.472	808.243	848.644	893.266	942.795
9	771.595	808.243	848.638	893.216	942.716
10	771.615	808.206	848.617	893.288	942.756
mean ($\bar{x}$)	771.573	808.249	848.629	893.248	942.758
s	0.092	0.034	0.021	0.032	0.046
error (ppm)	65	43	64	72	9

5.3.7 Bipolar Extraction

The concept of bipolar extraction using an ion trap/TOFMS was independently introduced by Mordehai et al. [17] and Chambers et al. [15]. Conventional extraction techniques for an ion trap/TOFMS involve the application of a negative voltage pulse to the exit endcap (unipolar extraction). Bipolar extraction involves simultaneous application of a positive voltage pulse to the entrance endcap and a negative voltage pulse to the exit endcap. Theoretical calculations using an ion simulation program (SIMION) were used by both authors to demonstrate that improvements in sensitivity and mass resolution are expected with bipolar extraction. Chambers et al. also reported an improvement experimentally as their mass resolution values increased from ~750 to ~2200 using an ion trap/reflectron TOFMS [15].

In light of these findings, a series of bipolar extraction experiments were carried out using the ion trap/linear TOFMS. One of the more difficult aspects of applying the bipolar extraction technique was trying to synchronize the two different high voltage pulse generators as was discussed in the experimental section. Table 5.7 shows a comparison of results obtained using unipolar extraction and bipolar extraction for PEG. Note that the mass spectra were calibrated using the same procedure as described in section 5.3.6.2 for an internal standard with isotopic resolution.

From the table, both the peak area and the mass resolution values obtained using bipolar extraction are comparable with the results obtained using unipolar extraction at low mass-to-charge ratios, but are significantly lower at higher mass-to-charge ratios. The errors in mass accuracy using bipolar extraction are larger than unipolar extraction, although theoretically, a more uniform field exists across the ion trap. Consequently, the use of bipolar extraction did not improve the performance this ion trap/linear TOFMS. However, the effect of the different rise/fall times of the high voltage pulse generators on these results cannot be determined. Note that the drastic improvement in mass resolution Chambers et al. observed may have been due largely to an unoptimized system. The optimal mass resolution value they obtained with their reflectron TOFMS before the application of the bipolar technique was only 750 [15]. This is well below mass resolution values of up to 3300 fwhm reported by Lubman et al. using a similar system [6].

Table 5.7 Comparison of negative extraction (only) versus bipolar extraction for PEG.

	x = 9	10	11	12	13	14
Negative extraction						
Mass accuracy error (ppm)	-10	7	11	6	9	11
Peak area (arb. units)	110	208	249	222	164	109
Mass resolution (fwhm)	1193	1159	1122	1075	1034	1004
Bipolar extraction						
Mass accuracy error (ppm)	-38	-47	-46	-45	-37	-12
Peak area (arb. units)	107	194	227	197	148	94
Mass resolution (fwhm)	1202	1136	1072	1020	955	887

5.3.8 Summary

The ion trap/linear TOFMS records mass spectra at an acquisition rate compatible with high speed separation techniques. The results presented in this chapter illustrate some current limitations of this instrument. One major limitation of this ion trap/linear TOFMS related to the deceleration and focussing of ions into the ion trap. Specifically, the results shown in this chapter indicate that the kinetic energy of ions entering the ion trap is a crucial variable for optimizing mass resolution, upper mass limit, and for maximizing the mass-to-charge ratio range observed for a mass spectrum. The kinetic energies of analyte ions entering the ion trap are adjusted using two different methods. One method involves the use of a buffer gas within the ion trap itself. The large flow rates of buffer gas necessary to reduce the kinetic energies of larger analytes results in a significant degradation of mass spectral quality. Another method of reducing the velocities of ions entering the ion trap is by adjusting the ion optics.

The current ion optics setup, consisting of the three focussing plates, was not sufficiently reducing the kinetic energy of the ions before they enter the ion trap. It has been shown that the presence of a rf-only quadrupole lens drastically reduces the kinetic energy of the ions when it is operated at high pressures [18]. Furthermore, signal intensity is not compromised as the ions were kept in a tightly focussed packet. By changing the ion optics to this type of configuration, the quality of the mass spectra should significantly improve. The rf-only quadrupole lens would particularly benefit the analysis of proteins as only small amounts of buffer gas would be required for trapping the analyte. Consequently, improvements in both peak area and mass resolution would be expected. In addition, a larger mass range and a reduction of mass-to-charge ratio discrimination should also occur. In fact, the addition of a rf quadrupole for ion focussing has resulted in improvements in sensitivity and no mass-to-charge ratio discrimination over a mass-to-charge ratio range of ~13 000 for an orthogonal TOFMS [15].

Finally, alternative methods of cooling ions in an ion trap, such as electrical ion cooling, are currently being investigated [20]. Because of the detrimental effects of the presence of buffer gas during extraction, these alternative cooling methods are expected to play a future role in development of the ion trap/TOFMS.

Many of the above limitations, due to problems such as space charge effects, mass-to-charge ratio discrimination, and kinetic energy of the ions entering the ion trap, were severe for large analytes. However, for smaller analytes, many of these limitations are not observed. Consequently, applications involving the electrospray ionisation ion trap/linear TOFMS were restricted to small analytes. The application of this instrument to larger analytes will be re-evaluated after suggested modifications to the instrument are made.

5.4 Literature Cited

1. *Time-of-Flight Mass Spectrometry;* Cotter, R. J., Ed. (American Chemical Society, Washington, DC, 1997,
2. Todd, J. F. J. *Mass Spectrom. Rev.* **1991**, *10*, 3.
3. Purves, R. W.; Li, L. *J. Microcolumn Separations* **1995**, 7, 603.
4. Michael, S. M.; Chien, M.; Lubman, D. M. *Rev. Sci. Instrum.* **1992**, *63*, 4277.

5. Michael, S. M.; Chien, B. M.; Lubman, D. M. *Anal. Chem.* **1993**, *65*, 2614.

6. Chien, B. M.; Michael, S. M.; Lubman, D. M. *Int. J. Mass Spectrom. Ion Proc.* **1994**, *131*, 149.

7. Qian, M. G.; Lubman, D. M. *Anal. Chem.* **1995**, 67, 234A.

8. Bernius, M. T.; Chutjian, A. *Rev. Sci. Instrum.* **1990**, *61*, 925.

9. Banks Jr., J. F.; Dresch, T. *Anal. Chem.* **1996**, *68*, 1480.

10. McLuckey, S. A.; Van Berkel, G. J.; Goeringer, D. E.; Glish, G. L. *Anal. Chem.* **1994**, *66*, 689A.

11. Smith, R. D.; Loo, J. A.; Edmonds, C. G.; Barinaga, C. J.; Udseth, H. R. *Anal. Chem.* **1990**, *62*, 882.

12. Major, F. G.; Dehmelt, H. G. *Phys. Rev.* **1968**, *170*, 91.

13. Stafford Jr., G. C.; Kelley, P. E.; Syka, J. E. P.; Reynolds, W. E.; Todd, J. F. J. *Int. J. Mass Spectrom. Ion Proc.* **1984**, *60*, 85.

14. Chernushevich, I. V.; Verentchikov, A. N.; Ens, W.; Standing, K. G. *J. Am. Soc. Mass Spectrom.* **1996**, 7, 342.

15. Chambers, D. M.; Thomas, S. W.; Grace, L. I.; Andresen, B. D. *Proceedings of the 43rd ASMS Conference on Mass Spectrometry and Allied Topics*; Atlanta, Georgia, May 21-26, 1995; p 1138.

16. Beavis, R. C. *Anal. Chem.* **1993**, *65*, 496.

17. Mordehai, A.; Karnicky, J.; Limbek, B.; Buttrill, S. E., Jr. *Proceedings of the 43rd ASMS Conference on Mass Spectrometry and Allied Topics*; Atlanta, Georgia, May 21-26, 1995; p 122.

18. Douglas, D. J.; French, J. B. *J. Am. Soc. Mass Spectrom.* **1992**, *3*, 398.

19. Krutchinsky, A. N.; Chernushevich, I. V.; Spicer, V.; Ens, W.; Standing, K. G. *Proceedings of the 43rd ASMS Conference on Mass Spectrometry and Allied Topics*; Atlanta, Georgia, 1995; May 21-26, 1995; p 126.

20. Weil, C.; Cleven, C. D.; Nappi, M.; Cooks, R. G. *Proceedings of the 44th ASMS Conference on Mass Spectrometry and Allied Topics*; Portland, Oregon, 1996; May 12-16, 1996; p 118.

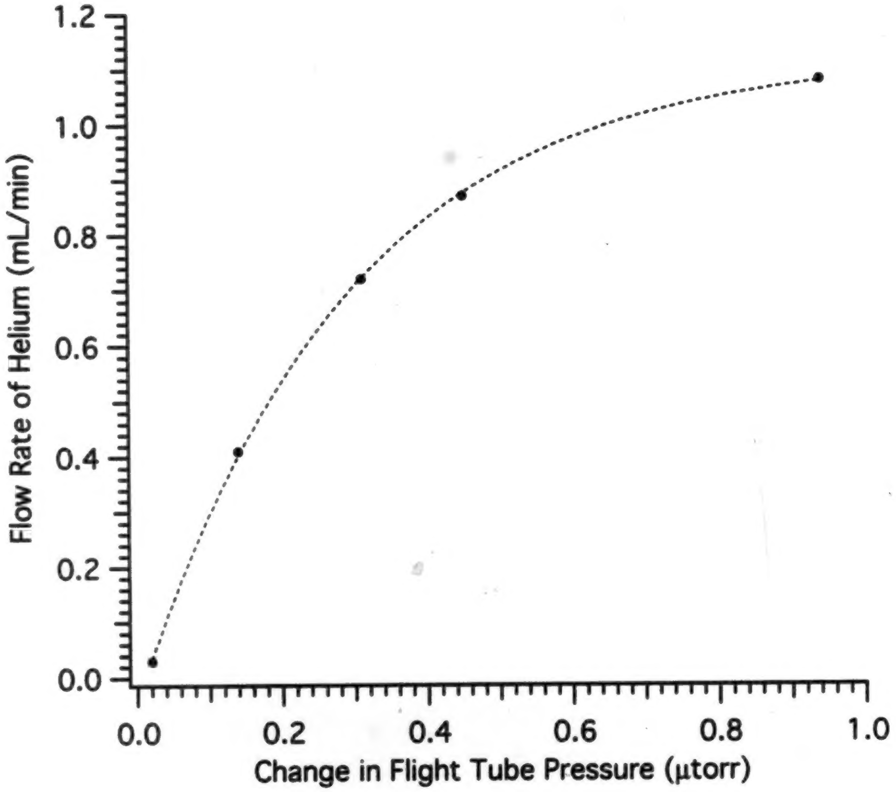

Figure 5.1 A plot of the flow rate of helium into the ion trap as a function of the change in pressure observed in the flight tube.

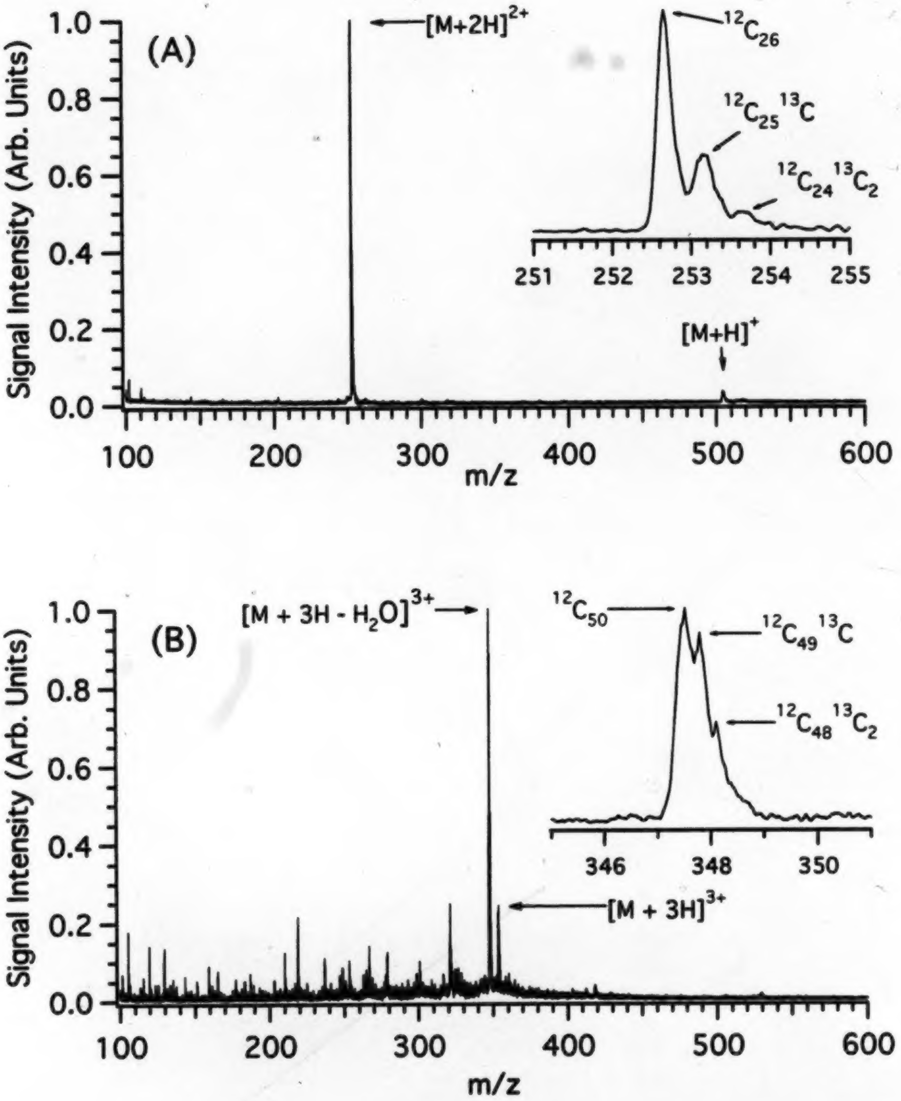

Figure 5.2 Resolution capabilities of the ion trap/linear time-of-flight mass spectrometer. (A) Mass spectrum of a small peptide, FIPK, showing isotopic resolution (inset). The rf voltage was 730 $V_{p\text{-}p}$ and the flow rate of helium into the trap was 0.20 mL/min. (B) Mass spectrum of bradykinin with mass resolution of 560 fwhm (inset). The rf voltage was 750 $V_{p\text{-}p}$ and flow rate of helium into the trap was 0.08 mL/min. The extraction conditions for both spectra are listed in the text.

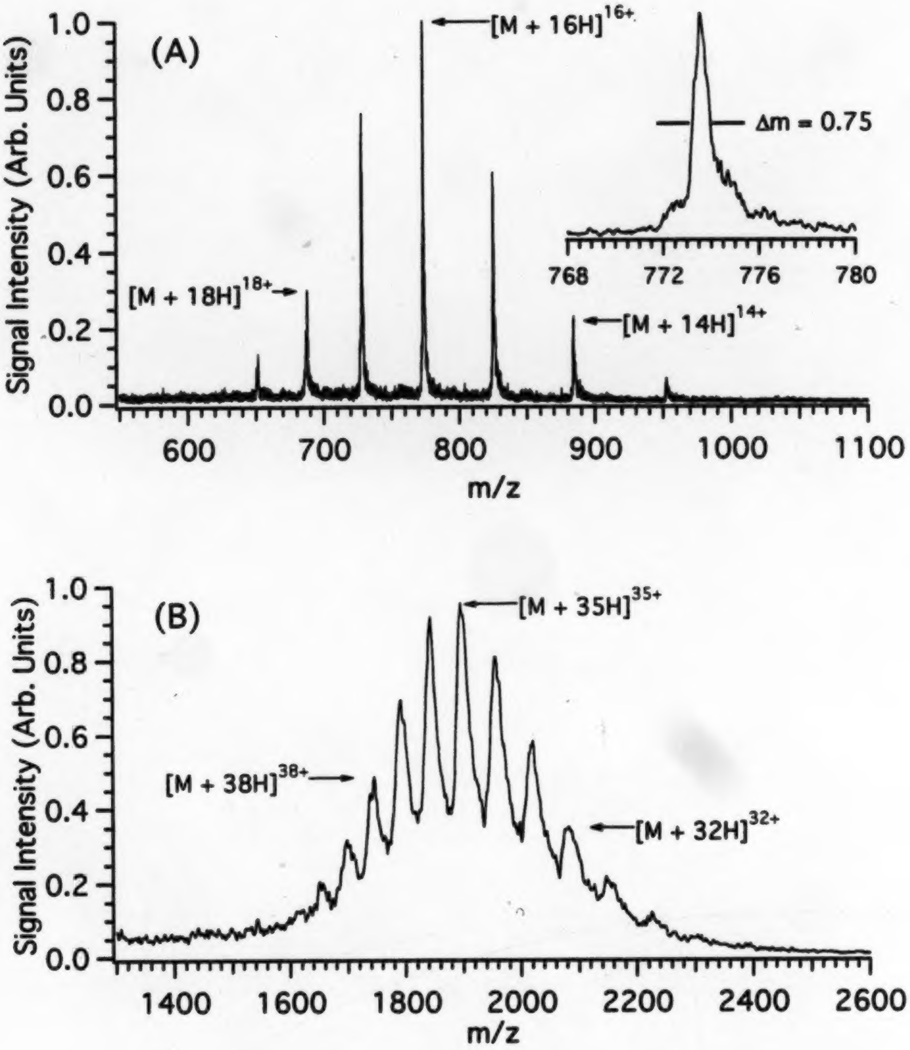

Figure 5.3 Mass resolution capabilities of the ion trap/linear time-of-flight mass spectrometer for larger analytes. (A) Mass spectrum of equine cytochrome c with a mass resolution of 1020 (inset). The rf voltage was 1650 V_{p-p} and the flow rate of helium into the ion trap 0.03 mL/min. (B) Mass spectrum of bovine serum albumin. The rf voltage was 2200 V_{p-p} and the rf frequency was 740 kHz. The trapping time was 100 ms and flow rate of helium into the trap was 0.17 mL/min.

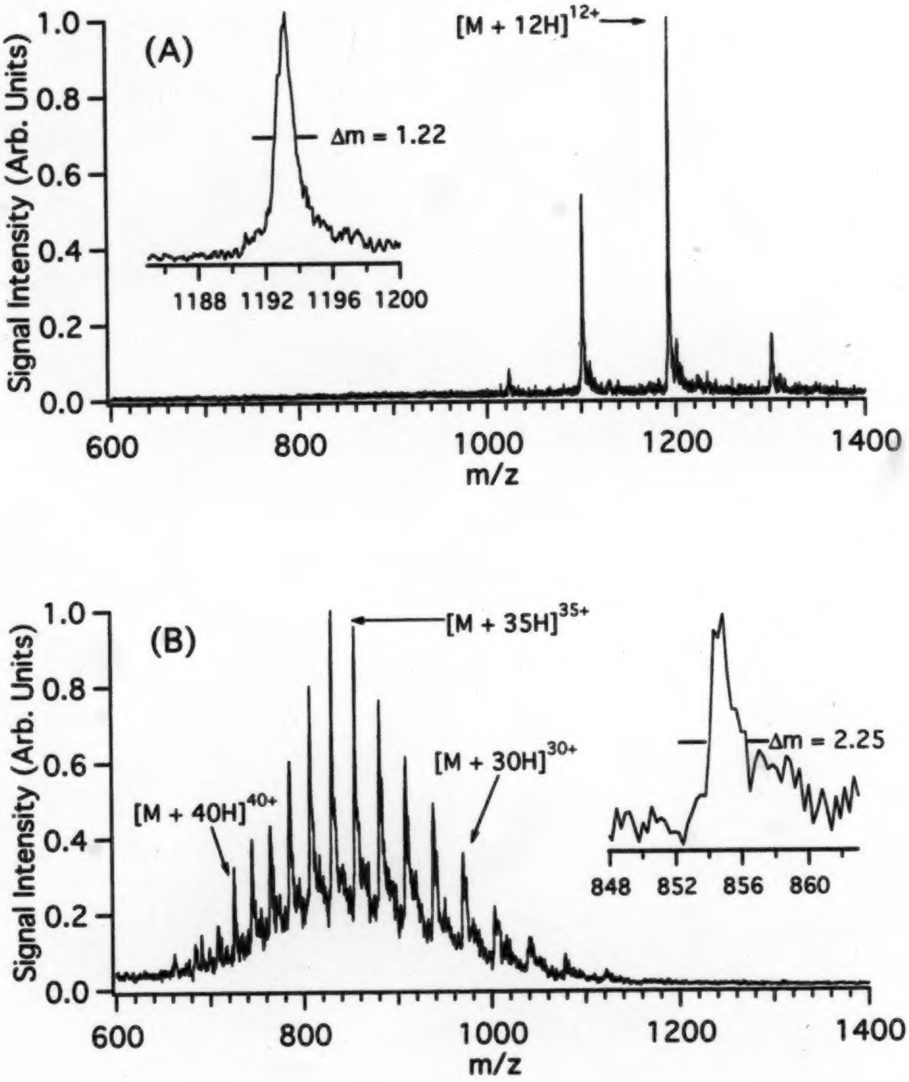

Figure 5.4 Mass spectra of (A) chicken lysozyme with a mass resolution of 980 (inset) and (B) bovine carbonic anhydrase II with a mass resolution of 400 (inset). (A) The rf voltage was 2150 V_{p-p} and flow rate of helium into the trap was 0.03 mL/min. (B) The rf voltage was 1240 V_{p-p} and flow rate of helium into the trap was 0.05 mL/min.

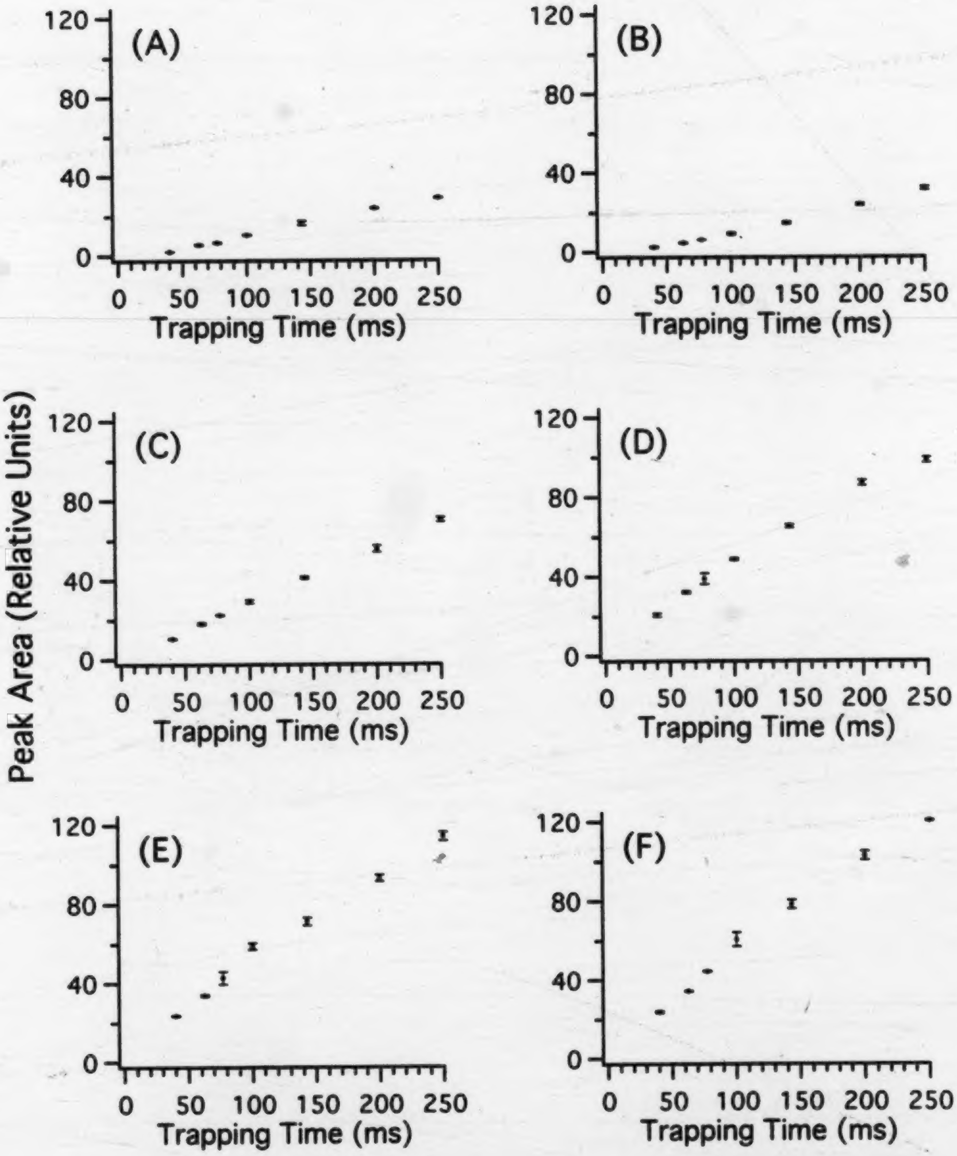

Figure 5.5 The effect of trapping time, for different flow rates of the helium buffer gas, on the peak area of FIPK. (A) 0 mL/min, (B) 0.03 mL/min, (C) 0.12 mL/min, (D) 0.40 mL/min, (E) 0.54 mL/min, (F) 0.72 mL/min. The rf voltage was 730 $V_{p\text{-}p}$.

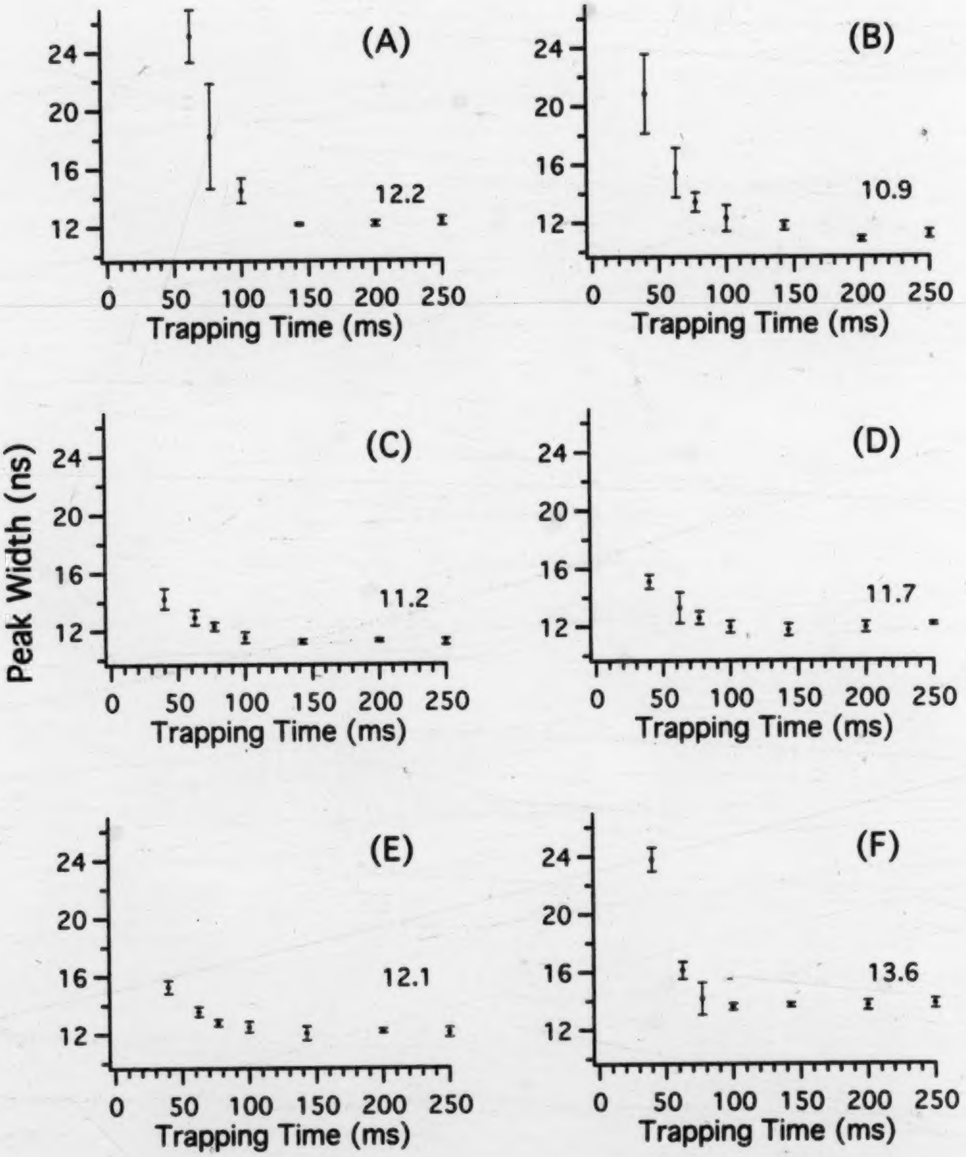

Figure 5.6 The effect of trapping time, for different flow rates of the helium buffer gas, on the peak width of FIPK. Conditions were the same as those given in Figure 5.5. The value of the minimum peak width is displayed for each helium flow rate.

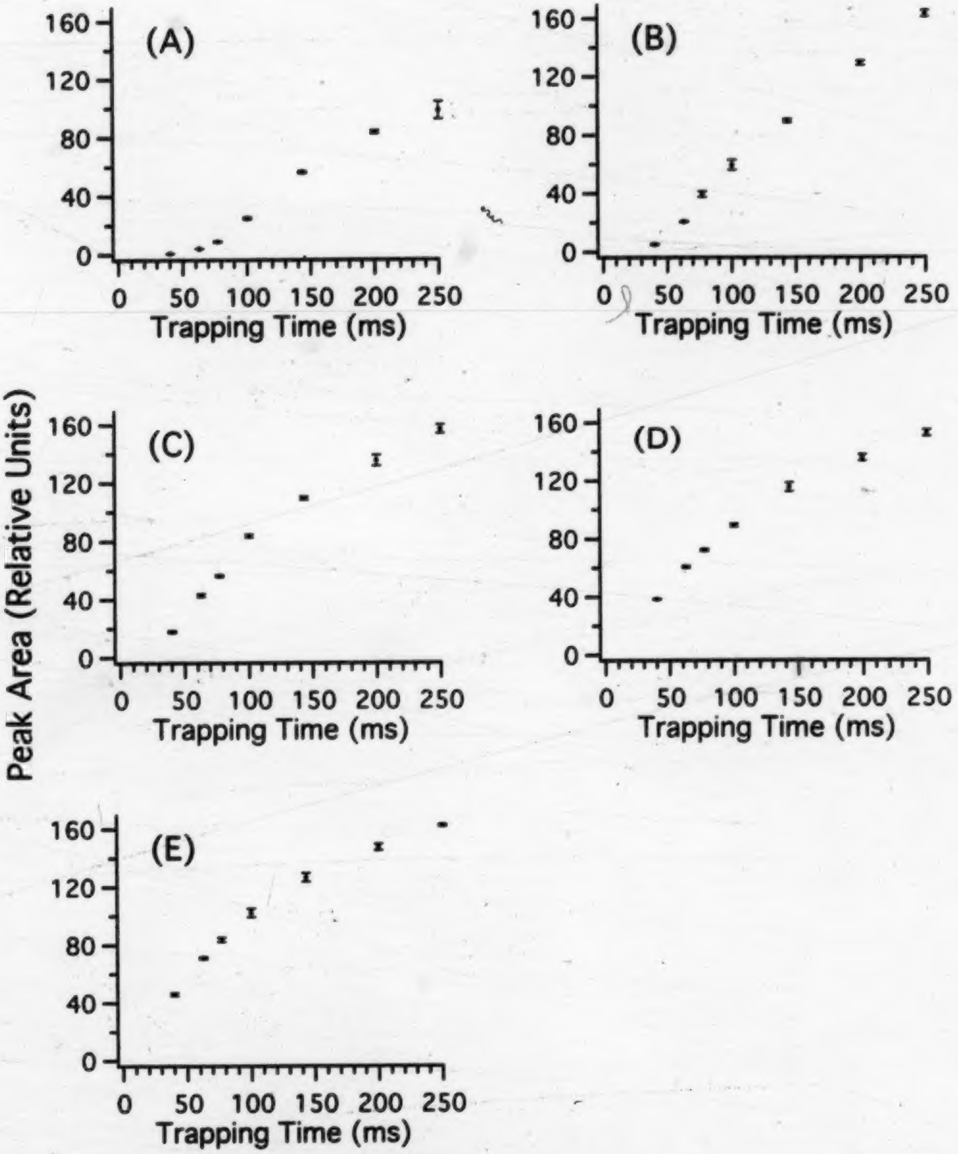

Figure 5.7 The effect of trapping time, for different flow rates of helium buffer gas, on the peak area of equine cytochrome c. (A) 0 mL/min, (B) 0.03 mL/min, (C) 0.07 mL/min, (D) 0.20 mL/min, (E) 0.40 mL/min. The rf voltage was 1650 V_{p-p}.

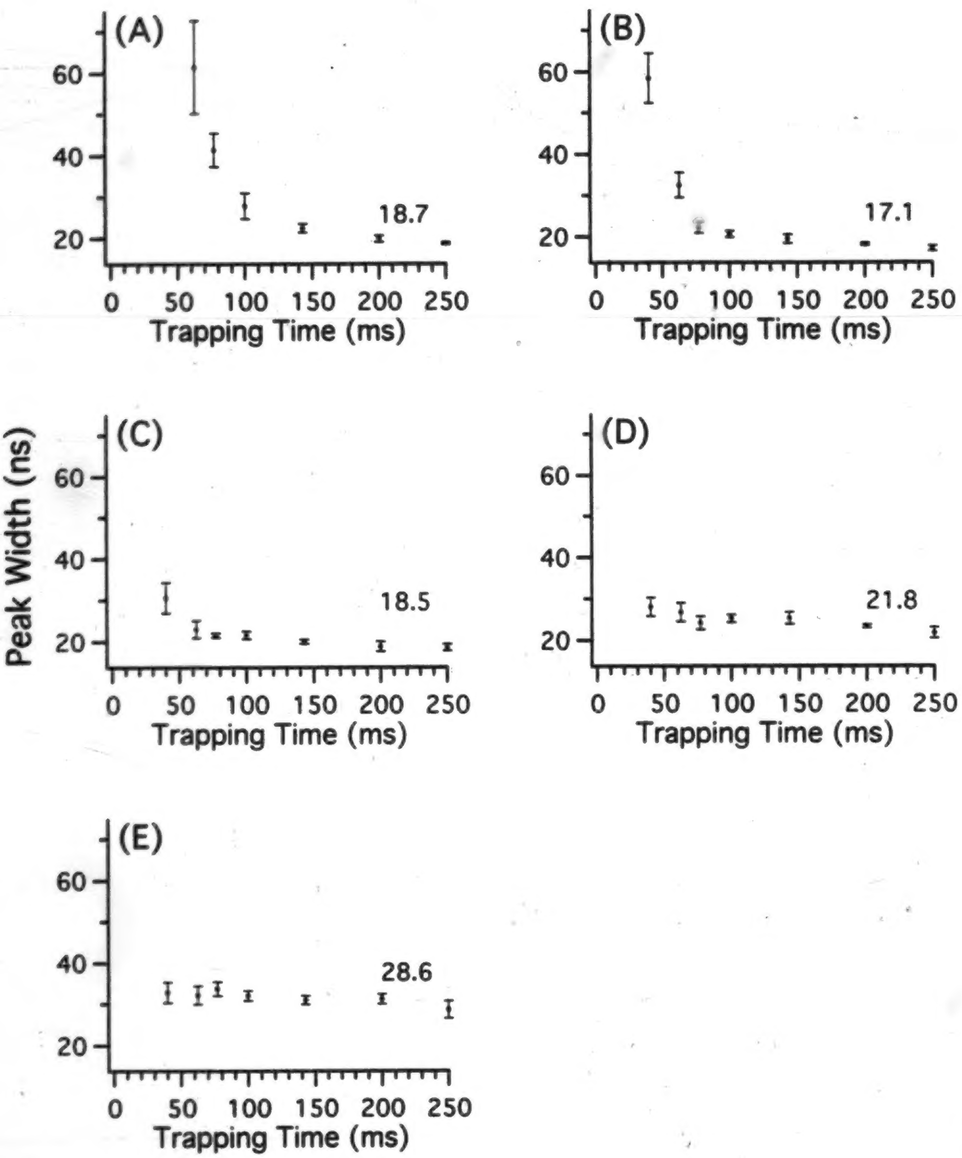

Figure 5.8 The effect of trapping time, for different flow rates of the helium buffer gas, on the peak width of equine cytochrome c. Conditions are the same as those given in Figure 5.7. The value of the minimum peak width is displayed for each helium flow rate.

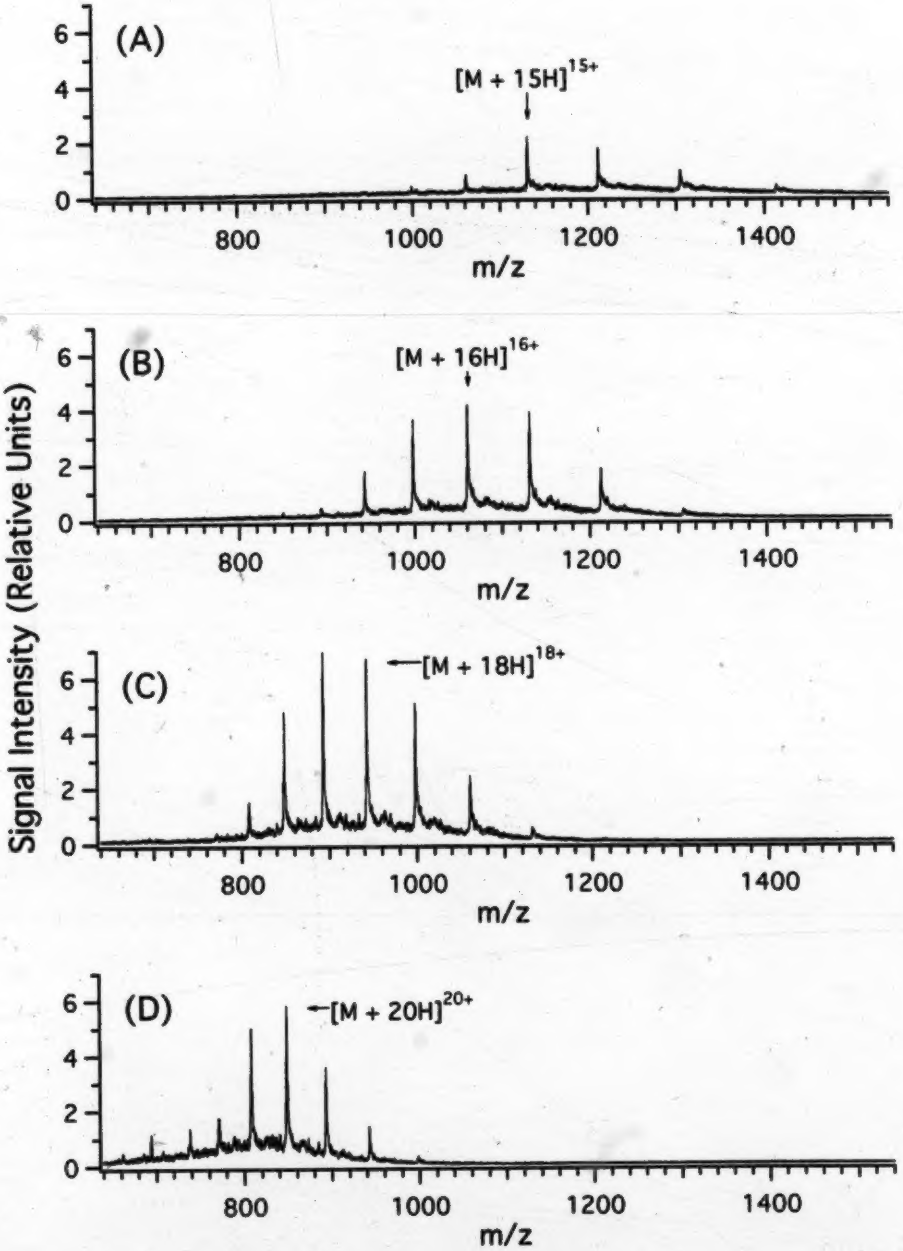

Figure 5.9 Mass-to-charge ratio discrimination observed for equine apomyoglobin. (A) rf voltage of 2250 $V_{p\text{-}p}$, (B) rf voltage of 2000 $V_{p\text{-}p}$, (C) rf voltage of 1750 $V_{p\text{-}p}$ and (D) rf voltage of 1500 $V_{p\text{-}p}$.

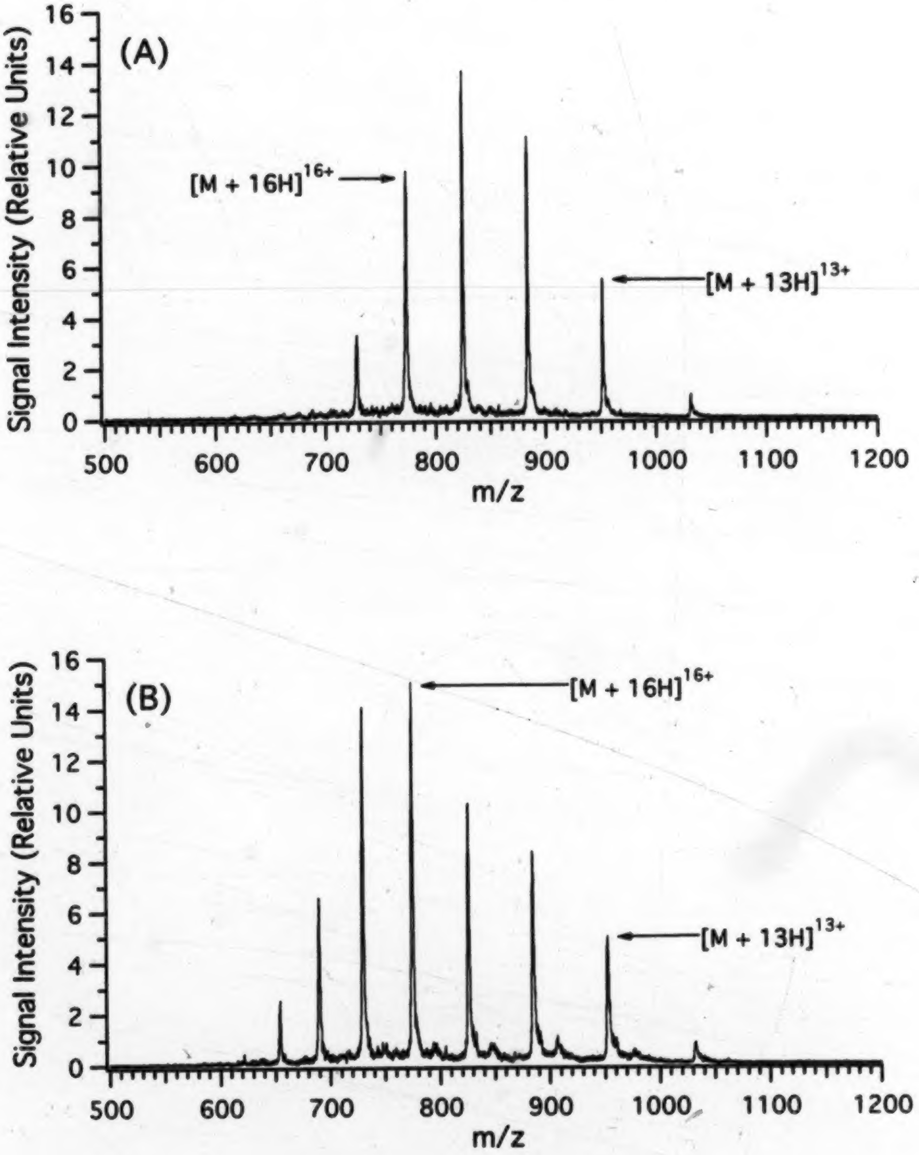

Figure 5.10 Effect of buffer gas on mass-to-charge ratio discrimination observed for equine cytochrome c. The helium flow rates are (A) 0.03 mL/min and (B) 0.32 mL/min.

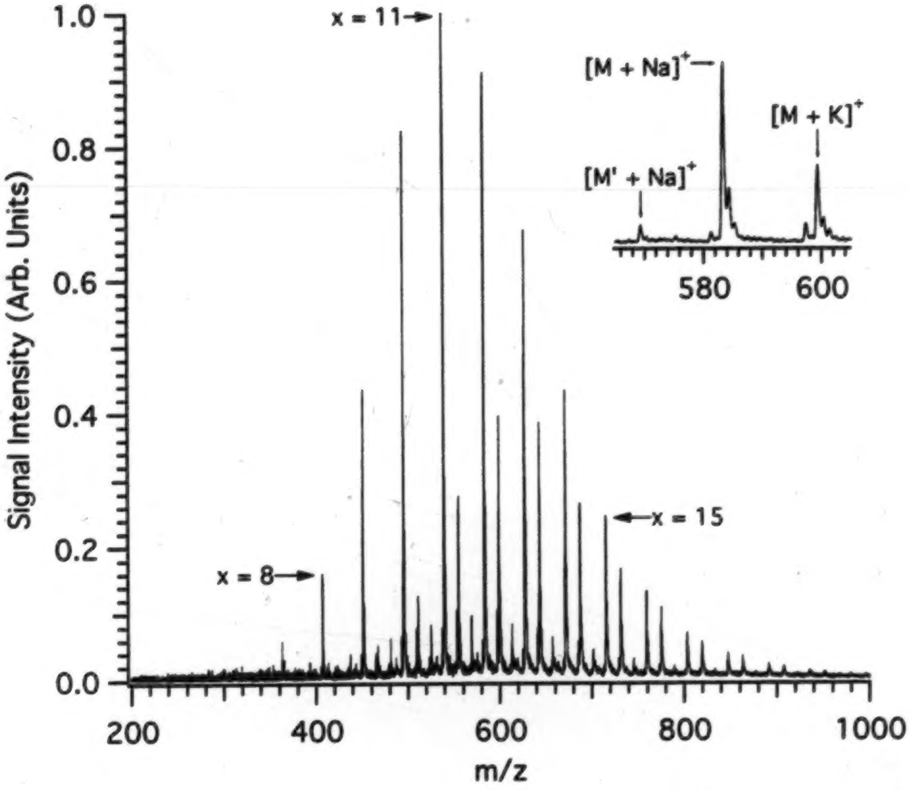

$$M = HO\text{-}(CH_2CH_2O)_x\text{-}CH_3$$

$$M' = HO\text{-}(CH_2CH_2O)_x\text{-}H$$

Figure 5.11 A mass spectrum of PEG with the three principle distributions (inset) and its corresponding structure.

Chapter 6

Quantitative Analysis Using an Electrospray Ionisation Ion Trap/Linear Time-of-Flight Mass Spectrometer[a]

6.1 Introduction

Electrospray ionisation mass spectrometry is increasingly gaining in importance in the biomedical field [1]. For example, electrospray ionisation has greatly simplified the application of quantitative liquid chromatography mass spectrometry methods to highly polar molecules in the pharmaceutical industry [1]. Traditionally, electrospray ionisation mass spectrometry and tandem mass spectrometry were commonly carried out using quadrupole mass analysers [2,3]. In comparison with the quadrupole mass analyser, an ion trap/time-of-flight mass spectrometer (TOFMS) [4,5] offers a potentially faster, more sensitive method for analysing pharmaceutical compounds. However, the quantitative capabilities of an ion trap/linear TOFMS have not been explored. In this chapter, sulphonamides are used to investigate the capabilities and limitations of an ion trap/linear TOFMS for quantitative analysis.

---

[a] A form of this chapter is in preparation for publication: R. W. Purves, W. Gabryelski, L. Li "Investigation of the Quantitation Capabilities of an Electrospray Ion Trap/Linear Time-of-Flight Mass Spectrometer for Quantitative Analysis". Data collection and data analysis were carried out by both R. W. Purves and W. Gabryelski.

Sulphonamides are antimicrobial agents that are extensively used to combat infections and/or promote growth in farm animals [6]. The level of sulphonamides in food products destined for human consumption is strictly controlled for several reasons. For example, exposure to these residues can reduce the effectiveness of human therapeutic drugs [7] and can also lead to allergic reactions in sensitive consumers [8]. Furthermore, some sulphonamides are thought to be carcinogenic [9]. Only meat products that contain sulphonamide residues below the maximum residue limit are allowed to enter the food chain [10]. Several techniques, including LC-UV [11] have been used to analyse sulphonamide residues. MS techniques, however, have the advantage of providing molecular weight information and structural data that aids in the confirmation of these residues. Detection of various sulphonamide mixtures has been carried out using electrospray ionisation or ionspray combined with LC [6, 12], capillary electrophoresis [13] or electrochromatography [14].

The focus of this chapter is on exploring considerations such as reproducibility, detection limits, and the linear range of a calibration curve. Reproducibility of the ion trap/linear TOFMS is examined for a series of injections and over an eight-hour period. Detection limits of five sulphonamides are examined and factors affecting the linearity at both ends of a calibration curve are also investigated.

6.2 Experimental

A detailed description of the ion trap/linear TOFMS used in this study was given in previous chapters [5,15]. For this chapter, the analyte was injected using a Rheodyne model 7520 injector (sample loop size of 0.5 μL). The voltages applied to the nozzle and the sampling plate were 40 V and 4 V, respectively. The first and third plates were grounded while the second plate was operated at -80 V. The rf voltage (800 V_{p-p}), was operated at 1 MHz and a range of trapping frequencies from 1 to 20 Hz was examined in this study. Data collection and data analysis were carried out using the same procedure described in Chapter 3 [16]. Note that the total peak area of an analyte for each injection was determined by measuring the area under the curve in the flow injection profile. The mass spectra presented in this study represent a consecutive sum of 40 ion extraction events obtained during the elution of the analyte, unless otherwise noted.

The flow rate of the helium buffer gas into the ion trap is a crucial variable as it has a strong influence on the peak area for low molecular weight analytes [15]. In particular, when a low buffer gas flow rate was used (i.e., less than 0.40 mL/min), small changes in the flow rate had a large effect on the peak area. When a higher flow rate was used (i.e., > 0.40 mL/min), the effect on the peak area by small changes in the flow rate was reduced. However, the use of a flow rate greater than 0.7 mL/min degraded the mass resolution. Consequently, a flow rate of 0.54 mL/min was used for this study as it gave the best compromise for maximizing peak area and mass resolution while minimizing fluctuations in peak area.

Five sulphonamides were examined in this study, their structures and corresponding exact molecular weights (to two decimal places) are given in Chart 1. Sulphadimethoxine (SDM), sulphamethazine (SMZ), sulphamerazine (SMR), sulphachlorpyridazine (SCP), and sulphathiazole (STZ) were the sulphonamides used. These sulphonamides were analysed using a solvent combination consisting of 80% acetonitrile, 20% water (v/v) and 2 mM ammonium acetate unless otherwise indicated. The sulphonamides were purchased from Sigma Chemical Company and used without further purification. Note that glass containers were used to store all of the solutions; the use of plastic containers was avoided as their use resulted in additional background peaks [17].

6.3 Results and Discussion

6.3.1 Solution Properties

In electrospray ionisation MS, the analyte distribution can be affected due to the formation of adducts from non-volatile sodium or potassium ions [18]. These adducts reduce the area of the analyte peak and therefore will adversely affect a quantitative analysis of the analyte. The addition of volatile buffers, such as ammonium acetate, to the analyte solution [13] restricts adduct formation and therefore is an important variable to be considered when analysing sulphonamides. Figure 6.1 shows the effect of varying the concentration of ammonium acetate on mass spectra obtained from continually infusing a 1 μM solution of SDM. Figure 6.1 (A) shows that with no ammonium acetate present, the mass spectrum is dominated by the $[M + Na]^+$ peak. Figures 6.1 (B) - (D) illustrate that the addition of ammonium acetate resulted in the preferential formation of the $[M + H]^+$ peak in the mass spectra. Furthermore, the intensity of the sodium adduct peak was dramatically reduced and ammonium adduct peaks were not observed. However, Figure 6.1 (D) shows that 10 mM ammonium acetate significantly suppressed the analyte signal. Consequently, a concentration of 2 mM ammonium acetate was used as experimentally it gave the best compromise between maximizing the peak area of the protonated molecule and suppressing the formation of the sodium adduct peak.

6.3.2 Detection limits and Linear Range

Figure 6.2 shows a mass spectrum obtained from an injection of a mixture containing 100 fmol of each of the five sulphonamides studied. Note that the most intense background peaks observed in this figure were sodium and potassium adduct peaks. Seven injections of a mixture of 5 fmol of each component, and seven injections of a mixture of 25 fmol of each component, were carried out. The signal-to-noise (S/N) ratios for each sulphonamide in the mixture were calculated; Table 6.1 shows the median values of these S/N ratios. The S/N values were limited at these low levels by the chemical background noise.

Table 6.1 S/N ratios for 5 sulphonamides examined in this study.

Sulphonamide	S/N ratio 5 fmol	 25 fmol
sulphadimethoxine (SDM)	7	38
sulphachlorpyridazine (SCP)	-	7
sulphamethazine (SMZ)	5	24
sulphamerazine (SMR)	5	34
sulphathiazole (STZ)	-	12

Note that S/N ratios for mixtures prepared using 0.05 mM ammonium acetate were slightly improved (up to a factor of two) compared with the mixtures prepared using 2 mM ammonium acetate. However, the use of 0.05 mM ammonium acetate should be restricted to qualitative determinations because the linear range of a calibration curve (see below) using 0.05 mM ammonium acetate was less than an order of magnitude.

For all five sulphonamides studied, a linear response for a plot of peak area versus injection amount was obtained for almost three orders of magnitude. Figure 6.3 shows a typical calibration curve for SDM with an expanded view of the low end of the curve shown in the inset. For each point on the calibration curve, seven injections were carried out and the error bars represent one standard deviation. The results for all of the sulphonamides were similar; the upper limit of linearity and the lower quantitation limit shifted depending upon which sulphonamide was being studied.

The lower limit of quantitation was restricted by the chemical background noise. Figure 6.4 shows a mass spectrum (only 25 consecutive ion extraction events) obtained from an injection of 5 fmol of SDM. The peak corresponding to the protonated molecule of SDM in this figure is barely discernable from the chemical background noise. Note that to improve the detection limit, and therefore the lower limit of quantitation, tandem mass spectrometry techniques could be carried out on the analyte of interest [19] and a corresponding fragment peak monitored. The relative improvement in noise reduction is expected to be greater than the loss of analyte signal, thereby improving the S/N ratio for low level injections.

Figure 6.3 shows a negative deviation from linearity at the upper end of the calibration curve. The detection system, the electrospray ionisation source, and the ion trap, are all potential causes of this deviation. When the detection system was examined, the amplifier provided a linear response over the range in question. Furthermore, the voltage drop across the MCP plates was changed, from the usual setting of 900 V across each plate, to different values to change the gain. If the detection system was causing the deviation to occur, the injection amount where the negative deviation begins would change as the gain was varied. The deviation in linearity was still observed at the same place in the calibration curve, consequently, the detector was not the cause of the non-linearity.

To determine the effect of the ion trap on the upper limit of the calibration curve, the following experiment was carried out. Three solutions of SDM (1 pmol, 4 pmol, and 10 pmol) were analysed using different trapping times. The peak areas were calculated, and the ratios of the peak areas at different trapping times are presented in Table 6.2.

Table 6.2 Determination of the Upper Limit of Quantitation.

	Ratio of Peak Areas of SDM	
Trapping Time (ms)	(4 pmol / 1 pmol)	(10 pmol / 1 pmol)
1000	3.3	5.4
500	3.4	6.9
250	3.6	7.4
100	3.9	8.6
50	4.1	9.6

In the linear region of the calibration curve, when two different amounts of an analyte were injected, the peak area ratio was approximately equal to the ratio of the injected amounts. Consequently in Table 6.2, a linear response would correspond to peak area ratios of approximately 4 and 10 in columns 2 and 3, respectively. If the deviation in Table 6.2 was only caused by the electrospray ionisation source, the peak area ratios would have been non ideal, but they would have remained constant as the trapping time changed. However, as the trapping time was increased, the peak area ratios decreased. These results imply that the ion trap was a significant factor in causing the negative deviations from linearity in the calibration curve. A possible explanation is that high number densities of ions in the ion trap were limiting the number of ions that were stored, thereby limiting the dynamic range [20]. Note that this experiment does not, however, exclude the electrospray ionisation source as a contributing cause to the deviation from linearity. Recent results obtained using a quadrupole mass analyser suggest that limitations due to the electrospray ionisation source may also play a significant role in causing deviations from the upper limit of the calibration curve [17].

6.3.3 Reproducibility

The reproducibility of the electrospray ionisation ion trap/linear TOFMS was also examined. The reproducibility was sensitive to considerations such as the tip-capillary connection, the condition of the electrospray needle tip, and the inner diameter of the electrospray needle [17]. Generally, relative standard deviation (RSD) values ranged from 4 to 7% for each injection amount. Figure 6.5 shows repeat injections of SDM at 10 fmol, 100 fmol, and 1 pmol. The reproducibility over an 8-hour day was also examined and shown in Figure 6.6 (A) is a graph of the peak area of SDM obtained during this period. The use of peak area alone gave an RSD of 8.1%. However, when SMR was added as an internal standard, shown in Figure 6.6 (B), the RSD value was reduced to 6.2%.

6.3.4 Multicomponent Analysis

Since a TOF mass analyser obtains a complete mass spectrum with every extraction event, multicomponent analysis is a major advantage of using this combination. Multicomponent analysis is used for determining coeluting analytes or, for certain applications in which the separation step is omitted, it is used to analyse the extract directly. Calibration curves for individual sulphonamides in a mixture of sulphonamides, with varying concentrations, were obtained to determine if changing the concentration of the other components in the mixture would change the peak area of the analyte of interest. In general, if the TOTAL peak area of all sulphonamides in the mixture was below a certain critical value, then the calibration curve for the analyte of interest was unaffected by changing the relative amounts of other sulphonamides present in the mixture. However, once this critical value of total peak area was reached (independent of which specie(s) was/were dominant), reduction in the peak area of the analyte of interest was also observed.

To illustrate this point, a calibration curve for SDM was obtained with low amounts of SCP, SMR, SMZ, and STZ present in solution. The calibration curve was very similar to what was shown for SDM alone in Figure 6.3. However, when a series of calibration curves for all five of the sulphonamides were simultaneously obtained, the results, shown in Figure 6.7, show deviations from linearity at lower injection amounts than Figure 6.3. The calibration curves were obtained by injecting SDM, SCP, SMR, SMZ, and STZ using a constant molar ratio of 1:4:1:1:2, respectively. This ratio was used so that the corresponding peak areas for all five sulphonamides were approximately equal for every injection. Figures 6.7 (A) - (E) show that all the sulphonamides, including SDM, are only linear for only about one order of magnitude. Note that the value for total peak area where the deviation from linearity occurs in these figures is approximately the same as the value for peak area where the deviation from linearity occurs in Figure 6.3.

Again, the decreasing trapping efficiency, due to the high number densities of ions discussed in section 6.3.2, is believed to be a major reason for the deviation from linearity. As the critical value of total peak area was increasingly exceeded, deviations from expected peak area values of the analyte of interest became more pronounced. Consequently, a quantitative multicomponent analysis can only be carried out if the total peak area of all the sulphonamides is below the critical value.

6.3.5 Summary

In summary, the addition of ammonium acetate to the solvent mixture was a necessary step when using the electrospray ionisation ion trap/linear TOFMS for quantitation as it limited the formation of sodium and potassium adducts. Three of the five sulphonamides studied were detected when 5 fmol were injected. The calibration curves for all the sulphonamides studied were linear for almost three orders of magnitude. The lower limit of quantitation was restricted by the chemical background noise. The use of tandem mass spectrometry techniques would significantly reduce the noise and therefore improve the S/N ratio at the low levels. The upper limit was determined, at least in part, to be restricted by the trapping character of the ion trap.

6.4 Literature Cited

1. Gelpi, E. *J. Chromatogr. A* **1995**, *703*, 59.
2. Fenn, J. B.; Mann, M.; Meng, C. K.; Wong, S. F.; Whitehouse, C. M. *Science* **1989,** *246*, 64.
3. Smith, D. R.; Loo, J. A.; Edmonds, C. G.; Barinaga, C. J.; Udseth, H. R. *Anal. Chem.* **1990**, *62*, 882.
4. Michael, S. M.; Chien, B. M.; Lubman, D. M. *Anal. Chem.* **1993**, *65*, 2614.
5. Purves, R. W.; Li, L. *J. Microcolumn Separations* **1995**, *7*, 603.
6. Porter, S. *Analyst* **1994**, *119*, 2753.
7. Haagsma, N.; Pluijmakers, G. J. M.; Aerts, M. M. L.; Beek, W. M. J. *Biomed. Chromatogr.* **1987**, *2*, 41.
8. Brady, M. S.; Katz, S. E. *J. Food Prot.* **1988**, *51*, 8.
9. Woodward, K. N. *Human Exp. Toxicol.* **1992**, *11*, 60.
10. Boison, J. O.; Keng, L.-Y. *J. AOAC Int.* **1995**, *78*, 651.
11. Long, A. R.; Short, C. R.; Barker, S. A. *J. Chromatogr.* **1990**, 87, 87.
12. Perkins, J. R.; Parker, C. E.; Tomer, K. B. *J. Am. Soc. Mass Spectrom.* **1992**, *3*, 141.
13. Johansson, I. M.; Pavelka, R.; Henion, J. D. *J. Chromatogr.* **1991**, *559*, 515.
14. Dekkers, S. E. G.; Tjaden, U. R.; van der Greef, J. *J. Chromatogr. A* **1995**, *712*, 201.
15. Purves, R. W.; Li, L. *J. Am. Soc. Mass Spectrom., in press.*
16. Coulson, L. D.; Nagra, D. S.; Guo, X.; Whittal, R. M.; Li, L. *Appl. Spectrosc.*, **1994**, *48*, 1125.
17. Purves, R. W.; Gabryelski, W.; Li, L. manuscript in preparation.

18. Griffey, R. H.; Sasmor, H.; Greig, M. J. *J. Am. Soc. Mass Spectrom.* **1997**, *8*, 155.

19. Qian, M. G.; Lubman, D. M. *Rapid Comm. Mass Spectrom.* **1996**, *10*, 1911.

20. McLuckey, S. A.; Van Berkel, G. J.; Goeringer, D. E.; Glish, G. L. *Anal. Chem.* **1994**, *66*, 689A.

Chart 1

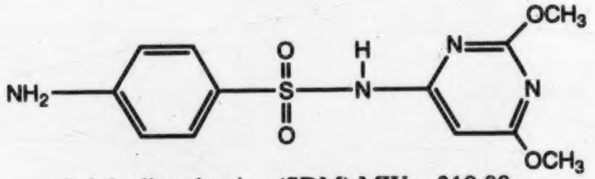
OCH3
N
N
OCH3
O
S
O
H
N
NH2

Sulphadimethoxine (SDM) MW = 310.08

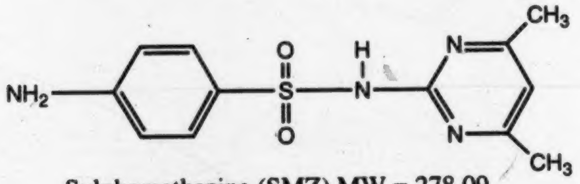
CH3
N
N
CH3
O
S
O
H
N
NH2

Sulphamethazine (SMZ) MW = 278.09

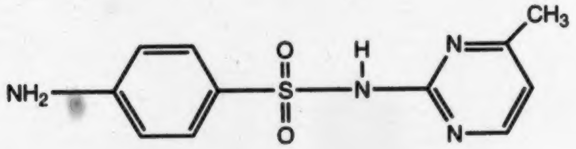
CH3
N
N
O
S
O
H
N
NH2

Sulphamerazine (SMR) MW = 264.07

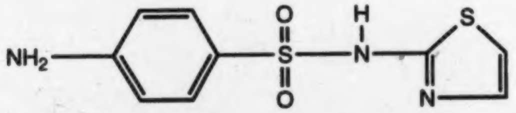
S
N
O
S
O
H
N
NH2

Sulphathiazole (STZ) MW = 256.02

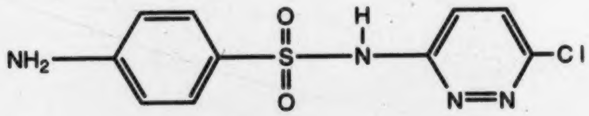
Cl
N=N
O
S
O
H
N
NH2

Sulphachlorpyridazine (SCP) MW = 284.02

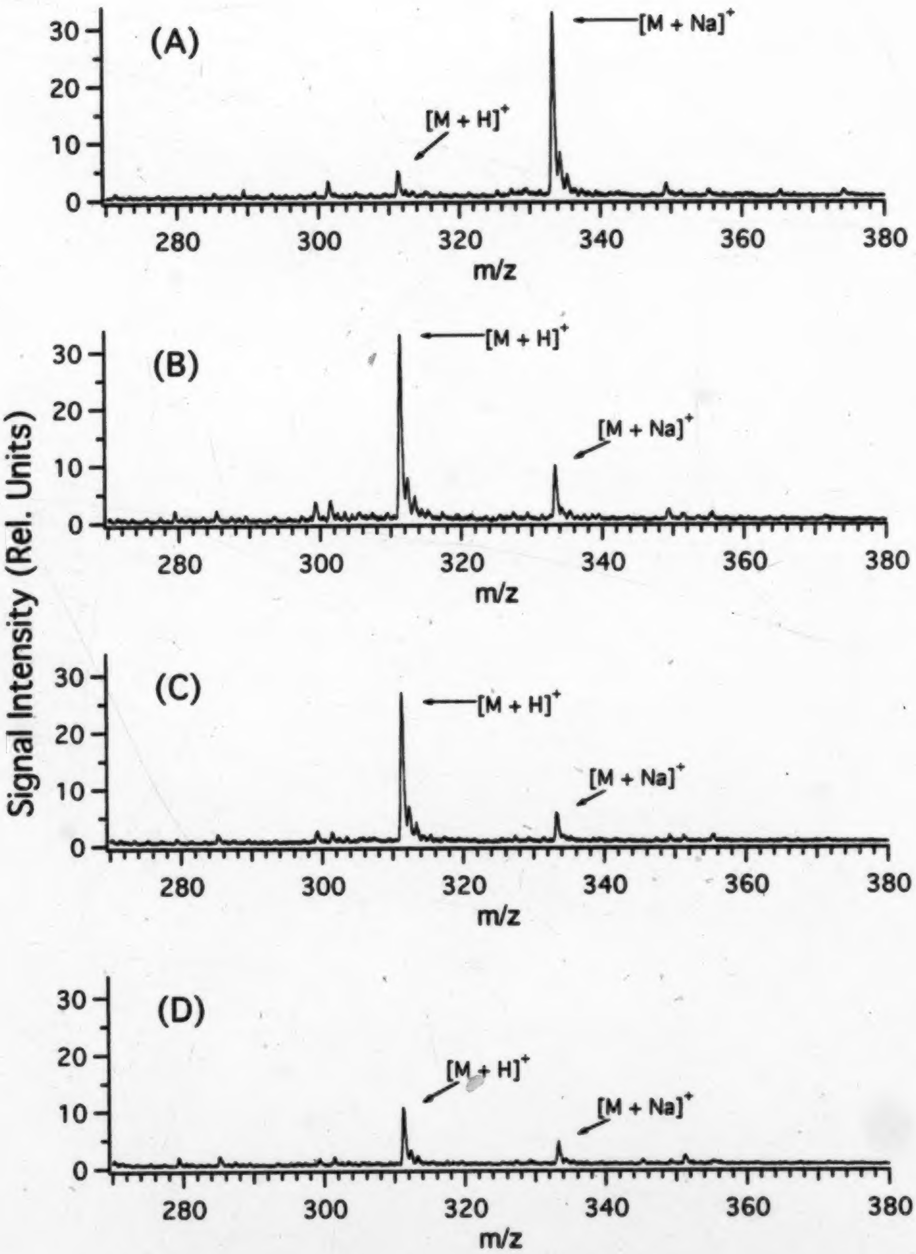

Figure 6.1 Effect of changing the concentration of ammonium acetate on the mass spectra of SDM. (A) No ammonium acetate added, (B) 0.5 mM ammonium acetate, (C) 2 mM ammonium acetate, and (D) 10 mM ammonium acetate.

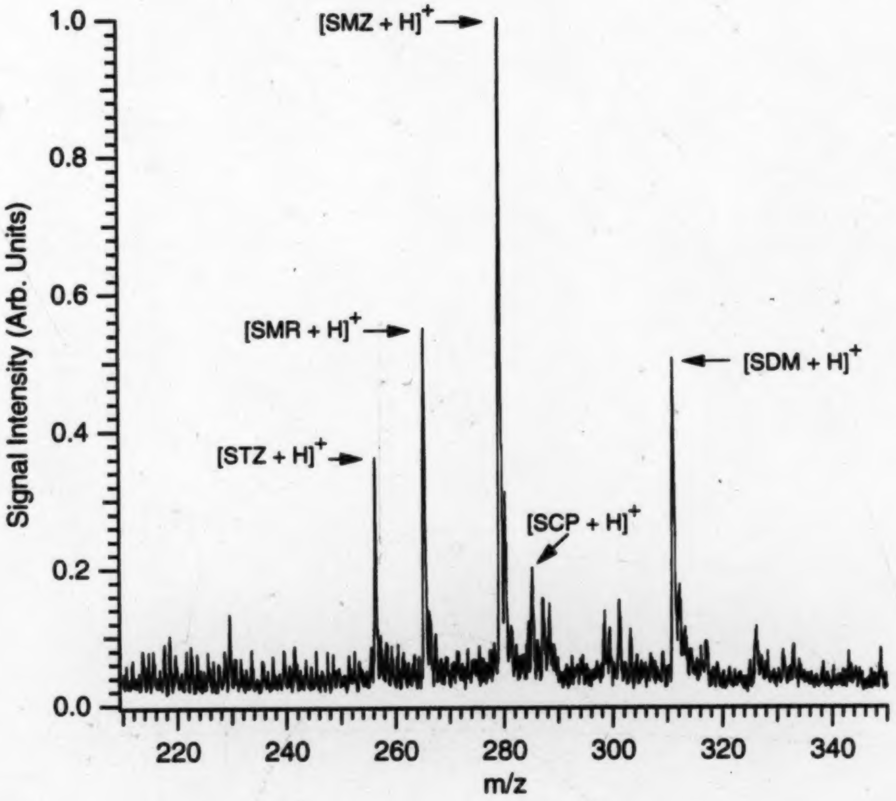

Figure 6.2 Mass Spectrum obtained from an injection of a mixture of SDM, SCP, SMZ, SMR, and STZ. The mixture contained 100 fmol of each sulphonamide. See description in text.

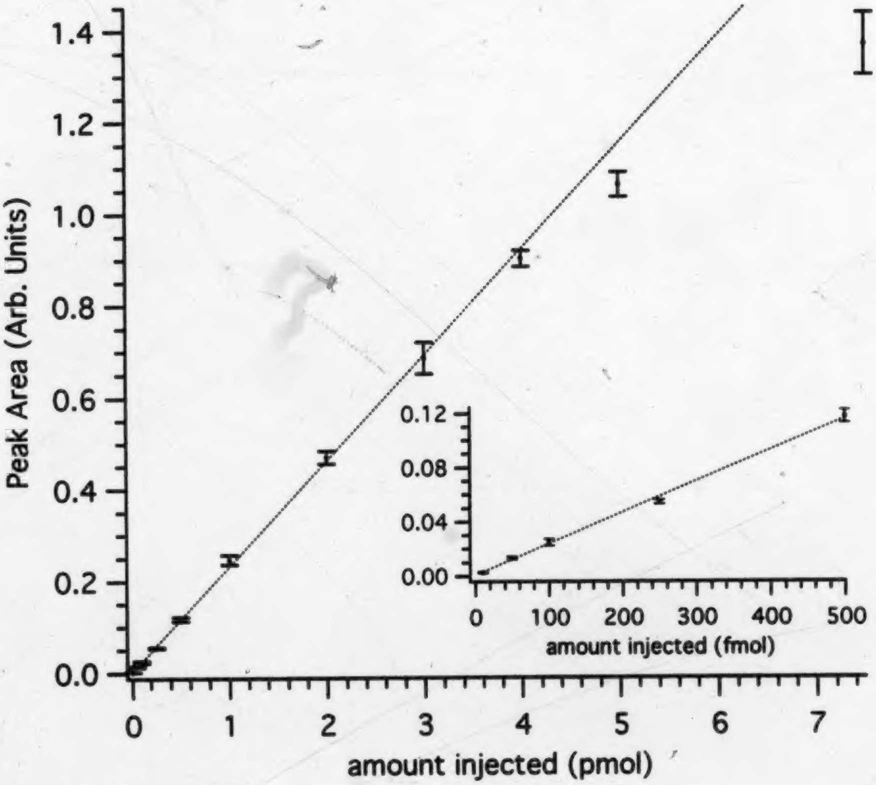

Figure 6.3 Calibration curve for a series of loop injections of SDM with an expanded view of the low end of the curve shown in the inset.

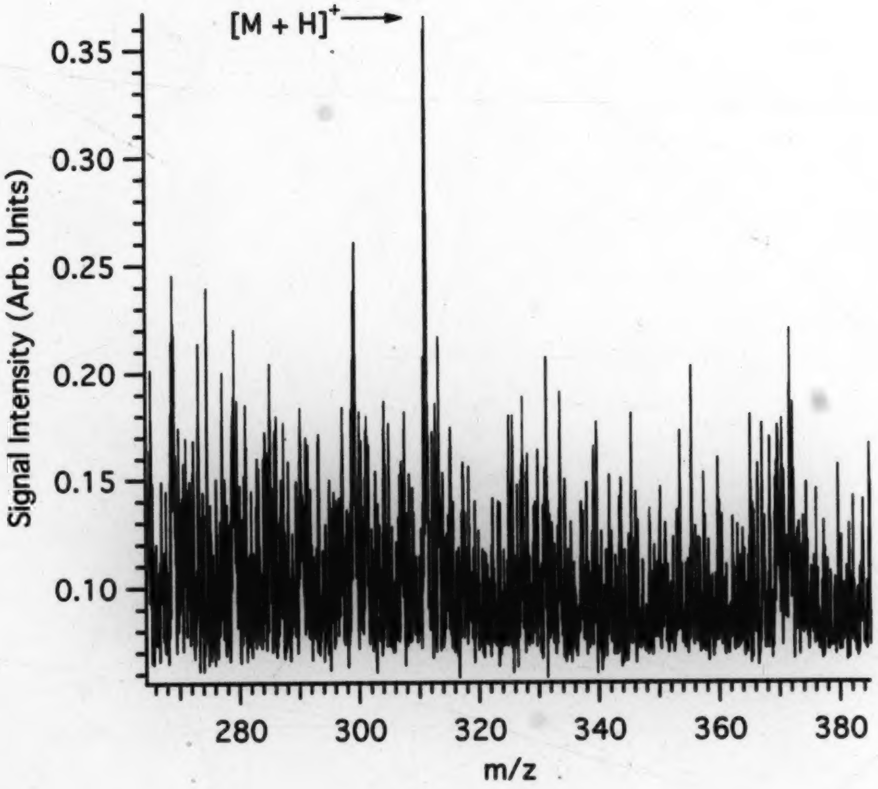

Figure 6.4 Mass spectrum of an injection of 5 fmol of SDM showing the limitations due to the chemical background noise using an electrospray ionisation ion trap/linear TOFMS. Note that only 25 ion extraction events were summed for this mass spectrum.

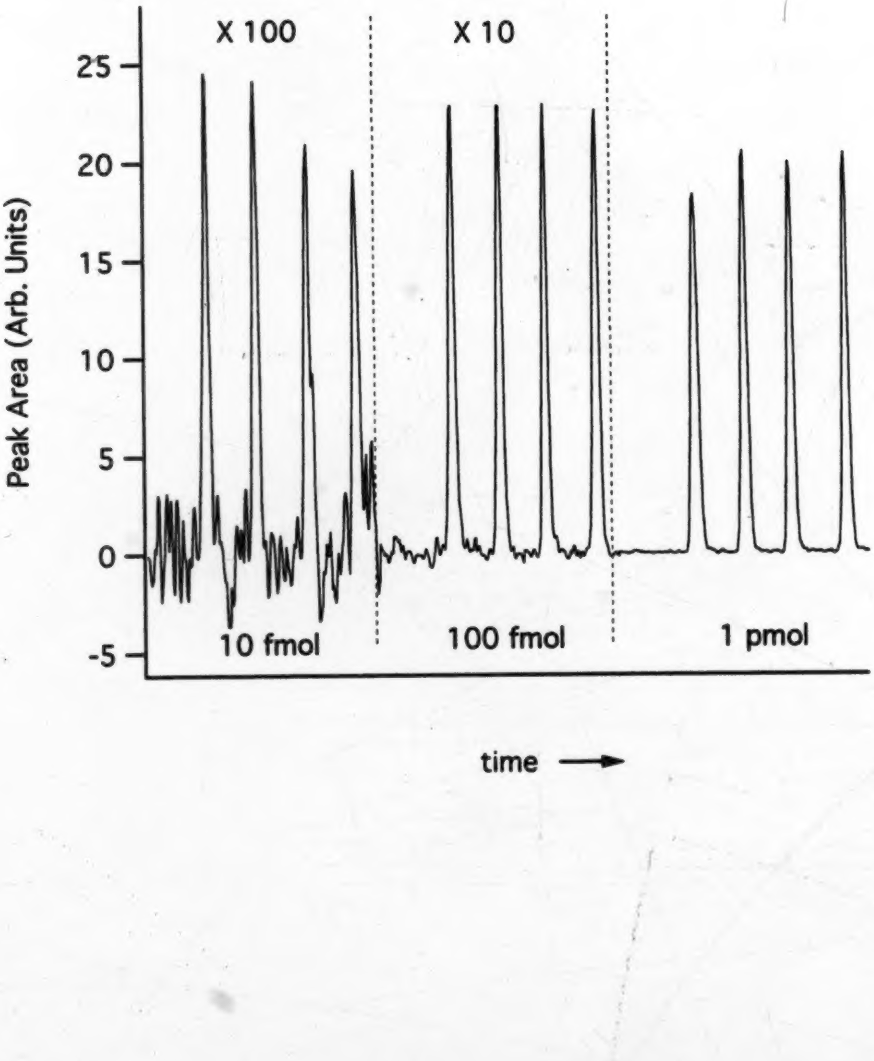

Figure 6.5 Reproducibility of the electrospray ionisation ion trap/TOFMS illustrated using repeat injections of SDM at 10 fmol, 100 fmol and 1 pmol.

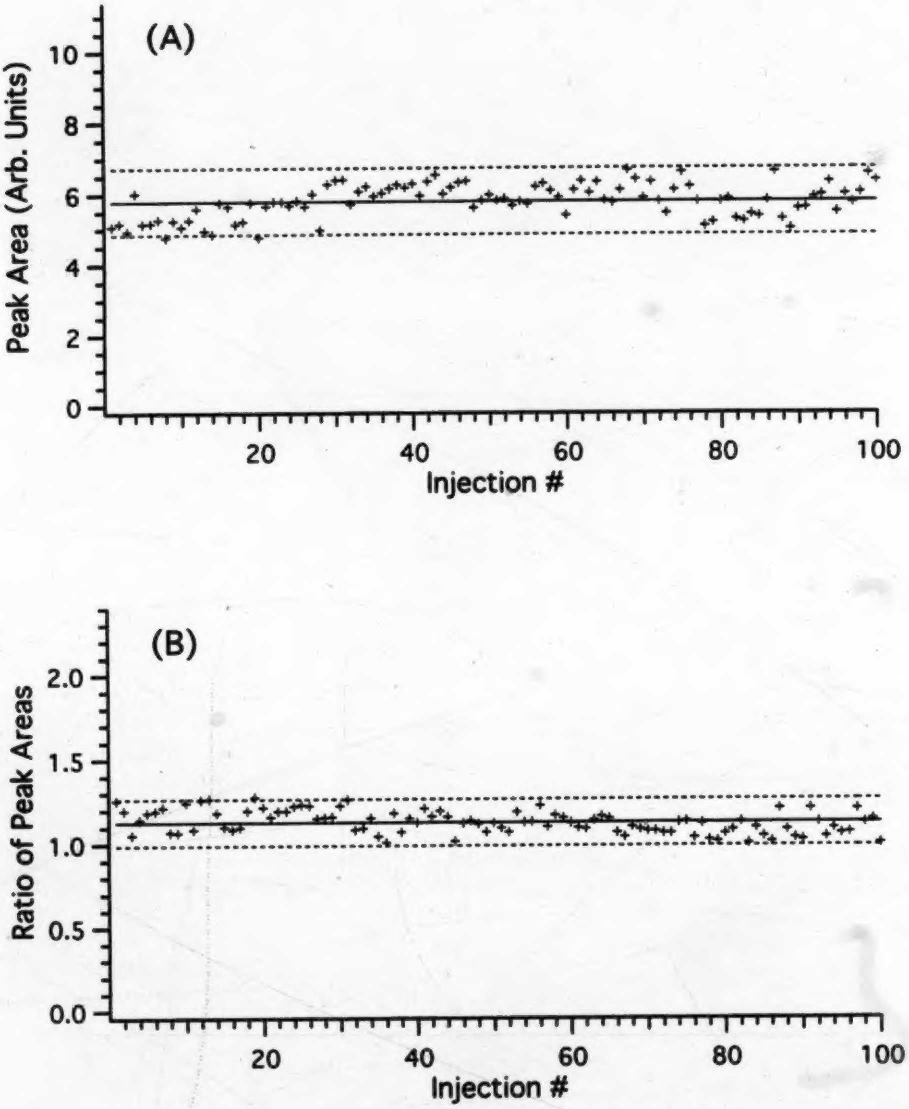

Figure 6.6 Repeat injections of SDM over an eight hour period. (A) Area calculated using a calibration curve, (B) a ratio of peak areas calculated using SMZ as an internal standard.

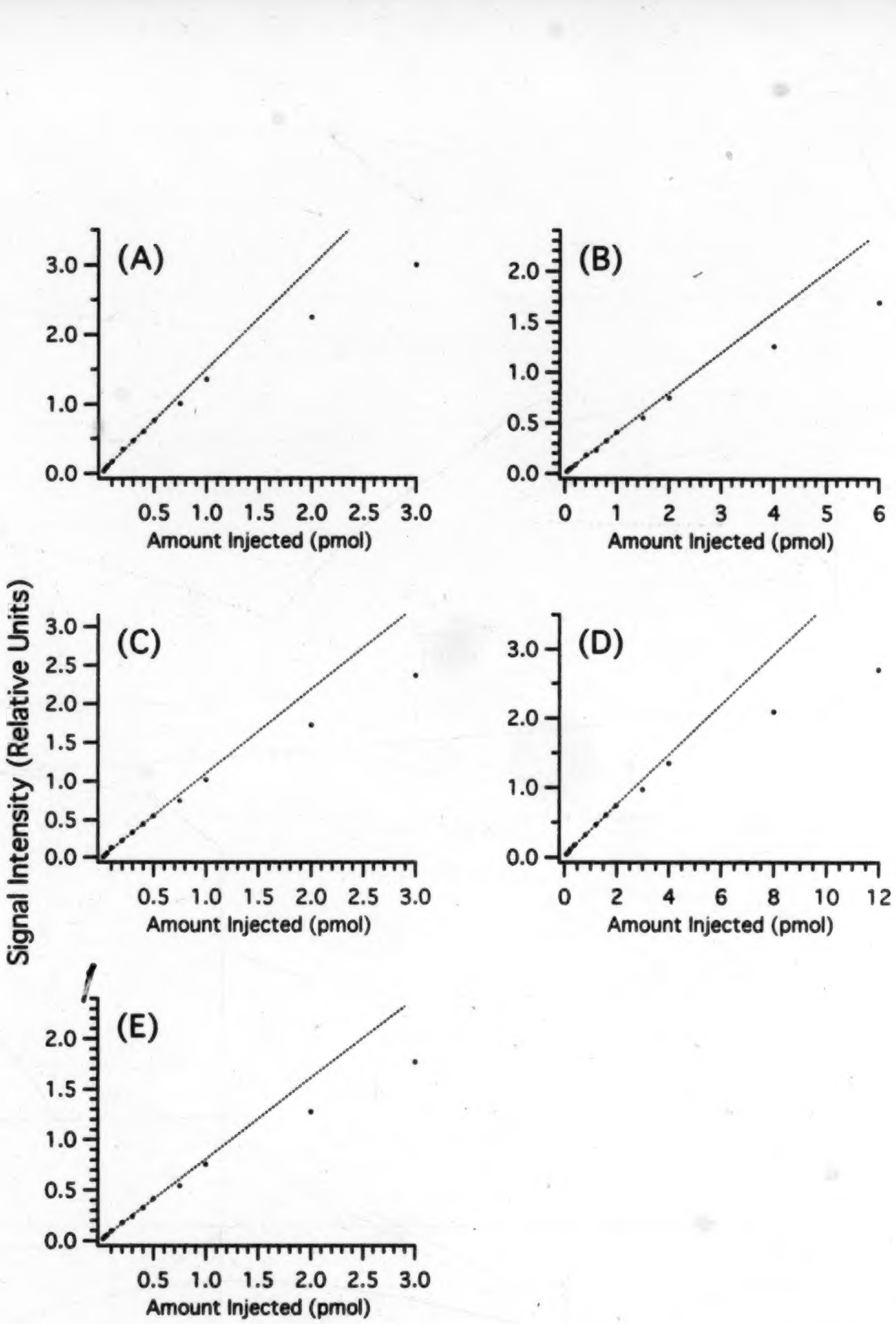

Figure 6.7 Calibration curves for (A) SDM, (B) STZ, (C) SMZ, (D) SCP, (E) SMR obtained simultaneously from a mixture. See text for details.

Chapter 7

Detection of Phenylthiohydantoin Amino Acids Using Electrospray Ionisation Ion Trap/Linear Time-of-Flight Mass Spectrometry[a]

7.1 Introduction

One of the most common methods used to determine the sequence of a peptide or protein is Edman degradation [1]. This technique sequentially removes the N-terminal amino acid from a protein using the sequencing reagent phenylisothiocyanate (PITC). The final products of Edman degradation, phenylthiohydantoin (PTH)-amino acids, are commonly analysed using high performance liquid chromatography (HPLC) with UV detection. Constant refinement of HPLC-UV techniques [2,3] has allowed for routine sequencing of low picomole amounts of polypeptides [4]. Although this is an effective means of analysis, the use of a mass spectrometer (MS) for detection of PTH-amino acids offers several advantages. For example, mass spectrometry provides the molecular mass and structural information of modified or unusual amino acids that cannot be identified with a

---

[a] A form of this chapter is in preparation for publication: W. Gabryelski, R. W. Purves, L. Li "Detection of Phenylthiohydantoin amino acids using an Electrospray ionisation Ion Trap/Linear Time-of-Flight Mass Spectrometer". Data collection and data analysis were carried out by both W. Gabryelski and R. W. Purves.

UV detector. An HPLC-MS analysis of PTH-amino acid derivatives has been carried out using thermospray ionisation [5]. However, studies involving the use of electrospray ionisation for detection of PTH-amino acids have not been reported. Electrospray ionisation has been used to analyse the final products of other protein sequencing reagents designed to give improved sensitivity [6-8]. A major problem with these methods, however, is that improved detectability does not lead to improved sequencing sensitivity mainly due to background contamination [7].

An electrospray ionisation ion trap/linear time-of-flight mass spectrometer (TOFMS) should allow for a highly sensitive analysis of PTH-amino acids. A preliminary study into the use of an electrospray ionisation ion trap/linear TOFMS as a detector for PTH-amino acids is presented in this chapter. This study investigates the sensitivity of the technique for 20 PTH-amino acids and explores a direct analysis of a mixture of six of the less detectable PTH-amino acids using the ion trap/linear TOFMS.

7.2 Experimental

The electrospray ionisation ion trap/linear TOFMS has been described in detail in previous chapters [9,10]. All of the 20 PTH-amino acids used in this chapter were purchased from Sigma and used without further purification.

The PTH-amino acids were analysed using a solution of 0.05 mM ammonium acetate in 80% acetonitrile and 20% water (v/v). This level of ammonium acetate results in a larger signal intensity for the analyte than the 2 mM ammonium acetate solution used in Chapter 6. The analyte was injected using a Rheodyne model 7520 injector (sample loop size of 0.5

μL). The only change made to operation of the instrument compared with the conditions used in Chapter 6 was that all the mass spectra were collected using a trapping time of 250 ms. Data collection and data analysis were carried out as was described in Chapter 6 [11].

7.3 Results and Discussion

7.3.1 Mass Spectra of PTH-Amino Acids

Except for PTH-(phenylthiocarbamyl(PTC)-cysteine), intense protonated molecule peaks were observed in the mass spectra of all the PTH-amino acids studied when mild conditions were used (i.e., a low voltage drop in the interfacial region). Figure 7.1 (A) shows an example of a typical mass spectrum for the PTH-amino acids using PTH-alanine. In the mass spectrum of PTH-(PTC-Cysteine), shown in Figure 7.1 (B), a molecular ion peak at m/z 373.0 was not observed. Instead, the peak observed at m/z 205.0 represents an intense fragment. Note that the peak at m/z 199 in the mass spectra of both compounds was caused by a contaminant from the injection system.

7.3.2 Detectability of PTH-Amino Acids

The detectability of 20 different PTH-amino acids was investigated using the ion trap/linear TOFMS. For each PTH-amino acid, five repeat injections were carried out for three different injection levels. The average signal-to-noise (S/N) ratios for the $[M + H]^+$ ion for each PTH-amino acid using the ion trap/linear TOFMS are presented in Table 7.1. Note that the PTH-amino acids are listed in decreasing order in the table starting from the highest S/N ratio for the 100 fmol injection.

Table 7.1 Signal-to-noise ratios of 20 PTH-amino acids using the ion trap/linear TOFMS.

PTH-amino acid	500 fmol	250 fmol	100 fmol
Histidine (H)	602	-	83*
Proline (P)	287	109	77
Arginine (R)	29**	-	45
Asparagine (N)	125	97	43
Valine (V)	130	64	24
Phenylalanine (F)	112	57	24
Alanine (A)	143	49	23
Leucine (L)	143	69	22
Tyrosine (Y)	69	38	20
Isoleucine (I)	78	41	18
PTC-Lysine (K)	75	35	18
Tryptophan (W)	67	37	18
Methionine (M)	61	33	18
Threonine (T)	82	40	16
PTC-Cysteine+ (C)	67	44	15
Glutamine (Q)	55	26	11
Glycine (G)	46	26	10
Serine (S)	39	18	7
Glutamic Acid (E)	32	18	7
Aspartic Acid (D)	30	16	5

* amount injected was 50 fmol

** low value is due to an adsorption phenomenon (see text)

+ intense fragment peak at m/z 205 was used to calculate S/N ratios

The table shows that all 20 PTH-amino acids were detected when at least 100 fmol were injected. This corresponds to approximately an order of magnitude increase in detection limits compared with the LC/MS study of PTH-amino acids by Parmanik et al. using thermospray and a quadrupole mass analyser [5]. The least detectable PTH-amino acids, PTH-glutamic acid and PTH-aspartic acid, are two species that are not easily protonated. In contrast, the more basic PTH-amino acids, PTH-histidine and PTH-arginine, are the more detectable compounds. The unusual results for PTH-arginine are a consequence of adsorption phenomena observed during the elution of this compound [12]. The flow injection profiles showed severe tailing of PTH-arginine over a very long time compared with the other PTH-amino acids. Note that when the same concentrations of the various PTH-amino acids were directly infused to the electrospray needle tip and the peak area was measured, PTH-arginine had the largest peak area of the 20 PTH-amino acids [12]. The S/N values shown in Table 7.1 are limited by the chemical background noise, a problem discussed in Chapter 6. Again, it is expected that the use of tandem mass spectrometry using an ion trap/TOFMS [13] could further reduce the detection limits.

7.3.3 Mixture Analysis

A major advantage in using TOF for mass analysis is the ability to collect a complete mass spectrum with every ion extraction event [14]. Note that with the electrospray ionisation ion trap/linear TOFMS, all 20 PTH-amino acids studied can be differentiated from their fragmentation patterns [12]. Consequently, a direct analysis of a mixture of unknown PTH-amino acids can be carried out. An example of this is shown for six of the less detectable PTH-amino acids used in this study. Figure 7.2 (A) shows the mass spectrum for a 1 pmol injection of each component in the mixture, while Figure 7.2 (B) shows the mass spectrum for a 250 fmol injection (single letter codes are given in Table 7.1). Note that for a 100 fmol injection, not all of the six PTH-amino acids were unambiguously determined. Again, the large chemical background noise effectively limited the limit of detection of these species.

7.3.4 Summary

In this preliminary study, all 20 PTH-amino acids, with the exception of PTH-(PTC-cysteine), produced mass spectra with intense molecular ion peaks. When the PTH-amino acids were analysed individually, all of the PTH-amino acids were detected when 100 fmol of the analyte was injected. Future work will involve combining a protein sequencer with the electrospray ion trap/linear TOFMS for the direct analysis of PTH-amino acids.

7.4 Literature Cited

1. Edman, P. *Acta. Chem. Scand.* **1950**, *4*, 283.
2. Zimmerman, C. L.; Appella, E.; Pisano, J. J. *Anal. Biochem.* **1977**, *77*, 569.
3. Johnson, N. D.; Hunkapiller, M. W.; Hood, L. E. *Anal. Biochem.* **1979**, *100*, 335.
4. Bures, E. J.; Nika, H.; Chow, D. T.; Morrison, H. D.; Hess, D.; Aebersold, R. *Anal. Biochem.* **1995**, *224*, 373.
5. Pramanik, B. C.; Hinton, S. M.; Millington, D. S.; Dourdeville, T. A.; Slaughter, C. A. *Anal. Biochem.* **1988**, *175*, 305.
6. Hess, D.; Nika, H.; Chow, D. T.; Bures, E. J.; Morrison, H. D.; Aebersold, R. *Anal. Biochem.* **1995**, *224*, 373.

7. Aebersold, R.; Bures, E. J.; Namchuk, M.; Goghari, M. H.; Shushan, B.; Covey, T. C. *Protein Sci.* **1992**, *1*, 492.

8. Basic, C.; Bailey, J. M.; Lee, T. D. *J. Am. Soc. Mass Spectrom.* **1995**, *6*, 1211.

9. Purves, R. W.; Li, L. *J. Microcolumn Separations* **1995**, *7*, 603.

10. Purves, R. W.; Li, L. *J. Am. Soc. Mass Spectrom., in press*

11. Coulson, L. D.; Nagra, D. S.; Guo, X.; Whittal, R. M.; Li, L. *Appl. Spectrosc.*, **1994**, *48*, 1125.

12. Gabryelski, W.; Purves, R. W.; Li, L. manuscript in preparation.

13. Qian, M. G.; Lubman, D. M. *Rapid Comm. Mass Spectrom.* **1996**, *10*, 1911.

14. *Time-of-Flight Mass Spectrometry;* Cotter, R. J., Ed. (American Chemical Society, Washington, DC, 1997).

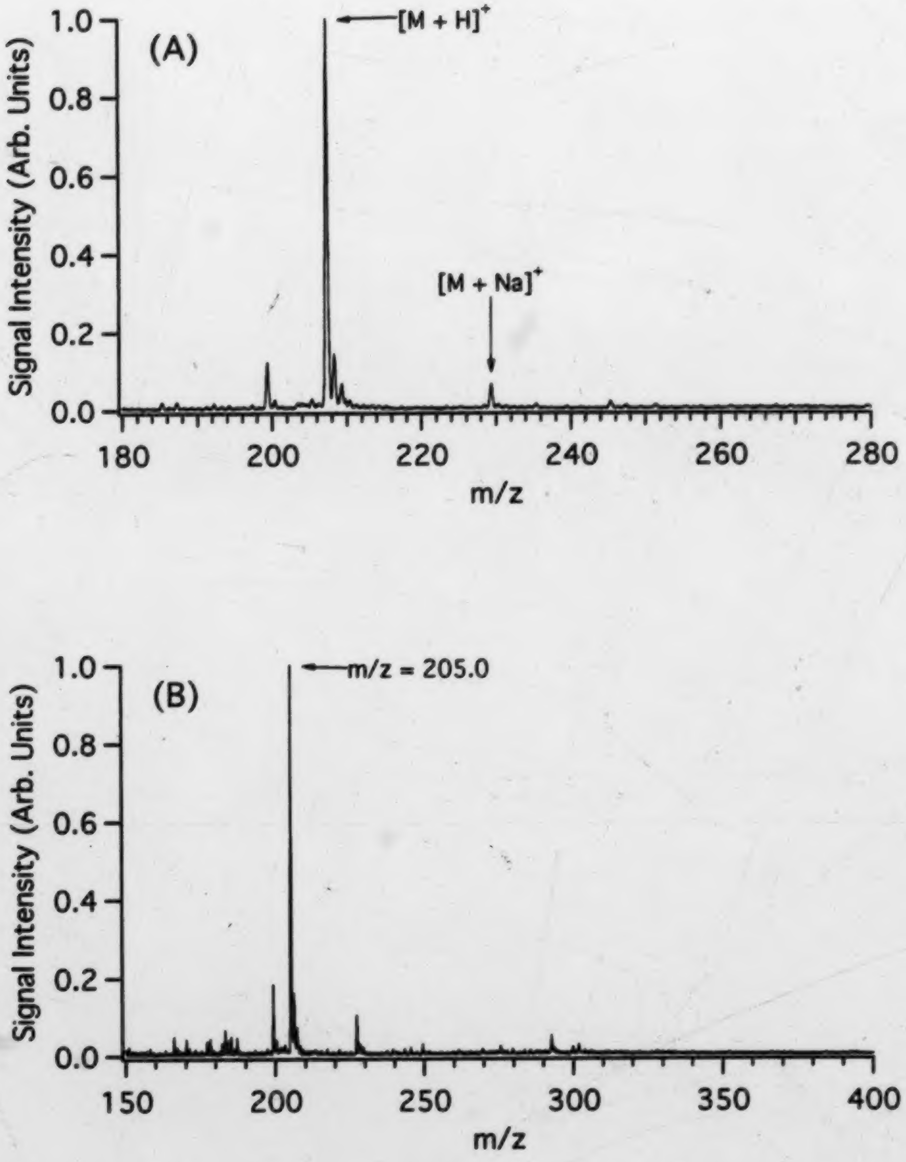

Figure 7.1 Mass spectra of (A) PTH-alanine, (B) PTH-(PTC-cysteine). See text for details.

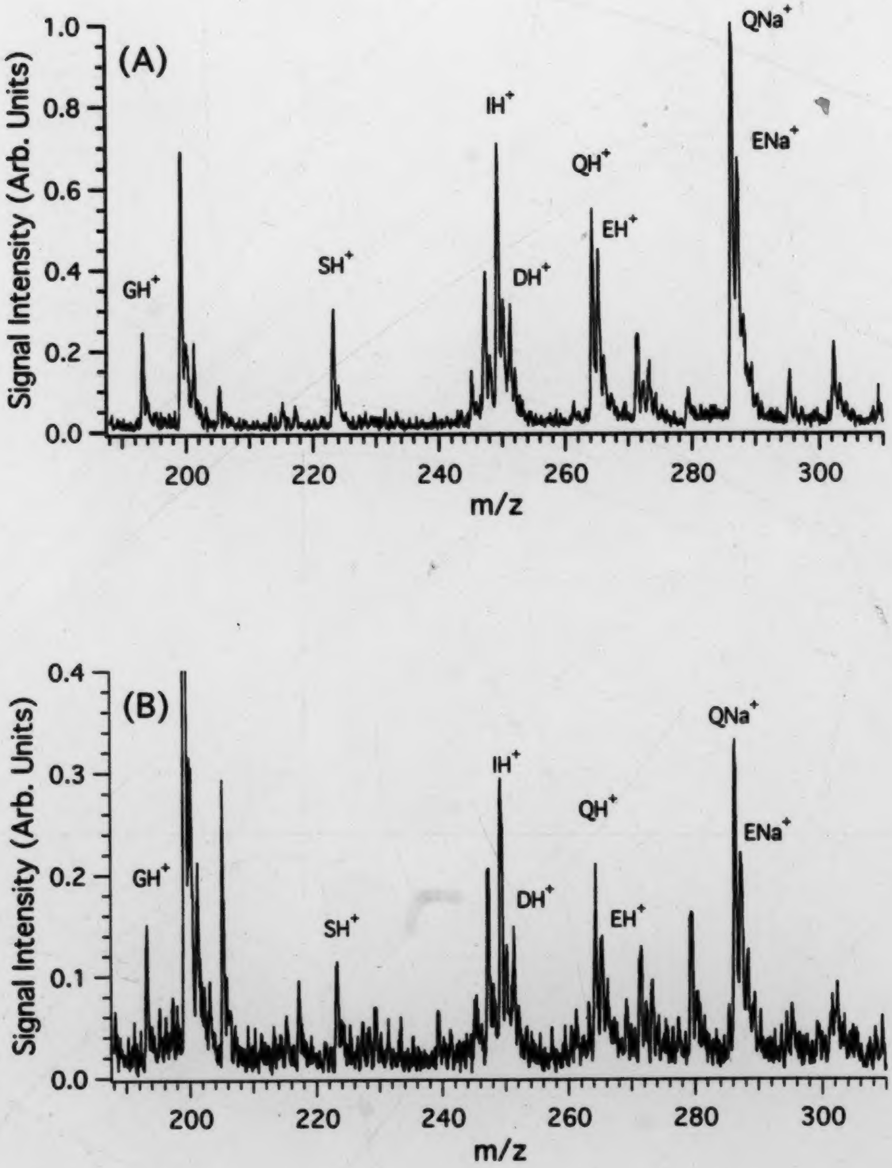

Figure 7.2 Mass spectra of a mixture of six PTH-amino acids, (A) 1 pmol and (B) 250 fmol of each compound injected. See text for details.

Chapter 8

Conclusions and Future Work

Electrospray ionisation is capable of producing gas phase ions from very large, complex, and fragile compounds. The use of a TOF mass analyser as a detector for electrospray ionisation mass spectrometry offers several advantages including speed and sensitivity. In Chapter 1, several different possible methods used for combining electrospray ionisation with TOFMS were examined. The construction and preliminary testing of an orthogonal extraction TOFMS was presented in Chapter 2. Poor sensitivity, which was largely attributed to the data acquisition system, was the primary reason why work with this configuration was discontinued.

An ion trap/linear TOFMS was constructed to maximize sensitivity and its potential as a detector for separation techniques was investigated in Chapter 3. This instrument gave unprecedented mass resolution values in comparison with previous electrospray ionisation linear TOFMS studies. The detection limits of the instrument were also examined using a series of injections of bradykinin.

In Chapter 4, two types of adduct formation that were observed with this instrument were examined; adduct formation that occurred in the ion trap and adduct formation that occurred in solution. Adduct formation that was occurring in the ion trap was due to residual gases from the silicon-based diffusion pump fluid. Adduct formation from solution was also examined, and in particular, the relevance of adducts to the mass spectral quality was also discussed.

The results from a characterization of the ion trap/linear TOFMS are reported in Chapter 5. Several variables were examined, several of which had not been previously investigated in the literature. The instrument was most suited for the analysis of small analytes (i.e., less than ~20 000 u). For these analytes, the optimal mass resolution values obtained with the ion trap/linear TOFMS were ~1200 fwhm. The application of the ion trap/linear TOFMS to the analysis of large analytes (i.e., greater than ~20 000 u) uncovered some limitations of the instrument. Studies on the effects of flow rate of helium into the ion trap showed that large flow rates of helium, necessary for efficient trapping of large analytes, resulted in decreased mass spectral quality. Furthermore, space charge effects and the kinetic energy of the ions entering the ion trap were also a concern when analysing large analytes. Possible solutions, including the use of a rf only quadrupole and electronic cooling methods were discussed.

The mass accuracy of the ion trap/linear TOFMS was examined and mass accuracy errors within 10 ppm are obtained using an internal standard when the peaks are isotopically resolved. For an external standard without isotopic resolution, the error is still better than 100 ppm.

The use of the ion trap/linear TOFMS for quantitative analyses was investigated by examining a group of sulphonamides and the results are presented in Chapter 6. A typical calibration curve for these compounds was linear for almost three orders of magnitude. The lower quantitation limit was restricted by the chemical background noise, however, the application of tandem mass spectrometry could potentially improve this limit. The potential for applying the ion trap/linear TOFMS to direct quantitative analysis of a mixture of compounds is also explored. The detectability of twenty PTH-amino acids was briefly investigated and these results are presented in Chapter 7. All of the PTH-amino acids were observed when 100 fmol were injected.

The ion trap/linear TOFMS enables fast, sensitive analyses of electrosprayed ions to be carried out. However, the instrument is still in the developmental stages and improvements still need to be made before its full potential for analytical applications can be evaluated. In particular, the implementation of an improved method of ion focussing (i.e., an rf-only quadrupole) could significantly improve the performance of the instrument. Also, the ability to carry out tandem mass spectrometry would not only reduce the chemical background noise, but it would also provide structural information of selected m/z ions.

Appendix A

Electronic Circuitry

Protection Circuit:

After a high frequency voltage spike irreparably damaged an amplifier, a protection circuit, shown in Figure A.1, was developed to protect the electronic components from similar future occurrences. All the required parts, listed in Table A.1, were available from the Electronics shop at the University of Alberta. Although simple in design, this circuit has been highly effective as it grounds both positive and negative high voltage transients. The following discussion explains the operation of the circuit for positive voltage transients and a similar argument can be made for negative voltage transients. Note that the detection system was designed to give a 50 Ω output and that care must be taken to use very short leads. Otherwise, long leads add inductance to the output that can result in an impedance mismatch and therefore degrade the quality of the mass spectra.

An input of 12 V is the maximum allowed by the amplifier before it is damaged. The maximum voltage resulting from an analyte signal before amplification is only ~ 0.3 V. To clip the level of a high voltage transient, while still allowing the analyte signal through, a signal diode was used. The additional circuitry in the diagram was required to bias the diode to ~2 V. The two resistors were used as a voltage divider that enabled the same power supply that was being used for the amplifier to be used for the protection circuit. The most important reason for biasing this circuit was that the input capacitance for charging the diode was reduced (i.e., a charging time was not required). The capacitor in the circuit supplied an immediate ground for high frequency voltage transients since the path to ground through the resistor was not adequate. The resistors were also used so that if the diode failed, 15 V would not be passed directly to the amplifier. Since the circuit was implemented (Oct., 1995), it has not failed.

Circuit to ground induced rf noise:

In developing a high voltage negative pulse generator that exceeded -500 V, new circuitry was used. The new high voltage negative pulse generator did not have a true ground and during the ion storage event an induced rf signal on the exit endcap was observed. This induced signal, dependent upon the rf voltage applied to the ring electrode, was ~150 V_{p-p} when the applied voltage was ~2000 V_{p-p}. To reduce the level of this "noise," the circuit, shown in Figure A.2, was developed. Again, all of the required parts, listed in Table A.1, were available from the Electronics shop. Note that a minimum pulse voltage of -300 V was required, otherwise the circuit would not operate. The series of diodes on the right side of the figure were used to ground any induced positive voltage on the exit endcap. The left side of the circuit, derived from Baker and Johnson[a], was used to ground the negative portion of the induced rf noise. The more elaborate circuit was required because the negative portion of the induced rf noise needs to be grounded while still enabling a negative voltage pulse to be applied to the exit endcap. The circuit required a series of metal oxide semiconductor field effect transistors (MOSFETs) since the voltage ratings of the individual MOSFETs were not high enough. By using the MOSFETs in this manner, the total voltage rating was the sum of the individual voltage ratings. For the majority of the time, the MOSFETs were in the "on" position. That is, the induced rf noise was shunted to ground through the MOSFET configuration. During a small window of time (microseconds), the circuit was shut off by applying a negative pulse as is shown in the bottom left hand corner. When the circuit was off, the rf voltage on the ring electrode was shut off and an extraction voltage was applied to the exit endcap. After application of the negative voltage pulse was completed, the left side of the circuit was turned back on. The induced rf noise was reduced by approximately two orders of magnitude.

---

[a] Baker, R. J.; Johnson, B. P. *Rev. Sci. Instrum.* **1993**, *64*, 1655.

Table A.1 List of parts for electronic circuitry.

	Component	Description
Protection Circuit	C_a	1 μF capacitor
	D	signal diode
	R_a	65 kΩ resistor
	R_b	10 kΩ resistor
Circuit to ground rf noise	C	200 pF capacitor
	D	1 kV fast recovery diode
	M	500 V, p-channel power MOSFET
	R_1	1 MΩ resistor
	R_2	1 kΩ resistor
	S	small signal MOSFET
	T	450 V transient suppressor
	Z	10 V zener diode

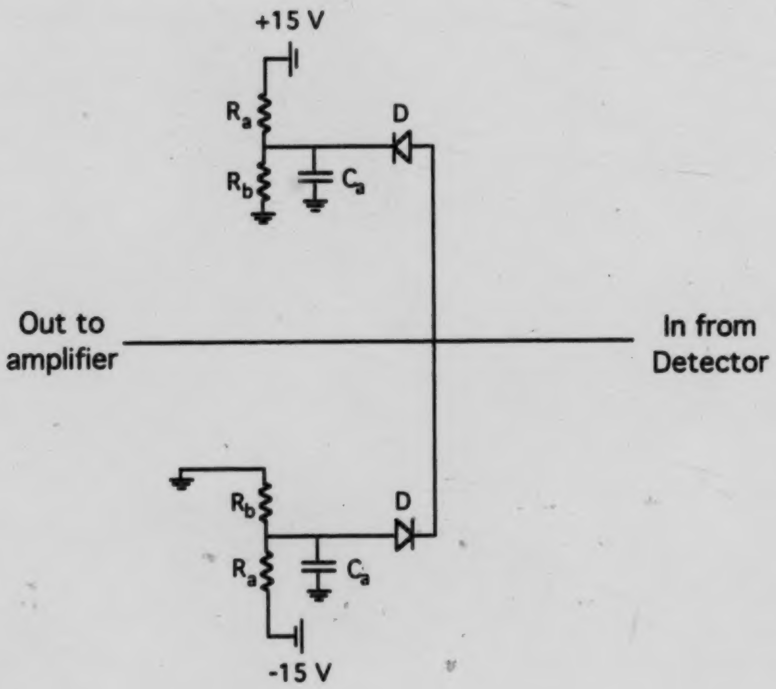
+15 V
R_a
D
R_b
C_a
Out to amplifier
In from Detector
R_b
D
R_a
C_a
-15 V

Figure A.1 Circuit developed to protect the electronic components.

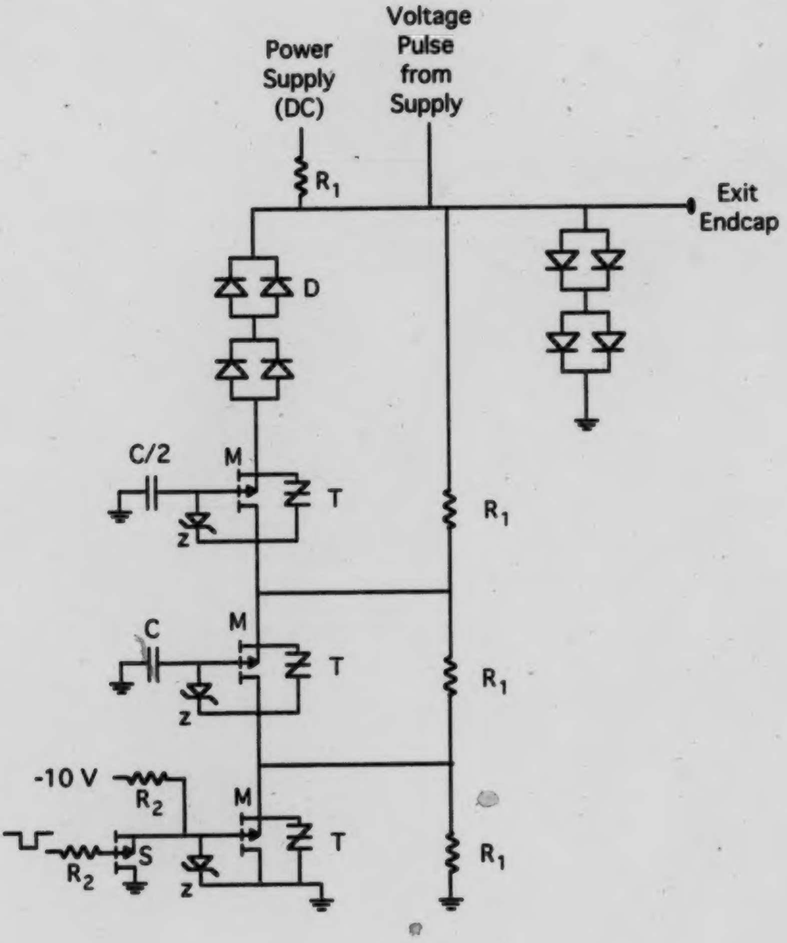
Voltage
Pulse
from
Supply
Power
Supply
(DC)
R1
Exit
Endcap
D
C/2
M
T
Z
R1
C
M
T
Z
R1
-10 V
R2
M
S
R2
Z
T
R1

Figure A.2 Circuit developed to ground induced rf noise on the exit endcap electrode.